Project Report

New Resilient Breakwater for Safety of Port and Harbour Against Tsunami

Submitted By

Principal Investigator:

Dr. Babloo Chaudhary

Department of Civil Engineering

National Institute of Technology Karnataka (NITK), Surathkal,

Mangalore, Karnataka 575 025, India

April 2025

General Information

(i) Project Title, Duration and Budget

Title of the Project	**New Resilient Breakwater for Safety of Port and Harbour Against Tsunami**
Duration of the Project	03 Years (2022-25)
Estimated Budget	45 Lakhs (Approx.)
Status of the organization	Central Government Organization

(i) Principal Investigator (PI)

Name of PI	**Babloo Chaudhary**
Academic Qualifications	Doctor of Engineering (PhD), Kyushu University, Japan
Affiliation	Assistant Professor, Dept. of Civil Engg., NITK Surathkal
Previous Research Experience	Postdoc (2016-2018), **Kyoto University, Japan** (*QS world rank 13 in Civil and Structural Engineering for year 2018*)
Address	Dept. of Civil Engg., NITK Surathkal, Mangalore 575014 Karnataka Email: babloomit@gmail.com; babloo@nitk.edu.in Phone: 0824-2473978 (O), 8724041225(M)

(ii) 1st Co-Investigator (CI)

Name of PI	Dr Sridhar G
Academic Qualifications	Doctor of Engineering (PhD), IIT Madras
Affiliation	Assistant Professor, Dept. of Civil Engg., NITK Surathkal, Mangalore

(iii) 2nd Co-Investigator (CI)

Name of PI	Prof. Katta Venkataramana
Academic Qualifications	Doctor of Engineering (PhD), Kyoto University, Japan
Affiliation	Professor, Dept. of Civil Engg., NITK Surathkal, Mangalore

(iv) Department and Organization Where Research is to be Performed

Name and address	Department of Civil Engineering National Institute of Technology Karnataka (NITK), Surathkal, Mangalore-575025, Karnataka, India
Status of the organization	Central Government Organization

ABSTRACT

Rubble mound (RM) breakwaters are vital coastal defence structures. Yet, past catastrophes such as the 2004 Indian Ocean tsunami and the 2011 Great East Japan Earthquake have exposed their vulnerability to seismic and tsunami-induced forces. Existing research offers limited insight into their complex failure mechanisms, particularly concerning the behaviour of foundation soils. This study addresses this gap through an integrated experimental and numerical investigation into the dynamic response of conventional RM breakwater. Moreover, a new reinforcing technique was developed to make the RM breakwater resilient against earthquake and tsunami. Using the New Mangalore Port breakwater as a prototype, two models were assessed: a conventional model and a reinforced configuration incorporating seabed-embedded sheet piles, gabions on outer slopes, and a crown wall with shear keys.

Under earthquake loading, shake table tests revealed that breakwater settlement is predominantly driven by the lateral spreading of loose foundation soils and increased pore pressure under strong earthquake loadings. Reinforcements in the form of sheet piles and gabions significantly reduced settlement and lateral displacement by 49.3% and 37.3%, respectively, while excess pore water pressure dropped by 35.6%. Numerical simulations confirmed that deeper and denser sand layers improved seismic performance.

Tsunami overflow tests demonstrated the reinforced model's superior resilience. Crest settlement and lateral displacement were reduced by 94% and 98%, respectively, due to the stabilizing effects of gabions and the crown wall. The incremental pore water pressure was also reduced by 35%, indicating enhanced seepage resistance. Damage analysis showed minimal dislodgement and scouring in reinforced models. Numerical studies supported these results and highlighted the critical influence of tsunami height and drawdown effects. At tsunami heights exceeding the breakwater crest ($h_t/H \geq 1$), the conventional model experienced large-scale deformation and failure, whereas the reinforced model maintained structural coherence. Drawdown scenarios revealed that lower sea levels ($h_s/H = 0.2$) significantly improved structural stability, reducing displacement and pore pressure while shifting failure modes from base to toe failure.

These findings emphasize the necessity of integrated reinforcement strategies—such as sheet piles, gabions, and crown walls—to enhance the resilience of coastal infrastructure against earthquake and Tsunami hazards, offering practical design insights for breakwater construction in disaster-prone regions.

TABLE OF CONTENTS

1. GENERAL

Breakwater is constructed to protect ports and harbours from the destructive effects of sea waves, currents and even tsunamis. The most common type of breakwater is rubble mound breakwater (RM breakwater). Armour, filter, and core layers are the main parts of RM breakwaters. In the armour layer, natural rocks or concrete blocks are employed as the building units. Breakwaters made of rubble mounds may exposed to environmental loadings, other than sea waves, such as earthquakes and tsunamis during their design life (Akarsh and Chaudhary 2024a). It was observed during the past tsunamis that breakwaters are vulnerable to tsunamis. For example, the 2004 Indian Ocean tsunami and the 2011 Great East Japan Earthquake and tsunami caused numerous damages to many breakwaters in Japan, India and other countries. Several breakwaters were damaged and even collapsed due to the earthquake and tsunami. Due to the breakwater's failure, the tsunami waves could not block by the breakwaters. Thus, the tsunami entered the port areas and led to catastrophic losses for the structures and lives. Therefore, the safety of the breakwater is crucial for safeguarding the buildings and people living near the port and harbour during such a severe calamity brought by tsunamis. It was discovered that most of the breakwaters collapsed due to geotechnical reasons (i.e. due to foundation failures). Unfortunately, very limited study has been done in the field. The available studies are almost restricted to composite breakwaters which are common breakwaters in Japan. Perhaps no countermeasure is available to make RM breakwater tsunami-resistant. Most of the breakwaters in India are RM Breakwaters. Therefore, the primary goal of this research is to develop novel techniques for RM breakwater in order to make it resilient against tsunami-induced damage. A resilient breakwater can prevent tsunami waves from entering the port or harbour, or at least it can reduce the damage that a tsunami does to port structures by cutting (reducing) the height of the tsunami waves. Thus, a resilient breakwater can protect the structures and people at the port from the devastating damage caused by a tsunami. The countermeasures for RM breakwater are developed using gabions, crown walls, and sheet piles. Since an earthquake generally precedes a tsunami, therefore countermeasures should be effective against both the earthquake (that precedes the tsunami) and tsunami. Several physical model tests would be conducted in the lab for a scaled model of the breakwater at New Mangalore Port. The main purpose of the tests is to understand the reasons and mechanisms of failure of the breakwater during an earthquake and tsunami. To this end, a series of shaking table tests and hydraulic model tests are done for the conventional breakwater model to provide earthquake loadings and tsunami overflow tests. Later, the novel technique was developed by

adding several countermeasure elements to the existing breakwater in order to develop a reinforced and tsunami-resilient breakwater. To evaluate the effectiveness of the novel technique, several physical model tests was be conducted, and the response of the breakwater are compared with those of conventional breakwater. Numerical analyses were also performed to make clear the mechanism.

2. BACKGROUND AND SIGNIFICANCE OF THE PROJECT

By reflecting and absorbing the wave energies of sea waves, breakwaters play an important role for safeguard of ports and harbours from their damaging consequences. However, it has been observed in past few decades that numerous breakwaters suffered damage from the past earthquakes and the ensuing tsunamis. For example, the 2004 Indian Ocean tsunami and the 2011 Great East Japan Earthquake and Tsunami caused several breakwaters to fail. The 2011 Great East Japan Earthquake and Tsunami destroyed several breakwaters in Japan, including the world's deepest breakwater at Kamaishi Port in Iwate Prefecture, Japan (Chaudhary et al. 2018a, 2018b, 2019). The tsunami waves entered the coastal areas due to the breakwater failure. The failure of the breakwater foundation was the key factor in the collapse of the breakwater . Due to such foundation failures, a number of breakwaters were damaged during the earthquakes and tsunamis. The tsunami penetrated the coastal districts and wreaked severe havoc there because the breakwaters were damaged and could not block the tsunami waves in the sea. In order to protect coastal areas from tsunami-induced destruction, it is vitally necessary to develop countermeasures to construct earthquake- and tsunami-resilient breakwater. Generally, tsunamis strike shortly after an earthquake. The effectiveness of a breakwater during a tsunami is significantly affected by the earthquake that precedes it. An earthquake increases the pore water pressure in the seabed soils, resulting in deformations in the seabed soils due to reduced bearing capacity. Breakwaters are also subjected to hydrodynamic and seismic inertia forces during an earthquake. These variables lead to a reduction in the shear strength of the foundation, which, at the end of the earthquake, results in settlement and lateral displacement of the breakwater. The effective height of the breakwater (above seawater level) lowers as a result of the excessive seismic subsidence. This reduction in height results in unfettered access for the tsunami into the coastal areas by overflowing the breakwater. In addition, the countermeasures must be effective to block the tsunami against tsunami Therefore, countermeasures should be devised to make the breakwater resilient such that they can protect a breakwater against both earthquakes and tsunami-induced damage.

2.1.Types of Breakwaters

Broadly, there are two types of breakwaters:

(i) Fixed type and

(ii) Floating type.

While floating breakwaters are created to float in the seawater, however, fixed breakwaters are constructed to rest on the seabed.

Based on the material used in the construction of the breakwater, the breakwaters are of three types:

(i) Rubble Mound Breakwater

(ii) Vertical Breakwater

(iii) Composite Breakwater

(i) Rubble Mound (RM) Breakwater

It is the simplest type of breakwater which is constructed by dumping of rubbles and stones into the seabed till the heap or mound emerges out of seawater. The core of a rubble mound breakwater is generally constructed with a core of quarry-run stone. The core is protected from wave action by rocks under layers, and an outer layer is composed of massive rocks or specially shaped concrete armour units. The breakwater is supported on a prepared foundation on the seabed. The rubble mound breakwater is shown in Figure 2.1(a). The advantages of this type of breakwater are that it is easy to construct and requires less technical support. Example-Bay mouth breakwater at Cherbourg Port, France. Due to ease of construction and economic cost, RM breakwaters are widely used around the world. Furthermore, most of the breakwaters in India are RM breakwaters. The advantages of RM breakwater construction over alternative techniques are primarily related to its low cost and simplicity. These breakwaters are relatively simpler to maintain and repair. The present study deals with the RM breakwater. The present project deals with the RM Breakwater.

(ii) Vertical Breakwater

The original concept of the vertical breakwater was to reflect sea waves, while that of the rubble mound breakwater was to break them. As shown in Figure 2.1(b), a vertical breakwater is a vertically faced structure extending directly over the seabed level (or a thin layer of rocks) to resist wave attack. It is usually reinforced concrete caissons pre-fabricated in a dry dock, then transported to the site and sunk into the seabed foundation. The inside chambers of the caisson

are filled with earth or rock to increase its mass. The advantage of this type is the minimum use of natural rock and less space requirement. Example-Mutsu-Ogawara breakwater, Japan.

(iii) Composite Breakwater

A composite breakwater is a combined structure consisting of a vertical structure placed on a rubble mound that is submerged at all tidal levels. This type of structure may be used in very deep-sea water where the volume of rock required for a rubble mound structure can be reduced, or when it is not practicable to design a vertical face structure to carry the design wave loading to the full depth. Figure 2.1(c) shows a composite breakwater. Example- Algeciras breakwater, Spain. The composite breakwaters are widely used worldwide due to their advantages over the former viz., less base width, economical use of the available materials, reduced environmental impact at construction and especially its suitability to deeper sea waters. By using caissons as the vertical wall, composite breakwaters provide an extremely stable structure even in rough, deep seas. Such strength has led to their use throughout the world. It should be noted that the world's deepest breakwater (breakwater at Kamaishi port, Japan) belongs to this category.

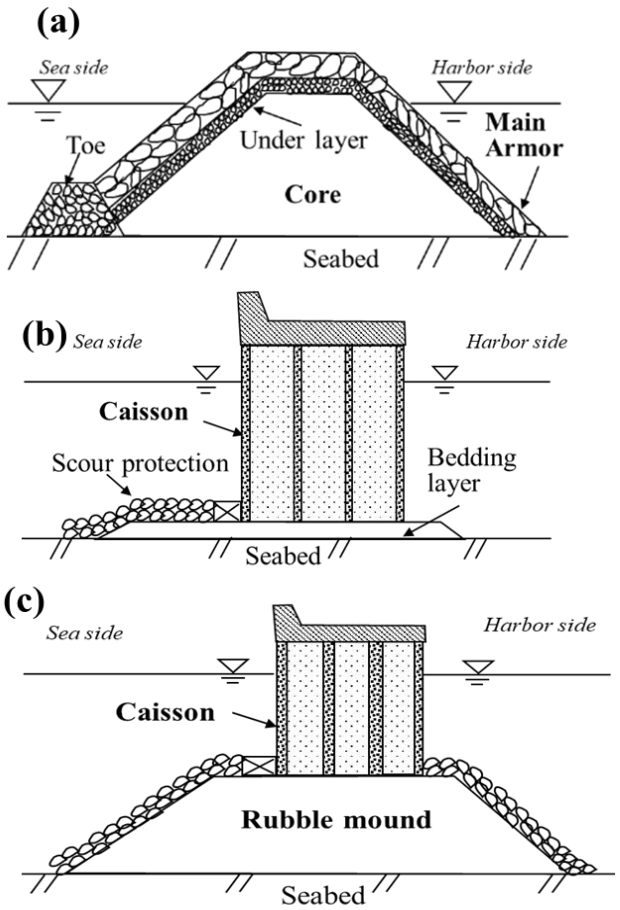

Fig. 2.1 Types of breakwaters (a) RM breakwater (b) Vertical breakwater (c) Composite breakwater

There are some special breakwaters, such as Curtain wall breakwaters, Steel pile breakwaters, Horizontal plate breakwaters, Floating breakwaters, Pneumatic breakwaters, Hydraulic breakwaters, etc.

2.2 Rubble Mound Breakwater

A rubble mound is a flexible heterogeneous assemblage structure of natural rubble consisting of quarried rocks in the core and natural or artificial armour as a protection cover. The word rubble means riprap and rock armour. It is generally trapezoidal in shape with flatter slopes on the seaside and steeper slopes on the harbour side with slopes 1:1.33 to 1:2. In any plan, rubble mound breakwaters consist of two sections, trunk and head sections. The head section is flatter than the trunk section, with slopes 1:3 to 1:5. Generally, the rubble mound consists of protective armour units, a crest provided with the concrete crown wall, one or two layers made up of granular material, berms, and a wide graded core as superstructure and Toe and bedding layer as foundation structures. The typical cross-section of the RM breakwater is shown in Figure 2.2.

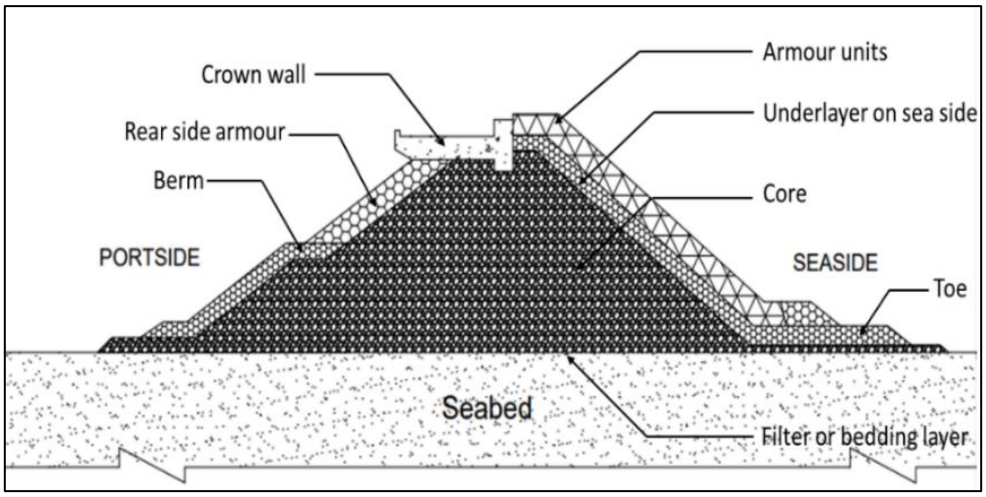

Fig. 2.2 Components of RM breakwater

The filter layer is a bottom layer provided above the sea bed as the surface preparation layer to avoid settlement and washing out / migration of finer core materials. The stones used in the filter may be 1–50 kg and size not less than 100 mm.

(a) Core

The core is the central and inner most part of RM breakwater consists variable sizes of quarry rocks, so that wave transmission is prevented and sediments shall not pass through the voids of the structure. The permeability of the core is lesser than the outer layers

because of wide graded stones. The weight of the individual stones varied from 50kg to 125 kg.

(b) Armour Units

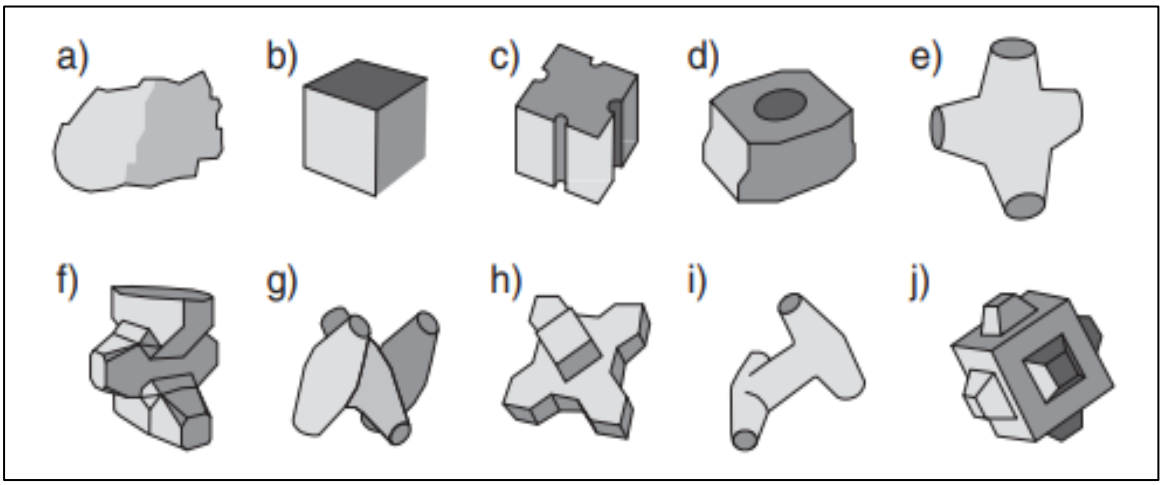

Fig. 2.3 Concrete armour units: (a) Rock, (b) Cube, (c) Antifer, (d) Haro, (e) Tetrapod, (f) Accropode, (g) Core-loc, (h) X-bloc, (i) Dolos and (j) Cubipod

Table 2.1 Armor type, shape, and it is contribution (after Akarsh and Chaudhary, 2024a)

Placement pattern	**Number of layers**	**Shape**	**Main contribution**		
			Self-weight	**Interlocking**	**Friction**
Random	Double layer	Simple	Cube, Modified cube, Antifer	-	-
			Tetrapod, tripod		-
		Complex	-	Dolos	-
	Single layer	Simple	Cube		Cube
		Complex	-	Accropode, Core-Loc, X-bloc	-
Uniform	Single layer	Simple	Haro	-	Seebee, Haro
		Complex	-	-	Cob, Tribar, diode

Armor units are used in the outer layers of RM breakwaters to protect the core from direct wave attack by dissipating the wave energy. To control the damage or failure of rubble mound from the wave action, the interlocking packing of armour units is very important. Up to 5 m water depth, natural stones are beneficial as they are cheaper, but above 5 m

water depth, the artificial concrete armour units are more advantageous in dissipating the wave energy. The stability of mound components mainly depends on the stability of the armour units placed on the seaside. Hence, armour should have sufficient weight. The armour's weight can be found in Iribarren, Hudson's, and Van der Meer's empirical formulas. The weight of the armour unit (W) depends on the significant wave height, and the weight of the other layers depends on the W. The thickness of the armour shall be a minimum of 300–500 mm. If the porosity is less, the waves will be reflected. So, it is adjusted between 35% and 55%. Different artificial concrete armour units like tetrapod (France, 1950), dolos (South Africa, 1963), accropode (France, 1980), core-loc (USA, 1996), cubipod (Spain, 2006), etc., can be used (ref. Figure 2.3) based on their application shown Table 2.1.

(c) Underlayers

The underlayers are made of granular material, which provides stability to outer armour layers and prevents the migration of core material through voids of armour units. The underlayers may be laid in one or more layers and increases the wave dissipation capacity of breakwaters. The underlayer is designed with a rule that the D15 of armour is less than five times the D85 of the layer.

(d) Toe

Toe is one of the important structures of breakwater, which provides scour protection, structural stability against the slip or circular failure, resistance against the armour sliding and prevents undermining. If toe protection is not used, the armour layer should extend below the maximum scouring depth and the slope is adjusted to have minimum scour. In deep waters and sandy conditions, the smaller size of the rocks could be used to support the armour. Sometimes, gabions are used to minimize the scouring depth.

(e) Berms

Berms are generally provided to increase the stability of armour units against wave energy dissipation and to use smaller gradation stones.

(f) Crest Height, Crest Width and Crown Wall

The crest elevation depends on the high-water level criteria, wave transmission, and return period and width depends on the allowable overtopping and construction requirement. The crest width and crest elevation are properly fixed, so that the overtopping and wave run-up shall not cause any damage on the harbour side. The crest width shall be a minimum

width of three to four armour stones. A crown wall of minimum of 2– 4 m is provided on the crest if pedestrians or vehicles need an access. The provision of crown wall reduces the amount of armour units, gives access for repair and maintenance, and supports for berthing.

Rubble mound dissipates the wave energy mostly by absorbing (about 60-70%) and partly by reflecting (about 30-40%) in contrast with other types. Armour units at the outer layer absorb most of the energy, and inner under-layers prevent transmission of the wave energy. The wave energy generated will be dissipated through the voids of these breakwaters, and there might be a wave runup caused by partial reflection. In India, rubble mound breakwaters are commonly used due to their easier construction, the requirement of smaller construction equipment, the availability of materials, and it is maintenance. These are economical if the depth of water is shallow and costly in deep waters due to the requirement of construction materials. The main advantage of the rubble mound is that failure is not sudden and can be repaired by adding stones to the flushed-out part.

2.3 Common Failure Modes of RM Breakwater

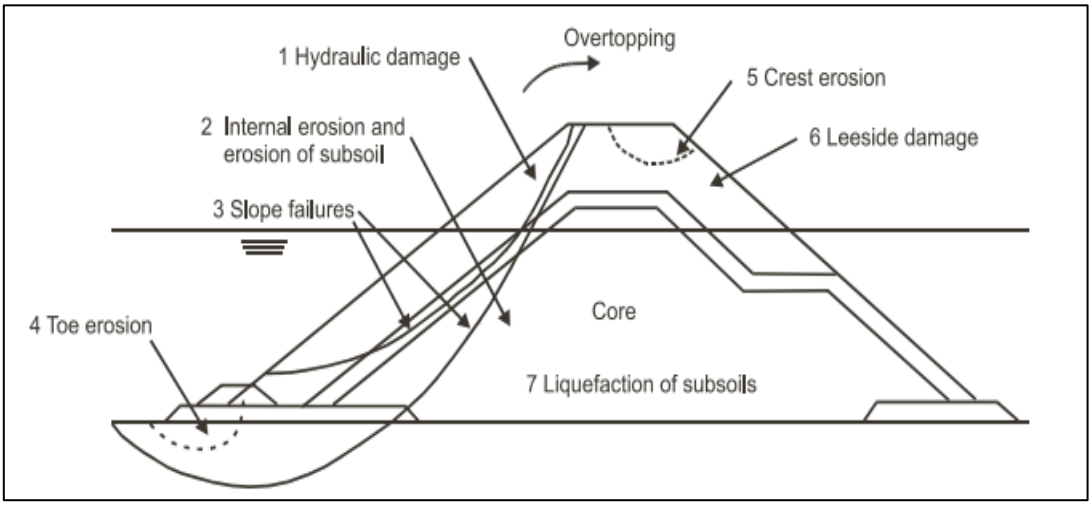

Fig. 2.4 Failure pattern of RM breakwater (CIRIA-C683, 2007)

RM breakwaters are subjected to harsh environmental circumstances such as repetitive wave loadings, hydrodynamic pressures, seismic and tsunami loadings. Depending on the intensity, frequency, and duration of the loadings, the responses of the RM breakwater to these circumstances would differ. According to CIRIA C683 (2007), the RM breakwater may either fail by wave actions or geotechnical instability as shown in Figure 2.4. The possibility of damage at the round head portion will be higher than the longer trunk of the breakwater.

Uncertain/ Repetitive Wave Actions: Hydraulic damages, toe erosion, severe overtopping, internal erosions, which ultimately leads to crest side erosion, seepage and leeside damages of breakwater. Hydraulic head-induced erosion of fine particles in case of improper filter functioning results in slope failure and settlement.

Geotechnical Risks:

- Deformation of seabed ground due to bearing capacity failure of the ground.
- Excessive total or differential settlement.
- Instability of rock armour slopes.
- Slope failure due to scoured portion and adjacent structures.
- Heaving, piping, and internal erosion.
- Loss of equilibrium of the ground due to uplift water pressure.
- Earthquake-induced settlement, horizontal displacement, and liquefaction of subsoil.

2.4 Earthquake

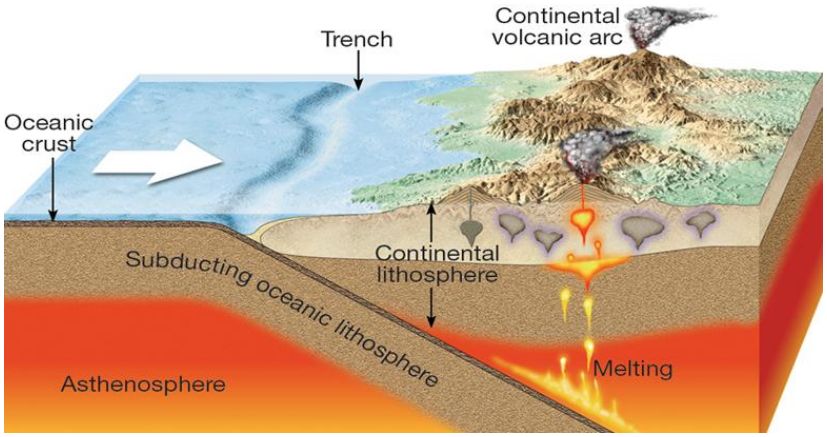

Fig. 2.5 Generation of an earthquake

An earthquake is the perceptible shaking of the earth's surface, resulting from the sudden release of energy in the earth's crust that creates seismic waves. Earthquakes are caused mostly by the rupture of geological faults but also by other events such as volcanic activities, nuclear tests, mine blasts, landslides, etc. An earthquake's point of initial rupture is called its focus or hypocentre. The epicentre is the point on the ground level directly above the hypocentre. Figure 2.5 shows the generation of an earthquake. An area's seismicity or seismic activity indicates the frequency, type and size of earthquakes experienced over time. Earthquake is measured by seismometer. The moment magnitude scale is the most common scale on which earthquakes larger than approximately 5 are generally reported for the entire globe. When the epicenter of

a large earthquake is located in offshore areas, the seabed may be displaced sufficiently to cause a tsunami. Earthquakes can also trigger landslides and occasionally volcanic activities.

Main reasons for an earthquake:

(i) Volcanic activities

(ii) Movement of tectonic plates

(iii) Man-made explosions

(i) Volcanic activities: Volcanic explosions are one of the most common causes of earthquakes in the neighbourhood of active volcanoes. Such earthquakes are known as volcanic earthquakes. This type of earthquake is caused either by the influence of the increasing pressure of volcanic gases or the subterranean movement of molten lava trying to come up on the earth's surface. They may occur before the volcanoes actually erupt on earth surface, which is due to the intrusion of dikes and other movement of lava. A great and violent earthquake may be caused in the region of the volcanoes when the final eruption occurs. However, such earthquakes of volcanic origin are generally less violent and more limited in extent than tectonic earthquakes.

(ii) Movement of tectonic plates: Tectonic earthquakes are triggered when the crust becomes subjected to strain, and eventually moves. Plate tectonic movements cause the majority of the earthquakes. The surface of the earth consists of 15 plates comprising the rigid upper mantle, and the oceanic and continental crust. There are six major plates and nine minor plates. When these plates (rocks) break or slide past each other at boundaries known as fault lines, they release shock waves. The shock waves are the result of the energy stored in the earth's crust due to the underground pressure of the earth’s inner core. Where two plates meet, it forms a plate boundary. There are three types of plate boundaries: Conservative, Constructive, and Destructive plate boundaries. Due to certain characteristics of the constructive plate boundaries, only moderate earthquakes are associated with them. It is the reason that only shallow focus earthquakes occur along the mid-oceanic ridges, the depth of their focus varying from 25 to 35 km. At the destructive plate boundaries, the most disastrous and deep focus earthquakes are caused. The Ring of Fire surrounding the Pacific basin represents the subduction edge of the Pacific plate thrusting deep into the crust and upper mantle. Due to plate collision and subduction of one plate beneath another a lot of molten lava comes up towards the earth. It is the main cause of the presence of active volcanoes along the Pacific Rim.

(iii) Man-made explosions: Seismic waves (shock waves) similar to the ones causing earthquakes can be generated by underground explosions. These explosions can be as a result of underground mining or during the construction of railroads, subways, or underground tunnels. However, some of the seismic waves produced by these activities are not as strong as those produced by real earthquakes. Underground nuclear tests are known to be dangerous and can produce powerful seismic waves similar to that of a natural earthquake.

Earthquakes typically consist of a series of tremors recorded by seismographs. The most significant event in this sequence is referred to as the mainshock. Smaller quakes that occur before the mainshock are termed foreshocks, while those that follow—usually of lesser magnitude—are known as aftershocks. These aftershocks are common in large seismic events, particularly when the fault rupture associated with the mainshock does not release the entirety of the accumulated strain energy (Bolt, 2023). The ground-shaking observed during an earthquake is a result of seismic wave propagation and is characterized in terms of displacement, velocity, and acceleration. This ground motion is captured by accelerometers, which generate accelerograms containing key information such as peak amplitude, duration, frequency content, and energy characteristics of the seismic event (Murthy, 2002).

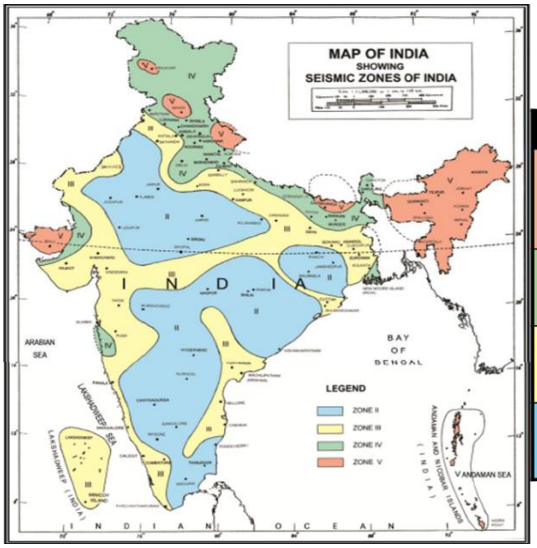

Zone	Magnitude
Zone V	Very High Risk Quakes of Magnitude ***8*** and greater
Zone IV	High Risk Quakes upto Magnitude ***7.9***
Zone III	Moderate Risk Quakes upto Magnitude ***6.9***
Zone II	Seismic Disturbances upto Magnitude ***4.9***

Fig. 2.6 Seismic zonal mapping of India (Source: IS:1893(1)-2016)

In the Indian context, the Ministry of Science & Technology and Earth Sciences has reported that approximately 59% of India's land area, encompassing all states, is prone to earthquakes of varying intensities. Based on historical seismicity and hazard assessment, the Indian seismic zoning map (IS 1893 (Part 1): 2016) divides the country into four seismic zones: Zone II, Zone

III, Zone IV, and Zone V (refer to Figure 2.6). These zones represent increasing levels of seismic risk, with peak ground acceleration (PGA) ranging from 0.10g in Zone II to greater than 0.36g in Zone V, considering a 10% probability of exceedance in 50 years.

2.5 Effects of Earthquake on Breakwaters

The coastal structures like RM breakwaters built on sea bed are vulnerable to other forces like earthquake and tsunamis apart from wave forces. Many breakwaters collapsed during the past earthquakes in Los Angeles (USA) in 1994, Kobe (Japan) in 1995, Kocaeli (Turkey) in 1999, Athens (Greece) in 1999, Sumatra (Indonesia) in 2004, and Tohoku (Japan) in 2011 and some are listed in Table 2. During these earthquakes, the breakwater lost its stability and allowed the tsunami water to overtop it. Hence, to protect the coastal areas from tsunamis, the seismic stability of breakwater is of utmost importance to avoid such devastating effects. Table 2.2 Breakwaters damaged during the past earthquake

Table 2.2 Breakwaters damaged during the past earthquake

Earthquake	Breakwater damaged	Description	Reference
The Great East Japan Earthquake and Tsunami (2011), $M_{w=}$ 9.0	Breakwaters at Miyako port, Ishinomaki port, Souma, Sendai-Shiogama, Hachinohe Port	Breakwaters were subjected to seismic motions and subsequent tsunami. The impact forces of tsunami pushed away the caissons and rubble mound scoured off. Due to the stability loss in foundation soils, the effective height of breakwater decreased and allowed tsunami water to enter coastal areas.	Kazama and Noda (2012); Suppasri et al. (2013); Bricker et al. (2015); Suganoa et al. (2014)
Chile Earthquake (2010), $M_{w=}$ 8.8	Breakwaters at Port of Valparaiso and Port of San Antonio	Lateral spreading and settlement of outer armor units of breakwater.	Edge et al. (2011)
Kocaeli Earthquake, Turkey (1999), Mw= 7.4	Breakwaters at Ergil Fishery Port, Izmit bay	The liquefaction of silty sand layer below the breakwater mound caused settlement breakwater of about 1.5 m along it is axis, flattening on cross-sections, and intrusion of lower rubbles into the sandy layer on sea side.	Gunbak et al. (2000); Yuksel et al. (2004); Sumer et al. (2007)
	Breakwaters at Esenkoy fishing harbour	Minor damage (Cracks along the crown wall)	

	Breakwaters at Cinarcik fishing harbour	The crown wall was cracked for about 30cm near backfill and concrete slabs were detached by sinking and swelling action.	
Kobe Earthquake (1995), M_w= 6.9	Breakwaters at Kobe Port	The loose saturated sandy soils be neath the breakwater liquefied exte nsively, there was subsidence of gr ound and vertical settlement of 20-30cm. There was large re-compression of soil after liquefaction.	Iai and Sugano (1999)
Patras Gulf Earthquake (1984), M_w= 4.5	Southern extensions of breakwater, Patras port of Greece	RM breakwaters was led on soft soils and the foundation was observed to be settle 3m to 4m post-earthquake, eventually failed.	Memos and Protonotarios (1992); Memos et al. (2001)
Alaska Earthquake (1964), M_w= 9.4	Breakwaters at Kodiak city and Seldovia	Minor damages of breakwaters obs erved due to earthquake at Kodiak city. Breakwaters were subsidedby 1.1m at Seldovia city.	Wilson and Torum(1972); Wang et al. (1978)

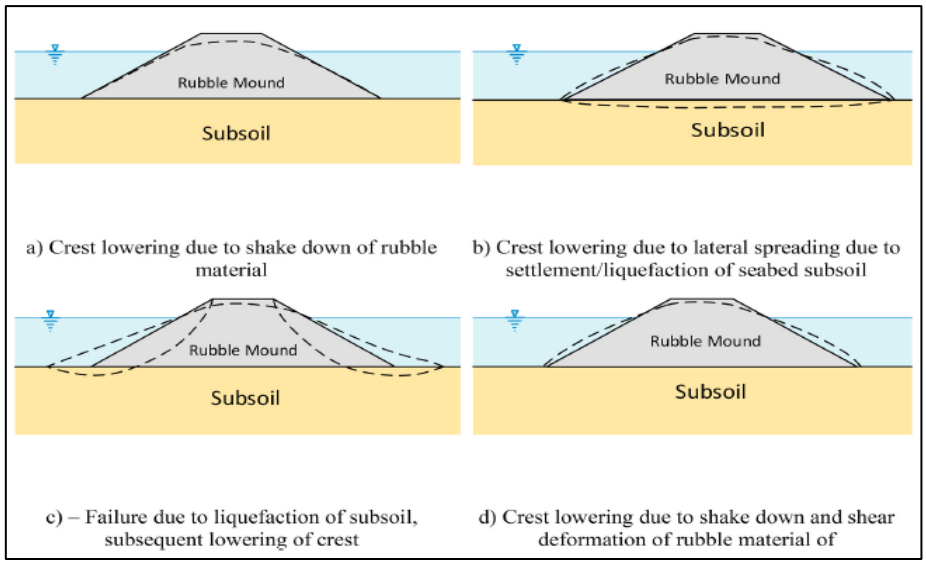

Fig. 2.7 Deformation of RM breakwater under the impact of an earthquake (PIANC, 2001)

Permanent International Association of Navigational Congresses (PIANC 2001) has given a brief discussion about RM breakwater behaviour during a seismic activity and details of that, is represented in Figure 2.7. The settlement of the crest will be evident in all the shown modes of failure. Under cyclic loading conditions, the seabed is prone to liquefaction. The liquified

zones are generally concentrated below the mound and toe regions under the earthquake loadings. The liquefaction process can trigger instant settlement of the structure above the seabed. Since breakwaters run in longer lengths, differential settlements are likely to occur. The key factors contributing to the RM breakwater's damage during the earthquakes were observed to be

- Increase in pore water pressure during the ground shaking,
- Deformations in the body of the breakwater, and
- Deformation of the seabed soils.

2.6 Tsunamis and their effects on breakwaters

Tsunami is a series of very long gravity waves generated by any rapid large-scale disturbance of the seawater generally due to underwater earthquake. Other causes may be volcanic eruptions, landslides, undersea landslides, underwater explosions and meteor impacts. All these can trigger a series of fast moving, long waves of initial low amplitude that radiate outward in a manner resembling the waves radiating when a pebble is dropped in a lake. Tsunami waves in deep oceans typically have heights of less than half a meter but can travel at a speed of more than 500 km per hour. When tsunami waves travel into shallow water, shoaling effects may result large waves and tremendous breaking activities near the shore, causing significant damage to coastal structures and human lives. Tsunami generation due to geological fault is shown in Figure 2.8.

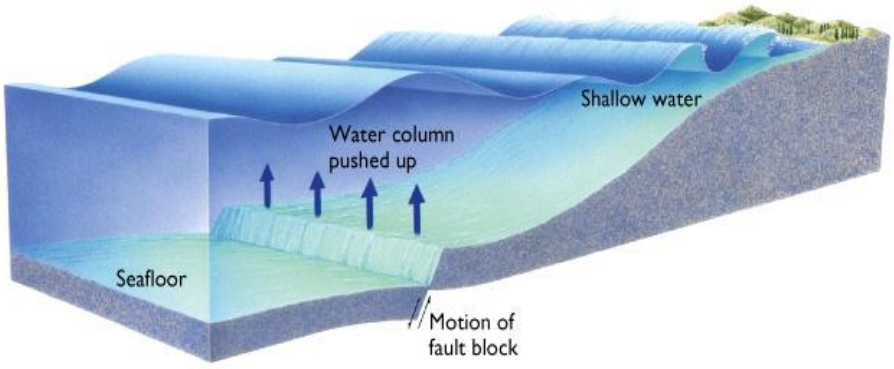

Fig. 2.8 Generation of tsunami waves due to geological fault

From the past experiences, it has been observed that most of the tsunamis are triggered by earthquakes. For example, Chile earthquake (1960), Alaska earthquake (1964), Indian Ocean earthquake (2004) and 2011 off the Pacific coast of Tohoku earthquake (2011) triggered tsunamis in the past. Strong earthquakes resulting in deformation of larger area led to severe tsunamis than smaller earthquakes. Generally, earthquakes having focus deeper than 30 km rarely cause tsunamis. But sometimes, certain earthquakes like Chile (1960) and Indonesia

(2004), which had a focal depth of more than 30 km, also triggered tsunamis. Tsunami possesses a lot of energy, moves at high speed and can travel greater distances. For example, in a typical ocean having a depth of 4 km, the travel speed of a tsunami is nearly equal to 700 km per hour. However, after entering shallow water (less than a depth of 30 m) the tsunami waves travel at a speed of only 60 km per hour. The speed of tsunami waves further diminishes as they move to shallower coastal water with an increase in height. Such rise in the height of tsunami waves to several meters near sea coast is due to the shoaling effect. As a result, when the tsunami reaches the coast, it may develop into a rapidly rising or falling tide i.e., a series of breaking waves. So, while designing the coastal structures, attention should be given to tsunami loading and earthquake loading in earthquake-prone zones.

Earthquakes and tsunamis are natural disasters that cause huge loss of property in terms of lives and the economy. Coastal structures are vulnerable to earthquakes and tsunamis. Many coastal structures such as breakwaters, seawalls, river dikes, groins, and jetties failed due to the past gigantic earthquakes such as the 2004 Indian Ocean Earthquake and 2011 Great East Japan Earthquake and subsequent tsunamis (Table 2.3).

Table 2.3 Breakwater's damage during the past tsunamis.

Location	Type of breakwater	Damages
The 2004 Indian Ocean Earthquake and Tsunami		
Hikkaduwa Port, Srilanka	RM Breakwater	▪ 1.2m high tsunami overflow occurred over the breakwater. ▪ 6 to 8 ton weighed armour units were displaced.
Mirissa Port, Srilanka	RM Breakwater	▪ 1.5 m high tsunami overflow occurred over the breakwater. ▪ Armour blocks in the crest and harbour side were scoured.
Puranawella Port, Srilanka	RM Breakwater	▪ Tsunami overflowed 2.5 m height above the breakwater. ▪ Primary armour blocks were scoured at several locations.
Chennai Port, India	RM Breakwater	▪ Tetrapod armour blocks were displaced. ▪ A part of the breakwater was tilted eastward about 20 degrees
Cuddalore Port, India	RM Breakwater	▪ The rubble mound was damaged severely.
Kayamkulam Inlet, India	RM Breakwater	▪ The northern side of the breakwater was eroded.
Ennore Port, India	RM Breakwater	▪ The North breakwater was displaced 1 to 2 meters with the direction of the southeast.

The 2011 Great East Japan Earthquake and Tsunami		
Kamaishi port, Japan	Composite Breakwater	▪ Designed as a tsunami-resistant breakwater for lesser peak impact height. Caissons were displaced and the rubble scoured.
Ofunato port, Japan	Composite Breakwater	▪ Designed as a tsunami-resilient breakwater for lesser impact height. Caissons were displaced even before the peak tsunami wave.
Noda port, Japan	Composite Breakwater	▪ Tsunami waves overtopped the breakwater by 12.24 m. ▪ Caissons and 3-ton armour units were displaced.
Miyako Port, Japan	Composite Breakwater	▪ Mound scoured and caisson Slid by the tsunami waves
Souma Port, Japan	Composite Breakwater	▪ Mound scoured and caisson Slid by the tsunami waves
Hachinohe Port, Japan	Composite Breakwater	▪ Mound scoured and caisson Slid by the tsunami waves
Ishinomaki Port, Japan	Composite Breakwater	▪ Mound scoured and caisson Slid by the tsunami waves
Taro Port, Japan	RM Breakwater	▪ Tsunami waves overtopped the breakwater by 16 m. ▪ The rubble mound collapsed.

(i) Damage of Coastal Structures Due to the 2004 Indian Ocean Earthquake and Tsunami

The 2004 Indian Ocean Earthquake (9.1-9.3 M_w) occurred on 26 December 2004, with the epicenter off the west coast of Sumatra in Indonesia. The undersea mega-earthquake occurred due to the subduction of the Indian Plate by the Burma Plate, which triggered a series of devastating tsunami waves. The maximum tsunami height of approximately 50 m was measured in the Banda Aceh region of Indonesia (Suppasri et al., 2012). It was one of the deadliest natural disasters in recorded history. Indonesia was the hardest hit country, by the tsunami followed by Sri Lanka, India, and Thailand. The tsunami, accompanied by the earthquake, propagated in the entire Indian Ocean and caused extensive damage. The reported number of casualties is approximately 300,000 (230,000 killed in Indonesia, more than 29,000 deaths in Sri Lanka, more than 10,000 in India, more than 5,000 in Thailand, and 82 deaths in the Maldives by the tsunamis) and more than 22,000 are still missing. Large numbers of buildings, river dikes, road embankments, and railway lines were damaged severely. Several coastal structures were reported to have failed across fourteen affected countries (Nakano, 2008 and Suppasri et al., 2012).

In India, the Andaman and Nicobar Islands, the coastal areas of Tamil Nadu, Andhra Pradesh, and Kerala were severely affected, and many structures were damaged (Patnaik et al., 2012 and Narayan et al., 2005). The breakwater at Rangat Bay Harbor in Middle Andaman (India) was reportedly damaged by the earthquake and tsunami (Mondal and Rai, 2008). The tsunami arrived in Andhra Pradesh and Tamil Nadu along the southeast coast of the Indian shortly after 9:00 a.m. At least two hours later, it arrived in the state of Kerala along the southwest coast. Tamil Nadu, Pondicherry, and Kerala were extensively damaged, while Andhra Pradesh sustained moderate damage. The presence of seawalls on the Kerala coast and some of the Tamil Nadu coast helped to reduce the impact of the waves. However, when the seawalls were made of loose stones, the stones were displaced and carried a few meters inland. The state of Kerala experienced tsunami-related damage in three southern districts, Ernakulam, Alappuzha, and Kollam, which are densely populated by villagers. The tsunami struck the Kerala coast due to the diffraction of the waves around Sri Lanka. The worst affected area in Tamil Nadu was Nagapattinam district, with a reported 6,051 fatalities caused by a 5 m (16.4 ft) tsunami, followed by Cuddalore district, with many villages destroyed. At the same time, many villages from many districts in the state of Andhra Pradesh were destroyed. In the Krishna district, the tsunami created havoc in Manginapudi and on Machalipattanam Beach, which came like a running wall of water. The most affected was Prakasham District. The tsunami arrived in the Andaman and Nicobar Islands minutes after the earthquake, and it caused extensive devastation to the islands' environment. Specifically, the Andaman Islands were moderately affected, while the island of Little Andaman and the Nicobar Islands were severely affected by the tsunami.

(ii) Damage of Coastal Structures due to the 2011 Great East Japan Earthquake and Tsunami

The 2011 Great East Japan Earthquake hit the coast of Japan on 11 March 2011. The epicentre was approximately 70 km East of Tohoku, and the hypocentre was at an underwater depth of approximately 30 km. It was the most powerful earthquake (9.0 M_w) ever recorded to hit Japan and the 4th most powerful earthquake in the world since modern record-keeping started in 1900. The main shock was preceded by a number of large foreshocks, with several aftershocks. One of the major foreshocks was a 7.2 M_w. Following the main earthquake on 11 March, a 7.9 M_w aftershock was recorded. The earthquake triggered powerful tsunami waves that reached heights of up to 40.5 meters in Miyako area (Iwate Prefecture), and travelled up to 10 km inland (Sendai). The tsunami attacked the

whole Pacific coasts of Japan from Hokkaido to Chiba Prefecture (Takahashi et al., 2011). A large number of buildings, river dikes, road embankments, railway foundations, coastal dikes, ports, and airports were damaged across the affected area due to compound disaster caused by the earthquake and tsunami which led to catastrophic losses for population and structures near coastlines (Hazarika et al., 2012 and 2013; Hara et al., 2012; Takahashi et al., 2011; Sugano et al., 2014 and Kazama and Noda, 2012). More than 15000 deaths were reported (NILIM, 2013).

Seismic subsidence, liquefaction, and landslides were also observed at many locations. Along the coast of Iwate, Miyagi, and Fukushima prefectures, there were 300 km of coastal levees; out of this, 190 km of levees were fully or half destroyed. The river dikes and their related structures were damaged at 2115 sites throughout the Tohoku and Kanto areas, including Iwate, Miyagi, Fukushima, Ibaraki, and Saitama Prefectures, as well as the Tokyo Metropolitan District (Oka et al., 2012). Levees in the coastal area were damaged mainly due to the combined effects of the tsunami and the seismic subsidence of the earth's crust (Sasaki et al., 2012). Fifteen ports were located in the disaster zone, and the breakwaters at almost all the ports (in the affected areas) were severely damaged (Mori, NILIM, 2013). The effects of the tsunami on the ports in the northern Tohoku region were large. However, the effects of the earthquake were large on the south of Ishinomaki and Sendai Shiogama Ports (Kazama and Noda, 2012). At some breakwater mouths, the scouring depth was more than 10 m (Takahashi et al., 2011). The geotechnical or foundation damage was the main reason for the failure of the breakwaters.

These breakwaters were damaged mainly due to the failure of their mounds. It was reported (MLIT, 2011 & 2013; Arikawa et. al, 2012 & 2013; Sugano et al., 2014 and Chaudhary et al. 2017) that the main reasons for the failure of these breakwaters include (i) High water pressure imposed on the breakwater by tsunami waves, (ii) Decrease in bearing capacity due to increasing in pore water pressure and seepage in the foundation ground and (iii) Scouring of the mound, toe erosion and joint failure by the tsunami waves. However, Japan has had many experiences of disasters caused by tsunamis (e.g., the 1896 Meiji Sanriku tsunami, the 1983 Nihon-kai Chubu earthquake tsunami, and the 1993 Hokkaido Nansei-oki earthquake tsunami). Still, the 2011 tsunami was more devastating (higher level tsunami) than the previous tsunami. This is the reason that some tsunami breakwaters also failed, and devastation occurred on such a large scale.

3. LITERATURE REVIEW

3.1. General

There hasn't been much research done on the effects of tsunamis on RM breakwaters and the development of countermeasures. Despite being a sizeably large construction and an important part of many coastlines, study on RM breakwaters (subjected to tsunami) has only lately started to garner interest from scientists, particularly in the wake of the 2004 Indian Ocean tsunami. Little attention has been paid around the world in the past to developing a tsunami-resistant breakwater. This research area became popular among researchers, especially after the tsunami caused by the 2011 Great East Japan Earthquake and tsunami. Very few researchers have developed countermeasures for breakwater against tsunami. But, almost all of them are limited to composite breakwaters. Perhaps, no research work has been done related to development of countermeasures for RM breakwater against earthquake and subsequent tsunami. It seems, no codal provision is available to mitigate such damage of a RM breakwater. Since, Japan is one of the most affected countries by the tsunamis, therefore most of the research in this area have been done or are ongoing in Japan. Furthermore, most of the breakwaters in Japan are composite breakwaters. It is the main reason that most of the available research works are limited to composite breakwaters.

Very limited research has been done for RM breakwater for development of countermeasures against earthquake and tsunami. The available research works are limited to either (i) field investigation for damage of RM breakwaters during past tsunamis or (ii) stability evaluation of RM breakwaters subjected to tsunami. Very few attempts have been made to develop countermeasures for RM breakwater. Most of them are related to either earthquakes or tsunamis. Probably, the effects of the earthquakes and subsequent tsunamis has not yet been considered. Moreover, all the disturbing factors (e.g., seepage, scour, toe erosion, top scour) during tsunami were not considered together in the studies. Some of them don’t even consider seabed soils, which is very important for the stability evaluation of RM breakwater. As seepage through seabed soils during tsunamis, and deformation of seabed soils during an earthquake can have significant impacts on the stability of RM breakwater during an earthquake and subsequent tsunami. This literature review tries to gather significant work that can provide insight into the scenario of an RM subjected to tsunami impact.

3.2. Behaviour of RM Breakwaters Subjected to Earthquakes

Cihan and Yuksel (2011) investigated how RM breakwaters with and without toes changed in response to cyclic loads. The investigation came to the conclusion that toes might significantly reduce the lateral deformations and settlement of RM. The findings brought to light a crucial aspect about the core layer's involvement to lateral and vertical movements. It was observed that the core layer deformed more than the armour layer in both directions. The hydrodynamic pressure that the water exerts during seismic loadings was ignored by the analyses. The study concluded that adding a toe element to a breakwater could minimise deformations caused by cyclic stresses.

Cihan et al., (2012) evaluated the homogenous RM breakwater built entirely of armour material and the second type of model constructed entirely of core material. Shake table tests were conducted in both dry and wet conditions. It was observed that breakwater crown settlement was greater in water than it was in dry settings, and that dry conditions also provided better resistance to deformation under higher seismic accelerations. The experimental findings also showed that the core-only breakwater produced more settlement than the one with armour. The slope stability analysis by Newmark’s method and Bishops method using WINSTABL software has also proved that the critical condition of dry condition reached at 0.37g acceleration and that of wet at 0.19g acceleration. Numerical modelling was done on finite element modelling software PLAXIS to determine the stress and strain distribution in rubble mound. The porosity of the rubble mound in two cases were determined after the experiments. The study highlights that the core material shown higher change in porosity compared to armour layer. It was inferred form the research that the deformations in breakwater increased with higher seismic accelerations. The study thus focused only on the behaviour of the RM breakwater alone and hence a rigid base was used throughout the evaluation.

Ye and Jeng, (2013) conducted significant research on the changes in the porous seabed and the behaviour of an RM breakwater under seismic loadings. This study was focused on the interaction of pore water and soil particles on the seabed subjected seismic motions. While the acceleration of these particles was considered, the relative motion of the soil and porewater was ignored. whereas the acceleration of these particles was considered. During the seismic loadings, the seabed and breakwater could undergo vibratory motion that trigger secondary waves in the water. The authors suggest that these secondary waves have only feeble effects on the structure. In the numerical computation, the seismic input was applied to all the three

directions simultaneously. This approach was different from the usual method of applying seismic acceleration to the seabed and assigning other boundaries as viscous to avoid wave reflection. Since the study had not accounted tsunami wave impact, the hydrodynamic pressure on the breakwater was not considered. Further, the literature pointed out the unavailability of a hydro dynamic model for the combined effect of earthquake and tsunami. The study modelled unsaturated seabed which was justified by field data from previous research those proved that the seabed could have degree saturation less than 100%. From the numerical simulations, it was found out that the seismic wave amplified while passing through the porous seabed and rubble mound. The maximum amplification was observed along the width of the rubble mound where the two sloping faces might have been set to free to vibrate. The response spectrums derived from the numerical simulations highlighted that the dimensions of a breakwater should be selected such that the structure will never have a natural frequency that may match with the frequency of a strong ground motion. It was observed from the study that the response of seabed as well as breakwater sections was maximum in the width wise direction when compared with other two orthogonal directions. The amplification of a seismic wave along the seabed was found to be more towards the surface of seabed. The authors suggest incorporating the relative movement of rubble and water when a seismic wave is transmitted though the water inundating the armour block of a breakwater.

The settlement of the breakwater crest and the liquefaction of the seabed beneath were proposed as the two primary mechanisms of failure of an RM breakwater by Cihan and Yuksel (2013) through experimental and numerical analyses. Since, it was observed that deformations along the length-wise direction were minimal, a one-dimensional shaking was used in the trials. To build the breakwater materials in the requisite density and porosity, a different laying system was developed. Before and after the horizontal shaking, the breakwater's profile was measured using the profile recorders. The study was able to understand how the breakwater behaved in two different tetrapod armour layer placements. The authors' computer studies revealed that it is possible to model breakwater components, including the concrete armour layer, as a soil layer without sacrificing the accuracy of predicting its responses. The compatibility of the numerical simulation results was demonstrated by a comparison between the positions of the distorted areas assessed by numerical simulation in the Finite Element programme, PLAXIS. It was noted, nonetheless, that the measured values from the actual scenario were higher than the outcomes of the numerical simulation. The modelling of armour units as a single layer whereas, in reality, they were discrete particles interlocked against one another, provided

justification for this. The investigation came to the conclusion that the tetrapod armour units had demonstrated superior resistance to seismic loading when stacked in an identical fashion with one leg pointing outward and perpendicular to the slope. With an increase in ground motion acceleration, an increase in crown settling was observed. Since the study was solely concerned with the behaviour of the breakwater, a hard base was assumed.

Zhao et al. (2018) developed the numerical model using integrated FVM-FEM to know the interaction between sea waves, currents, submerged breakwater and sea bed. The authors used VARNAS equation to develop fluid field and Biot's poro-elastic model for porous sea bed. They observed liquefaction and shear failure in upper seabed layers around the breakwater. In addition, Zhao et al. (2020) numerically investigated the dynamic behaviour of breakwater constructed over a loose liquefiable sandy seabed considering responses like EPWP development, plastic strains generation and degradation of soil stiffness due to seawater-breakwater-seabed interactions. They observed the progressive and asymmetric settlement of breakwater due to successive cyclic loadings and the seabed liquefaction observed on the seaward side.

In the investigations carried out by Najma and Ghalandarzadeh, (2019), shake table tests were performed to investigate the liquefaction of the seabed beneath the breakwater. Two layers of sand beneath a composite breakwater with a caisson on top of an RM breakwater were modelled. The results of the experimental investigation demonstrated that during the seismic loadings; and RM breakwater widening, the bottom soil was laterally shifted. Furthermore, the bottom on both sides of the breakwater was seen to be surging downhill and vertically. The study concluded that enclosing the existing liquefiable seabed in denser sand avoided damage from liquefaction-induced liquefaction and also reduced the penetration of RM into the bottom under seismic loading.

A breakwater contains a high percentage of large to small fragments that rest randomly in a mound, but have little particle adhesion. Ghalandarzadeh et al. (2021) examined seismic behaviour and deformation of rockfill breakwaters by shaking table tests. They used scaled model of a cross-section breakwater from South Pars Petrochemical Port, South Iran as prototype. For the breakwater considered by them, permissible settlement was limited (differential settlement is not allowed) in order to allow installation of oil and gas pipeline racks on crest. Nine models were considered (7 models -without piles and 2 models-with piles) and parameters like displacement, pore water pressure, accelerations were studied. The scaling

factor selected was 1:160. Two types of core material were used by them, finer core and coarser core along with other parts. The authors stressed that, along with scaling the grain size, it is necessary to adjust permeability. The authors found that, the use of coarser core material which do not soften during an earthquake will be best material for breakwater. Also, from deformation studies, they got to know that, increase in acceleration will have larger impact on deformation of breakwater compared to the combined effect of inertial and hydrodynamic forces. The effects like rolling down of armours, dislocation of surface component materials, volume change (densification) and slumping of core were observed by them during earthquake loadings in the breakwater without piles. As densification of upper core part did not control the settlement in the fine-grained core, they proposed the cross-section to be considered with twin-pile system in landward side and scaled models of piled breakwater was analysed against seismic loadings. The coarser core pile supported breakwater experienced minor settlement. The finer core pile supported breakwater experienced softening and deformation. The piles did not prevent large deformation but pipe racks were found in it is initial position. They concluded that, the piled breakwater was good in resisting settlement but did not have sufficient control over horizontal displacement under earthquake loadings and they recommended isolation system to have control. Numerical model studies were not performed by the authors.

Recently, Zhang and Ye (2023) investigated the seismic stability of revetment breakwater founded on coral sand. They observed softening of foundation soils and sinking of breakwater due to pore pressure development under the attack of high amplitude seismic waves.

3.3. Behaviour of RM Breakwaters Subjected to Tsunami

In the study carried out by Bricker et al. (2012), it was demonstrated that the tsunami waves overtopping could cause damage to the breakwater foundation. It was made very apparent in the handbook of coastal disaster mitigation for engineers and planners (Bricker et al., 2015) that the standard scour avoidance techniques alone could not prevent the geotechnical breakdown of a breakwater by punching. As the tsunami's height rose, it was seen that the overtopping jet of water gradually drifted away from the breakwater. The study also showed that the distance between the caissons resting on top of the RM made the failure of the leeward side of the breakwater more likely. The leeward side of an RM breakwater is clearly susceptible to serious damages during waver overtopping, and the extent of such damage would be greater in the absence of a crown wall or caisson, according to these studies.

Hazarika et al. (2013) investigated the damage to waterfront structures (e.g., coastal dikes, quay walls, and breakwaters) in the northern area of the Tohoku region (Aomori prefecture and northern Iwate prefecture). The investigation was focused on the geotechnical and structural aspects of the damages to coastal dikes, quay walls, and breakwaters due to the 2011 earthquake and tsunami, as well as the backlash. Analyses of the damage and their nature indicate that, in the north of Tohoku, rather than the earthquake itself the compound disaster brought by the tsunami was more rampant. The investigations reveal that the force of tsunami, the force of overtopping tsunami and the force of backrush were responsible for the scouring of the mound of breakwaters and seawalls resulting in the catastrophic failure of such structures.

The studies performed by Guler et al. (2015) looked into how tsunamis would affect RM breakwaters. The experiments were carried out using a model of the RM breakwater at Haydarpasa Port, Turkey. The experimental findings demonstrated that the existing breakwater could not survive even mild tsunami attacks. As a result, it was suggested that the breakwater on the harbour side be made wider. The overflow of tsunami waves over the breakwater was continued for a while until breakwater damaged. By setting off earthquakes at several potential locations and measuring the associated height of the tsunami waves at shore, the height of tsunami waves was calculated by numerical modelling. The experimental findings also showed that the random organisation and interlocking of the debris between the rubbles play a role in the failure of the crown wall when water is overtopping it.

Aniel-Quiroga et al. (2018) provided information on experimental findings after subjecting an RM breakwater to tsunami impact. The breakwaters were modelled after the ones that already exist along Mediterranean coast of Spain. Investigations were done into the behaviour of breakwaters with and without crown walls. In the experiments, it was noted that the model with the crown wall had greater drawdown-related breakwater damages on the seaside. It was also noteworthy that the breakwater without a crown wall had suffered less damage at a higher wave height, which was explicable by RM armour units' potential stability responses during wave action.

An important factor in determining the amount of water that will pass through an RM breakwater during a tsunami attack is the permeability of the core. This parameter also affects the possibility of uplift pressures developing beneath the crown wall and some material rearrangement in the core as a result of hydraulic pressure. The estimation of core permeability using laboratory experiments based on Darcy's law has been extensively described in the study

done by Recio and Oumeraci (2008). The duration and amplitude of the impacting waves both affect how much water will be channelled through the breakwater. So, as stated in the article by Oumeraci and Kortenhaus (2011), longer waves have a greater capacity to move water through the porous core of a breakwater. The study recommended that the transmission coefficient of the breakwater be calculated by adding the wave transmission by overtopping and through the breakwater.

It is challenging to assess how a wave decays after passing through the RM breakwater. The phenomenon of wave overtopping inside an RM breakwater was covered by Muttray and Oumeraci (2005). When a wave travels into the core, the water level there rises and may even reach the crest level, overtopping the waves internally. This behaviour grows as wave height rises, proving conclusively that internal wave overtopping would happen in the event of a tsunami. Changes in pore water pressure and internal wave height are connected. Thus, these two characteristics must be assessed in order to determine the damping effect of a breakwater core. In a thorough experimental examination, the RM model was subjected to both regular and irregular waves, with wave overtopping strictly prohibited. A weakness of the study is that the penetration of waves from the crest of RM was not taken into account. The study proposed a modified Forchheimer equation that, by accounting for turbulent losses, accurately forecasts the attenuation of waves travelling over the breakwater. The study also demonstrated how linear polynomial or quadratic techniques of resistance estimation can be used to approximate the hydraulic resistance involved in wave infiltration.

An essential approach of assessing the wave impregnation through armour units was employed in the numerical analysis by Dentale et al. (2018). In contrast to most other literature, where the armour layer was defined as a porous medium, the method used the Flow Within the Armour Units (FWAU) model, which allows the interaction of turbulent flow through the armour blocks to be analysed. As a result, the field conditions were not accurately simulated. The analysis made use of the FLOW-3D programme, which utilises the Volume of Fluid (VOF) technique and Reynolds Averaged Navier-Stokes (RANS) equations. Modelling the breakwater to more closely resemble actual field conditions was made possible by the technique of inserting armour units as distinct 3D pieces created in CAD software. The analysis's findings demonstrated that the proposed numerical method was more accurate than current equations at predicting the wave run-up, overtopping, and reflection coefficients.

Gent and Werf (2019) investigated about the effects of oblique waves on the reduction of wave overtopping. Two different types of crown walls were used to model an RM breakwater in a wave basin for the investigation. The effects of waves were applied to the crown walls both with and without a shear key. The armour blocks were kept more stable by utilising wire mesh and heavier blocks because the study was primarily concerned with the behaviour of crown walls. A tank that was attached to an overtopping chute was used to track the amount of water collected. In order to calculate the horizontal and vertical forces acting on the crown wall, the study provided reduction factors. Furthermore, having a key available on the wall tends to greatly diminish the uplift forces while increasing the horizontal forces. In order to compute the overtopping discharge caused by oblique waves, a reduction factor was also developed. The authors proposed that in order to lower the designed size of the structure, crown walls should be constructed while taking oblique wave stresses into account.

Goseberg et al. (2013) put forward the idea of using pumps with a proportional-integral-derivative controller in a closed-circuit flume system, where the volume of water in the storage reservoir is used to form the volume of water in the wave crest generated in the flume. By this, the authors successfully generated long waves of wave profiles resembling actual tsunami waves. The waves are long waves that cannot be generated in the usual flume. The authors also highlighted some important aspects to this type of wave generation. The 180^0 bend in circuit flume will cause spiral flows and secondary flows when the generated waves travel through the flume. These additional flows could cause energy loss to the generated long waves. The study is thus limited to the possibility of generation of the long waves. The impact of these waves on the model beach and the uncertainties in assuming a unit reflection coefficient to the beach model was not evaluated. On the contrary, the increase in volume of water due to the reflection of waves has been evaluated using pressure sensors, and correspondingly, the pump systems were adjusted based on algorithms so that the desired long waves were persistent in the wave flume. Although the article has limitations in using a circuit flume system for wave propagation, the method of wave generation suggested was innovative in recreating long tsunami waves at a laboratory scale without consuming large spaces.

3.4 Effects of Scale Down on Wave Overtopping Over Rubble Mound Breakwaters

Franco et al. (2009) conducted extensive research by comparing the actual prototype data with the model data to determine the effects of scaling in wave run-up and overtopping on a RM breakwater. The breakwater at Ostia, Italy was modelled in wave flume as well as a wave basin

for analysing under both 2D and 3D conditions. The studies were conducted as different sets. The initial set of experiments were conducted on the model of prototype breakwater. The other sets of experiments were conducted by modifying the seaward slope, permeability, and offshore distance. The results of these experiments concluded that the models have failed in creating wave overtopping under the scaled down actual storm data. To find the reason behind this, the authors have modified several parameters of breakwater to incorporate the filed dimensions and conditions. Despite of the efforts, it was found that all those parameters had negligible effects on the wave overtopping. Therefore, the article suggested that the breaking of waves at longer offshore distance before reaching the breakwater could result in higher turbulent water that could not be accurately modelled in the laboratory scale. The factors such as curvature in the breakwater alignment, wind speed etc. could not be quantified and modelled. These factors may result in the inaccurate overtopping of waves in flume and basin. Whereas the authors pointed out that, in the case of rubble mounds with steeper slopes on either side, the overtopping of waves can be modelled with higher accuracy. The authors also extended the study by determining the roughness coefficient of the breakwater with reference to a smooth breakwater slope.

The research performed by Lykke Andersen et al. (2011) highlighted the relevance of scaling down effects on small wave overtopping in RM breakwaters. Since, majority of RM breakwaters are designed for small wave overtopping heights, the inefficiency of scaling down the wave could seriously impact the model experimental results. The authors compared the difference in the effects on small and large-scale models. The large-scale model was 4 times larger than small scale model. The scale down effects on the Reynold's number was highlighted by the authors as one of the reasons that could cause the small overtopping in model. The scaling down of a prototype will also result in changing the type of flow through the rubble mound from turbulent to laminar. Further, another important aspect highlighted in the article was about the entrapped air in water used in the flume or basin. Generally, fresh water is used in studying model which will have lesser air entrapped bubbles compared to saline water. However, even if the model was subjected to saline water, the relative size of entrapped air bubbles will be considerably larger than that of actual sea water near prototype. Also, the volume of air entrapped will be lesser in model than in prototype. Therefore, it was pointed out that the average mass of water that run up the slope of rubble mound in prototype will be lesser than that of model. This would obviously result in higher overtopping in prototype and lower overtopping in model. The experiments concluded that the top geometry of the rubble mound

has great influence on the overtopping of waves. Effects of scaling were found to be lesser for rubble mounds with wider top widths.

3.5 Development of Resilient Breakwaters Against Earthquake and Tsunami

In the study performed by Chaudhary et al. (2018a, 2018b), new techniques of countermeasures were developed for a composite breakwater to make it resilient against an earthquake and tsunami-induced damage. Gabions and sheet piles are employed in the breakwater's foundation as reinforcing measures. Through experiments and numerical simulations, the effectiveness of the reinforcing countermeasures was assessed. The research works by Chaudhary et al., (2017a, 2017b, 2018a), Hazarika et al., (2015, 2017, 2019) developed novel techniques making a caisson-type composite breakwater as an earthquake and tsunami resilient structure. Through model testing and numerical analysis, the performance of the techniques was evaluated. Shake table testing and hydraulic model tests were carried out as part of model tests for various earthquake loadings and tsunami overflow in the lab.

The mitigation techniques for a composite breakwater (caisson type) were suggested by Chaudhary et al. (2019, 2018c) under the influence of a major earthquake and tsunami. The authors observed that the excess pore water pressure caused by a seismic event would not completely diminish when followed by a tsunami wave as evidence that this condition was crucial. The caisson at the top of rubble mound lying on a foundation of sand, served as the material for the composite breakwater. It was demonstrated experimentally that this circumstance causes a breakwater to move horizontally and vertically excessively. Therefore, sheet piles, gabions, and a geogrid layer were used to strengthen the breakwater foundation. According to the experimental investigation, the installation of sheet piles and gabions under the aforementioned critical loading conditions can limit the lateral movement of foundation soils and mound. The primary purpose of sheet pile was to stop water from seeping through the foundation dirt. A tsunami event's higher-level water profile difference between the harbour and seaside could cause water to seep through the foundation soil, causing the breakwater to sink. To reduce the impregnation of water through the mound from the seaward side, a special form of gabion was developed. On top of these gabions was a metallic sheet that served as an impermeable barrier for water to pass through it. Since the failure of the foundation was the only thing that interested the investigation, the breakwater was built robust enough to withstand the loadings. The presence of sheet pile walls has reduced the amplification of seismic waves, according to the acceleration time history data gathered after conducting shake table tests under 0.1g and 0.3g as foreshock and main shock, respectively. Breakwaters with strengthened

foundations were shown to have reduced caisson settlement. The lower readings from pore water pressure monitors in the foundation soils made this obvious. Lower value of excess pore pressure was the result of the RM settling to a lesser extent due to the geogrid membrane presence. The outcomes for horizontal displacement were similar. The additional weight and frictional resistance that gabions added prevented breakwater from moving horizontally. While the foundation soil's lateral movement had been lessened by the sheet piles. The article concluded that reinforced breakwaters were very successful compared to conventional or unreinforced breakwaters in withstanding the earthquake and tsunami-induced damage. After the seismic motions, the sheet pile wall's displacement was seen. To avoid this displacement, the authors advised using geogrid membrane to secure the sheet piles. Additionally, there was no connection between the offered gabions during the testing. Therefore, the authors proposed that in addition to linking the gabions, attaching them to sheet piles and caisson could increase the structure stability. In order to make a breakwater resilient towards earthquake and tsunami loadings, the study proposed a novel approach of incorporating geosynthetics into the breakwater foundation and enhancing the foundation's strength against earthquakes and tsunamis.

Some more research works related to breakwater stability and countermeasure development subjected to earthquakes and tsunamis are listed as below:

RAPSODI (2016), Joint Project between Japanese and European Research Organizations: After the 2011 Great East Japan Earthquake and Tsunami, several research organizations of Europe (e.g. NGI, DEU, METU, TU-BS, LWI) and Japan (e.g. PARI and NIMPAT) conducted a joint research project, RAPSODI (**R**isk **A**ssessment and design of **P**revention **S**tructures f**O**r enhanced tsunami **Di**saster resilience) and found that there is lack of information on the behavior of RM breakwater subjected to tsunami. To determine the behaviour of RM breakwater under tsunami, tests were conducted, and comparisons were made based on the damage that occurred during the 2011 Great East Japan Earthquake and Tsunami. It was observed that armor units displaced and scattered due to increase in buoyancy force and tsunami impact forces. In some cases, it was observed that crown unit could reduce the damage of the breakwater during the tsunami. However, in other cases, the crown unit slid from the top of the breakwater.

Chaudhary et al. (2018 a, b), Kyoto University, Japan: Countermeasures were developed for composite breakwater to make it resilient against earthquake and tsunami. As reinforcing

countermeasures, gabions and sheet piles are used in foundation soils of the breakwater. Performance of the reinforcing countermeasures was evaluated through experiments and numerical simulations. A series of shake table tests and tsunami overflow tests were conducted.

Hazarika et al. (2017, 2019), Chaudhary et al. (2017a, b) and Chaudhary & Hazarika (2018), Kyushu University, Japan: They have developed new countermeasures for composite breakwater against an earthquake and tsunami. The performance of the countermeasures was evaluated through model tests and numerical analyses. As a part of model tests, a series of shaking table tests, hydraulic model tests were conducted for different earthquake loadings and tsunami conditions. Numerical simulations were also performed.

Kazama and Noda (2012), Tohoku University, Japan: They performed detailed field survey for the damage caused by the 2011 Great East Japan Earthquake and Tsunami in Japan. Many coastal structures such as breakwater, seawall, etc. damaged in Japan by the tsunami. The breakwaters at almost all the major ports in the affected areas of Japan were damaged by the tsunami. Main reasons of failure of the breakwaters during the tsunami were (i) scour of rubble mound, (ii) seepage below the caisson, (iii) caisson sliding over the mound and (iv) joint failure.

Gular et al. (2015), Port and Airport Research Institute, (PARI), Japan: This study for RM breakwater at Haydarpasa Port, Istanbul, Turkey subjected to tsunami. Experiments were conducted at PARI, Japan for different models of RM breakwaters. The breakwater failed during the tsunami overflow tests. As countermeasure, crown unit was placed at the top of the breakwater which gave stability for some cases. However, the armor units washed away and crown unit slid for higher level of tsunami.

Jianhong et al. (2013), China Academic of Science, China: It is a numerical study dealing with the stability of a breakwater under a tsunami. It was observed that tsunami impact force, overtopping and overflowing of tsunami waves are the main factors causing damage to the breakwater.

Kikuchi et al. (2015), Tokyo Uni of Science, Japan: As countermeasure the authors used row of cylindrical piles in foundation of a composite breakwater in order to mitigate the effects of tsunami on the breakwater.

Quiroga et al. (2018), University of Cantabria, Spain: Experiments were conducted to determine the stability of RM breakwater under tsunami. In the study, tsunami impact forces and tsunami overflow are considered. It was observed that the damage on the breakwater under tsunami action varies from sea side to harbor side. The presence of a crown wall could reduce the damage on the harbour side.

3.6 Summary of Literature Review

Many breakwaters were damaged and even collapsed during the past tsunamis. Due to the failure of the breakwater, the tsunamis could not be blocked by the breakwater. Thus, the tsunamis entered the coastal areas, which led to devastating damage there. Therefore, it is of utmost importance to develop countermeasures for RM breakwater, which can make it resilient against tsunamis. Moreover, generally, earthquakes precede tsunamis. Hence, these countermeasures should be effective against both the earthquake and tsunamis. For the development of countermeasures against tsunamis, it is very important to first determine the reasons and mechanisms of the damage of RM breakwaters under the actions of an earthquake and tsunami. A joint project between Japanese and European Research Organizations was conducted after the 2011 Great East Japan Earthquake and Tsunami, several research organizations in Europe (e.g. NGI, DEU, METU, TU-BS, LWI) and Japan (e.g. PARI and NIMPAT) conducted a joint research project, RAPSODI (**R**isk **A**ssessment and design of **P**revention **S**tructures f**O**r enhanced tsunami **Di**saster resilience) and found that there is lack of information on the behaviour of RM breakwater subjected to tsunami. Some studies were conducted to determine the effects of earthquakes on the behaviour of RM breakwaters [Memos (2000), Ulker (2014), Yüksel et al. (2004), Cihan and Yuksel (2011 and 2013)], but these are limited to earthquake-only tsunami tests were not done. The seabed foundation soils can be liquefied during an earthquake, due to which seabed ground can lose the shear strength, and finally, the breakwater may collapse.

The main reasons for the instability of a RM breakwater subjected to an earthquake are:

- Deformations of the core of the breakwater
- Excess pore water pressure
- Seismic inertia forces acting on the breakwater
- Deformation of seabed soils

The effects of a tsunami on an RM breakwater were discussed by Chaudhary et al. (2018a, 2019), Aniel-Quiroga et al. (2018), Banijamali et al. (2017), Esteban et al. (2014), Guler et al.

(2015), some of them are for the composite breakwater. The main reasons for damage to breakwaters during tsunamis are

- Scour due to tsunami
- Sliding of the crown unit due to tsunami impact forces
- High seepage through the breakwater body and seabed.

4. RM BREAKWATER SUBJECTED TO AN EARTHQUAKE AND TSUNAMI

For countermeasure development, it is important to understand the behaver of RM breakwater subjected to earthquake and tsunami. Based on the past study done by PI and available literature, the expected behaviour of an RM breakwater under the actions of an earthquake and accompanying tsunami is depicted in Fig. 4.1.

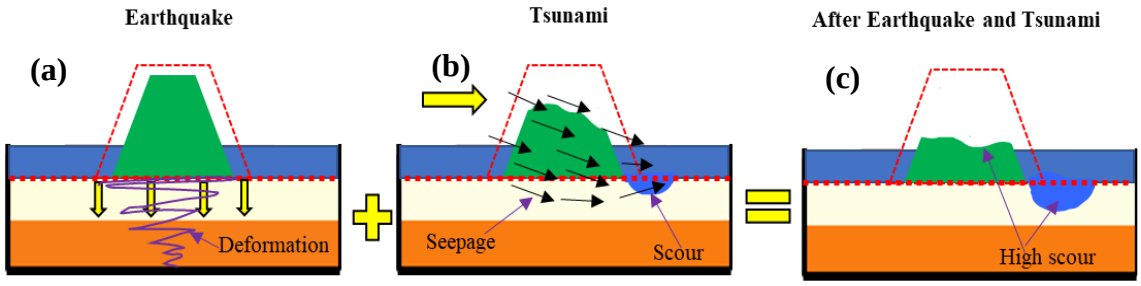

Fig. 4.1 Breakwater under actions of an earthquake and subsequent tsunami

The RM breakwater lacks a base foundation structure. Excessive pore water pressure (EPWP) in the seabed; and the breakwater body, generated by an earthquake, can weaken the structure and result in breakwater damage as shown in Figure 4.1a. The bottom seabed soils can deform in both the vertical and lateral directions as a result of the ground shaking caused by the earthquake, adding to the breakwater's instability. The height of the breakwater may decrease as a result of the earthquake-related damage and settlement. Because of this, a tsunami can easily overflow it.

Figure 4.1(b) depicts the effects of the tsunami on the RM breakwater. A breakwater is subject to the tsunami's impact forces. There is a difference in seawater level between seaside and harbour side of the breakwater. Due to which, seepage occurs through the body of the breakwater and the seabed soils in one direction as a result of the difference in seawater level. The arrows in Figure 4.1(b) depict the anticipated seepage during the tsunami. High seepage might result in soil piping on the seafloor. According to Chaudhary et al., (2018b , 2018c)

pipping of a seabed below breakwater as a result of the tsunami was one of the key factors of the failure of the breakwater. In addition, tsunami waves have the power to overflow and scrape the crest of the breakwater. The rear side of the breakwater and the seabed next to the breakwater are scouring by the overflowing tsunami wave as shown in Figure 4.1(b). Finally, the combined impacts of the tsunami impact force, scouring, seepage, and pipping can cause a breakwater to collapse completely during the tsunami (Figure 4.1c).

5. RESEARCH OBJECTIVES

Breakwaters are essential structures for ports and harbours, which protect ports and harbours from the destructive impacts of sea waves. The breakwaters can also be used to protect the port from tsunamis. For instance, the breakwater (caisson type composite breakwater) at Kamaishi port in Japan was built to protect the port from tsunamis of height 5 -6 metres. On the other hand, the 2004 Indian Ocean Tsunami damaged many Indian ports. In India, RM breakwaters are primarily utilised to shield ports from sea wave disturbances. Therefore, the primary goal of the research project is to develop a new technique for making the RM breakwater of an Indian port (e.g. New Mangalore Port) as a tsunami-resilient structure. The tsunami-resilient breakwater can thus prevent or significantly decrease the height of the tsunami. Thus, damage to the ports caused by a tsunami can be mitigated.

Numerous composite breakwaters in Japan were damaged due to the 2011 Great East Japan Earthquake and Tsunami. Moreover, the 2011 Great East Japan Earthquake and tsunami caused numerous breakwaters in Japan to collapse, including those in Shinchi, Soma, Yamamoto, and Ishinomaki. Researchers and the Japanese government then did investigative work, and it was found that most of the breakwaters collapsed mainly owing to the failure of their foundations. The tsunami's overflow eroded the mound, and caissons slid over it and submerged in the seawater. The tsunami invaded the coastal areas due to the breakwater's failure, causing severe destruction there.

The catastrophe served as a reminder of the necessity of developing countermeasures against tsunamis for breakwater. The development of countermeasures for composite breakwaters against the earthquake and subsequent tsunami has been attempted in the wake of the earthquake and tsunami, they were primarily created in Japan. However, RM breakwaters make up the majority of breakwaters in India. When a tsunami strikes, RM breakwaters behave differently than composite breakwaters. In order to make the RM breakwaters resilient against tsunamis, new techniques for countermeasures, particularly for the existing breakwaters, should be developed. Additionally, a tsunami never strikes alone. In most of the cases, an

earthquake comes before a tsunami. As a result, these procedures ought to be effective against both tsunamis and earthquakes (that precede the tsunami).

Objectives of The Project

The main objectives of the research proposal are as follows:

- To examine the stability of an existing RM breakwater of an Indian port (e.g., breakwater at Mangalore Port) under actions of an earthquake and tsunami. Stability of the breakwater is determined through experiments (shaking table tests and tsunami overflow tests) and numerical modelling.
- To develop a new reinforcing countermeasure for the breakwater in order to mitigate earthquake and subsequent tsunami-induced damage of the breakwater.
- To evaluate the effectiveness of the developed model by physical model tests.
- To carry out numerical analyses by Geotechnical software to elucidate the mechanism.

6. DESCRIPTION OF INNOVATIVE REINFORCED MODEL

This study introduces an innovative technique that combines several elements to enhance the resilience of rubble mound breakwaters against tsunamis. The approach incorporates a combination of gabion armour layers, crown walls with shear keys, and sheet piles, as shown in Figure 6.1. The details of the main components are mentioned below:

- **Gabion Armor Layer**

The gabion armour layer is a crucial addition to the conventional rubble mound breakwater. It consists of gabion baskets filled with stones or other heavy materials. These gabions are strategically placed over the existing rubble armour units. Their weight provides enhanced resistance against scouring caused by tsunami overflow. By using gabions, the breakwater's core layer remains protected, ensuring its integrity even during extreme tsunami events.

- **Crown Walls with Shear Keys**

Crown walls are constructed on top of the rubble mound. Their primary purpose is to safeguard the crest region from overflowing tsunami waves. Shear keys are incorporated beneath the crown walls. These keys enhance the wall's resistance against lateral forces generated by tsunamis. The combined effect of crown walls with shear keys improves the overall stability of the breakwater, preventing the dislocation of armour units due to lateral thrust from tsunami waves.

- **Sheet Piles**:

  Seepage through foundation seabed soils can reduce bearing capacity of seabed foundation soil, and thereby compromise the stability of the rubble mound breakwater under a tsunami. To address this issue, two rows of sheet piles are embedded in the seabed at both the seaside and harbour-side ends of the breakwater. These sheet piles act as cut off wall or barriers, efficiently blocking seepage through seabed soil during tsunami. By doing so, they contribute significantly to the breakwater's overall resilience.

In summary, this innovative approach—combining gabion armour layers, crown walls with shear keys, and sheet piles—provides a robust solution for NMPT rubble mound breakwater, making it better equipped to withstand tsunamis and protect coastal areas.

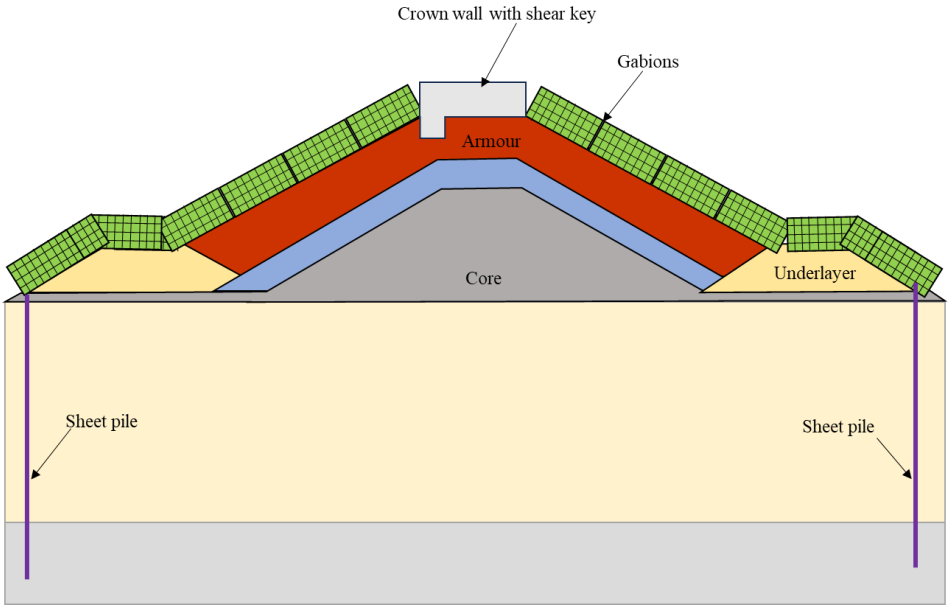

Fig. 6.1 Reinforced rubble mound breakwater model

7. METHODOLOGY

The study is conducted on the scaled down models of the existing rubble mound breakwaters at New Mangalore Port to understand it is behaviour against seismic loadings and tsunami. Initially, the prototype breakwater's physical properties were scaled down based on suitable scaling laws. For the physical model tests, materials are chosen by following the similarity rule and availability in the market. The materials were characterized before using in the physical modelling. Initially earthquake tests were conducted, followed by tsunami overflow tests.

As a part of physical model tests, a series of shake table tests were conducted to determine the behaviour of the breakwater under the actions of earthquakes. First of all, the tests were conducted in order to understand the reasons and mechanism of failure of the conventional (unreinforced) RM breakwater during an earthquake. Later, new countermeasures techniques

were developed to make the breakwater resilient against the earthquake-induced damage. After that, the physical model tests were conducted to evaluate the effectiveness of the developed reinforced breakwater subjected to the earthquake. Following that, tsunami studies were conducted with the conventional as well as reinforced models. The parameters such as settlement, horizontal displacement, excess pore water pressure, acceleration, etc, were monitored throughout the tests. A high-resolution camera is used to capture the deformation patterns under the earthquake and tsunami loadings. Along with this, 3D profiles were developed using Profile Mapper, an innovative mapper that uses ultrasound and laser technologies. Finally, numerical analyses were performed to clarify the mechanism involved.

7.1 Description of Prototype Breakwater

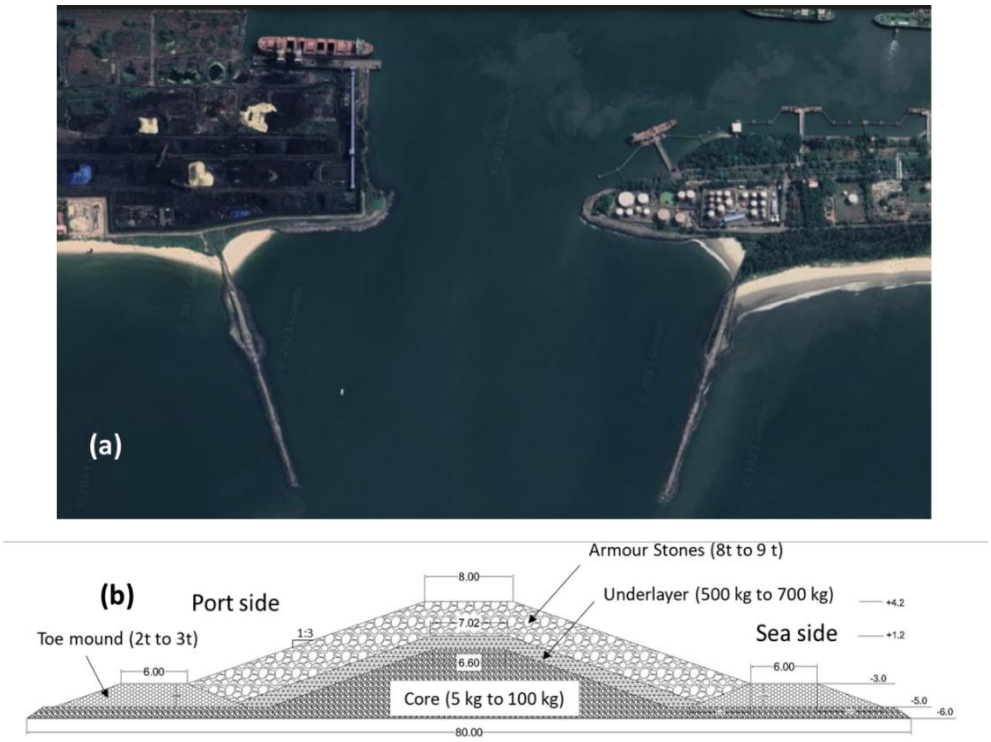

Fig. 7.1 NMPT breakwater location and (b) Cross-section of breakwater at NMPT

This research focused on a prototype breakwater located at the New Mangalore Port, Mangalore, Karnataka. The New Mangalore Port (NMPT) is a purposefully constructed facility designed to ensure operation under diverse weather conditions. It is geographically positioned at coordinates 12.9°N and 74.86°E, situated along the southwestern coast of India at the confluence of the Gurupura (Phalguni) River and the Arabian Sea. The port features two RM-type breakwaters, each extending over 770 meters, strategically constructed - one on the southern side and the other on the northern side - to safeguard the port from the disturbances

caused by sea waves. For the study, the cross-section of northern breakwater was considered. The depth of the breakwater cross-section is 10.2 m and width is 80 m (on seabed ground) (ref. Figure 7.1(a) for location). The breakwater cross section consists of armour stones on outer slopes, underlayer rubbles, core and toe mound on both sides of port and harbour as shown in Figure 7.1(b). Regarding seismic and tsunami studies, the terminal port in Mangalore comes under Zone III of the Seismic Zoning map of India given in IS 1893 (P1): 2016 and can be affected by a future earthquakes. Also, the port is located on the western coast of India, which is under more threat from tsunamis due to the proximity of the Makran Subduction Zone. Hence, it is crucial to evaluate its breakwater against these forces to keep up the safety of the port and the coastal area.

7.2 Development of Physical Models

The prototype dimensional parameters were scaled down using the scaling laws given by Iai (1989). The prototype-to-model ratio (N) is 80 for the present study. The various parameters of the model were scaled down based on the scaling law, and depicted in Table 7.1. The models were developed in the soil box and tsunami flume of shake table and tsunami apparatus respectively. So, the experimentation dealt with two models: (a) the Conventional breakwater model (without crown wall) and (b) the Reinforced breakwater model. The reinforced model was prepared with reinforcing elements like two rows of sheet piles in the foundation soils, crown walls on crest and gabion on outer slopes of the breakwater.

Table 7.1 Similitude laws for the experiment (Prototype to model ratio= 80)

Parameters	Prototype/Model ratio	Scale Factor
Length	N	80
Area	N^2	80^2
Volume	N^3	80^3
Mass	N^3	80^3
Density	1	1
Time	$N^{3/4}$	26.75
Stress	N	80
Acceleration	1	1
Frequency	$N^{-3/4}$	0.037
Displacement	$N^{1.5}$	715.54

Pore water pressure	N	80
Permeability	$N^{3/4}$	26.75

7.2.1 Shake Table Setup

The shake table at the Geo-disaster Prevention Lab of the National Institute of Technology-Karnataka, Surathkal, was used to provide earthquake loading in this study. The shake table consists of a square platform of 2m x 2m. In this study, a uniaxial shake table is used. On the shake table, a scaled model of the breakwater of NMPA will be created in the lab. The shake table is capable of producing sinusoidal input motion as well as real earthquake data. A suitable sinusoidal wave can be generated by an input wave generator system. The input system is connected with a servo-hydraulic linear actuator and a hydraulic power pack. The shake table's desired movement depends on the actuator's linear motion installed on the reaction frame. Data acquisition system (DAQs) records the output from the transducers used in the tests. A geodynamic software called bench analysis is used to extract the data, and the variation measured by transducers is visualised in the display system. The schematic representation of the shake table setup is shown in Figure 7.2.

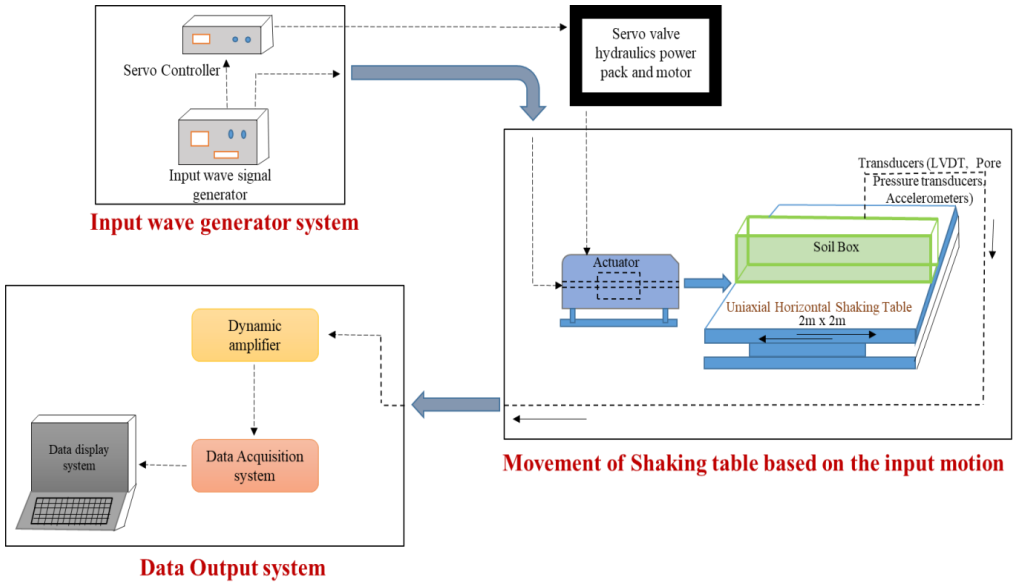

Fig. 7.2 Schematic diagram of shake table (after Akarsh et al. 2024b)

The model breakwater was constructed in a soil box of 155cm x 100cm x 50cm made with steel and transparent acrylic sheets (ref. Figure 7.3). These sheets were supported by C-channel steel frames. The corners were made water resistant. The soil box was firmly fixed on the

horizontal shake table using suitable bolts and nuts and placed along the axis of movement of actuator. In order to reduce the boundary effects, the breakwater model was placed centre and cushion type wave cum vibration absorbing synthetic layers were provided on extreme boundaries. According to Dou and Byrne (1997), it was possible to create free-field condition without the soft boundary walls due to large difference in input frequency and natural frequency of soil.

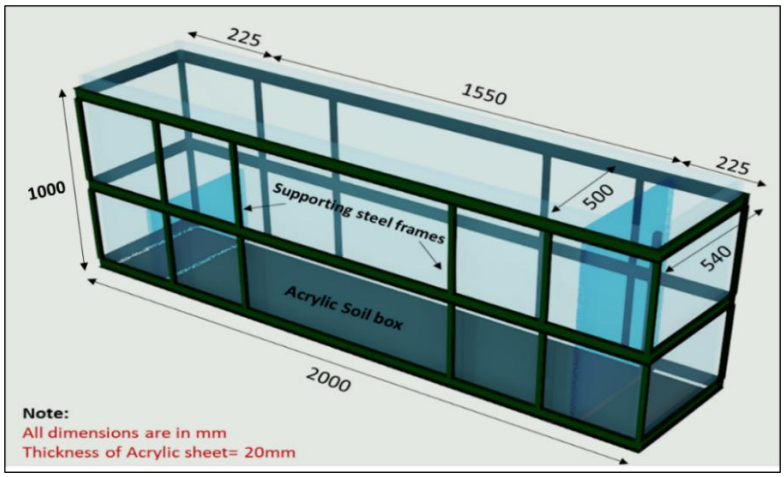

Fig. 7.3 Soil box setup (after Akarsh et al. 2024b)

7.2.2 Development of Breakwater Models for Earthquake Loadings Tests

For the development of physical models, two models were considered: (a) conventional model (without crown wall) and (b) reinforced model.

(a) Conventional model (without crown wall)

The conventional model comprises two main components: the foundation ground/soils and the breakwater body. The foundation ground is made of two layers of sand: an upper layer of loose sand representing the seabed and a lower layer of dense sand, simulating a hard stratum or bed rock. Due to the unavailability of the prototype's seabed soil details, the study utilized natural river sand for these purposes. The lower dense sand layer was compacted to achieve a relative density of 90% (Dr=90%) with a thickness of 100 mm, using a square tamper. Densification of the upper loose sand (Dr=60%) was accomplished via the air pluviation method. This was adopted to prepare homogeneous, repeatable sand bed specimens of required relative density instead of simply pouring a particular weight of sand into the soil box. A self-made, travelling air pluviator system designed at the Geo-disaster prevention lab was used for this study. The set-up mainly consists of: a hopper system of 20kg capacity, an orifice plate, a flow stopper, a supporting hollow box made with mild steel sheet on 3 sides and 1 side acrylic sheet and a

chain-pulley system for adjusting the height. Inside the acrylic box, 4 layers of diffuser sieves (2 layers of 6mm sieve on upper side followed by 2 layers of 5mm sieve) are placed parallel to each other with appropriate vertical spacing (Akarsh et al. 2024b). A schematic representation of the Pluviation system is shown in Figure 7.4. In the method of air pluviation, the three major factors that are to be considered include the height of fall, deposition intensity and relative diffuser ratio (Knodel et al., 1992). The required height of fall can be adjusted by attaching the sand hopper to a chain block pulley system that is attached to a roller system. The roller system can run through a rail fixed a horizontal rod placed along the length of the soil box/tsunami flume. The required height of fall is determined by calibration charts prepared specifically for the sand used in this experiment. The trap door beneath the sand hopper can be adjusted to maintain a constant deposition intensity.

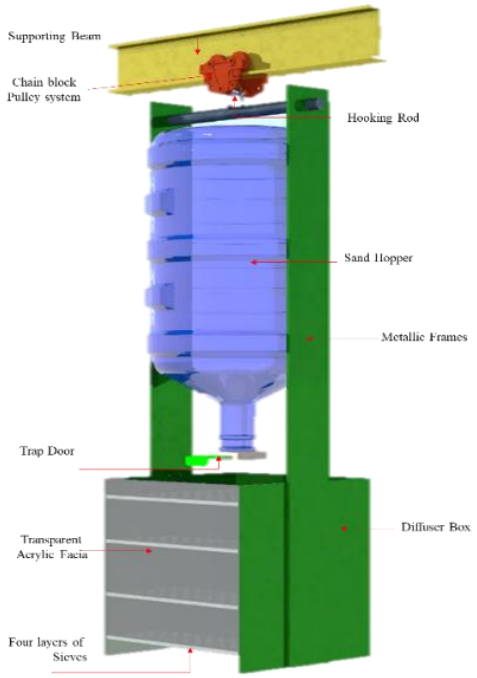

Fig. 7.4 Schematic representation of the pluviation set-up

The deposition intensity defines the total weight of the soil fallen from the hopper in unit time over a unit area (Dave and Murty, 2012). The deposition intensity is fixed such that for a particular height of fall, the sand will not be retained on any of the sieves in the diffuser box. In the study, the relative density of 60% is used for loose sand for upper layer. The pluviation box will be continuously moved throughout the soil box, and adjustment in height will be achieved by pulling the chain to achieve the required density. Care should be taken against accumulation of sand in the diffuser sieve and uninterrupted sand deposition. Hence, it is possible to achieve reliable relative density values by adjusting the height with two or more

diffuser sieves. The height of the fall will always be measured from the bottom of the lowest sieve plate to the top of the seabed. The relative density of the loose sand was kept at 60% (Dr=60%) with a thickness of 250 mm. The physical properties of the foundation soils used and their particle size distribution are shown in Table 7.2 and Figure 7.6, respectively.

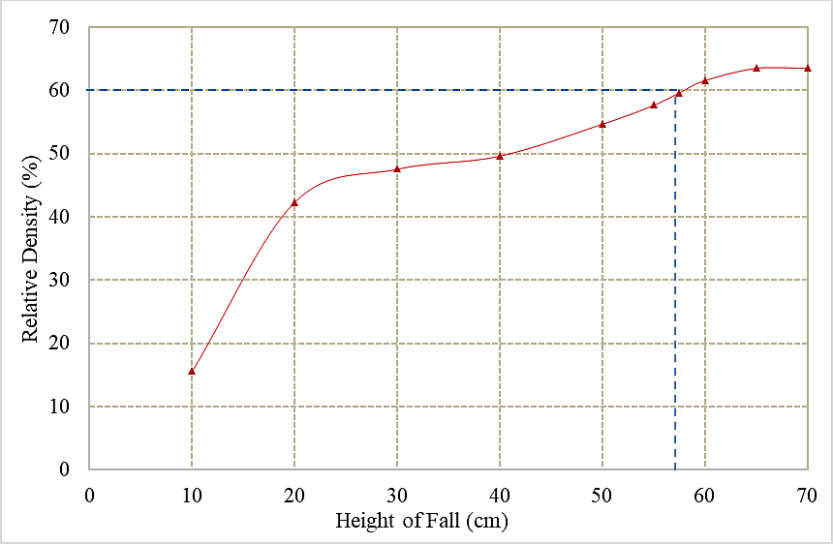

Fig. 7.5 Height of fall v/s relative density of sand)

Table 7.2 Properties of foundation soils (sand)

Parameters	Results obtained	Reference
Specific gravity, G	2.66	IS 2720 - P4 (1985)
Effective diameter, D_{10}	0.39 mm	
Coefficient of uniformity, C_u	2.524	
Coefficient of curvature, C_c	1.103	
Maximum dry density, γ_{dmax}	1.67 g/cc	
Minimum dry density, γ_{dmin}	1.49 g/cc	
Minimum void ratio, e_{min}	0.58	
Maximum void ratio, e_{max}	0.77	
Shear parameters for loose sand	ϕ_1 = 33.88 and C_1=0	IS 2720 - P39 (1977)
Shear parameters for dense sand	ϕ_2 = 37.89 and C_2=0	

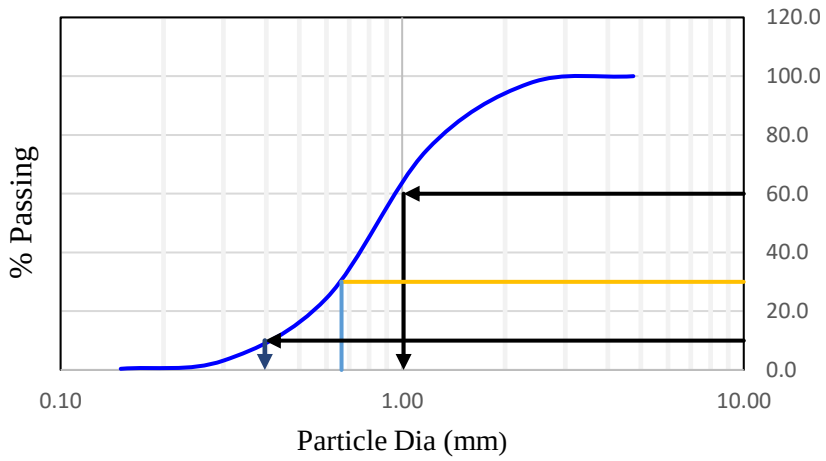

Fig. 7.6 Particle size distribution

The RM breakwater body was made of core, under layer armour layers and toe mound. These parts were prepared by various sizes of crushed stones and assigned with different colours (e.g., armour stones → red colour, underlayer → blue colour, toe mound → yellow colour and core → natural colour). The materials used in conventional breakwater was shown in last quarter progress report. The sizes of armour stones, toe mound stones, underlayer stones, core and were scaled down to (20-22) mm, (12-16) mm, (8-10) mm, (2-6) mm respectively. Initially, the core rubbles were densified in the central portion confining to its cross-section. Later, the underlayers and armour units were constructed on the trapezoidal breakwater core. The height of mound was 128 mm. The conventional model doesn't consist of crown wall (same as NMPT breakwater). After construction of dry model, water was allowed for saturation from the bottom to top; and it was adjusted to avoid sand boiling in the model. The tap water used as sea water in the study. The water was filled to a height of 96 mm (which is mean sea level in the prototype) above the foundation soils and kept it for 24 hrs to ensure complete saturation. The schematic representation of conventional model without crown wall is shown in Figure 7.7. To study the deformation pattern of foundation soil, thin layers of red coloured sands were provided at the distance of 100 mm, 200 mm, 300 mm and 350 mm from bottom near side face.

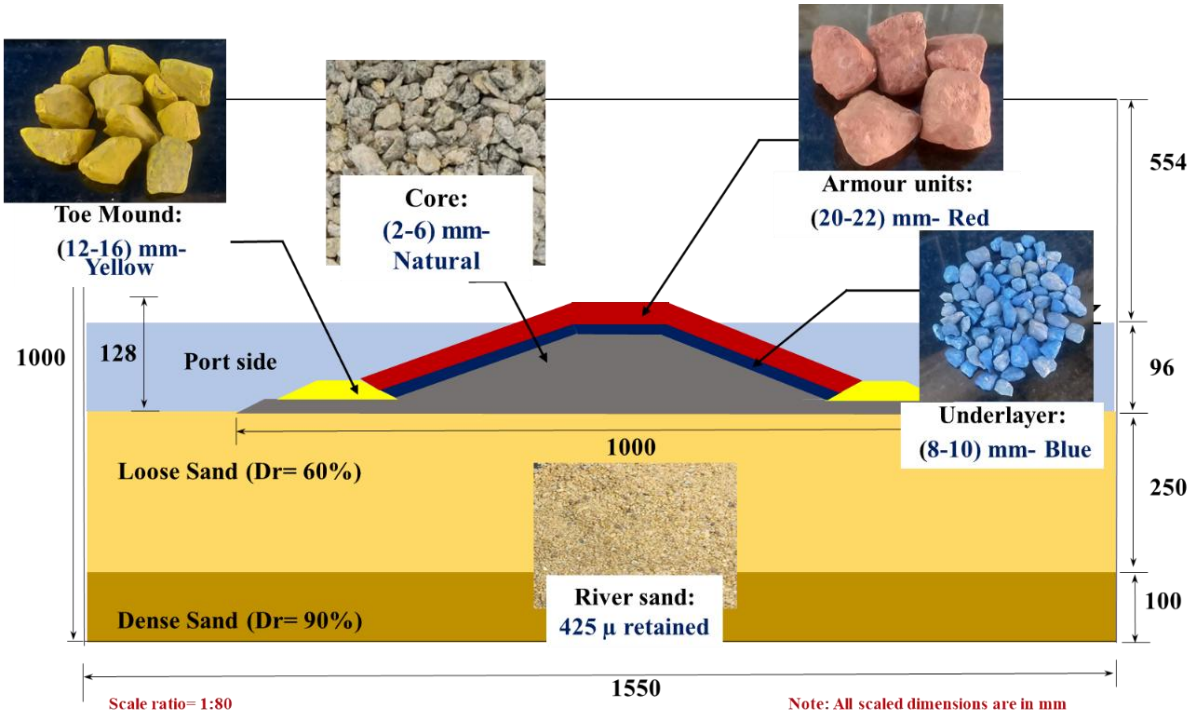

Fig. 7.7 Schematic representation of conventional model without crown wall

(b) Reinforced model

The novel reinforcing model consists of sheet piles in foundation soils, gabions as outer armour layer on both sides and the crown wall on the crest of breakwater body. In this model, the foundation soils were formed by two layers, lower dense sand (thickness=100 mm) and upper loose sand (thickness=250 mm) and constructed with same relative density as that of conventional model. In breakwater body, core material of 6 mm crushed aggregate, underlayer of 10 mm, toe mound of 16 mm and armour stones of 22 mm was used similar to the conventional model. Along with this, as a countermeasure for earthquake-induced damage, the countermeasure elements like sheet piles on extreme ends of the breakwater (embedded in foundation soils) and stone-filled gabions on outer slopes of the breakwater (above the armour layer). The same water level of 96 mm was used on both sides of breakwater body. The construction procedure used in reinforced model was similar to conventional model. The schematic representation of the reinforced model is depicted in Figure 7.8.

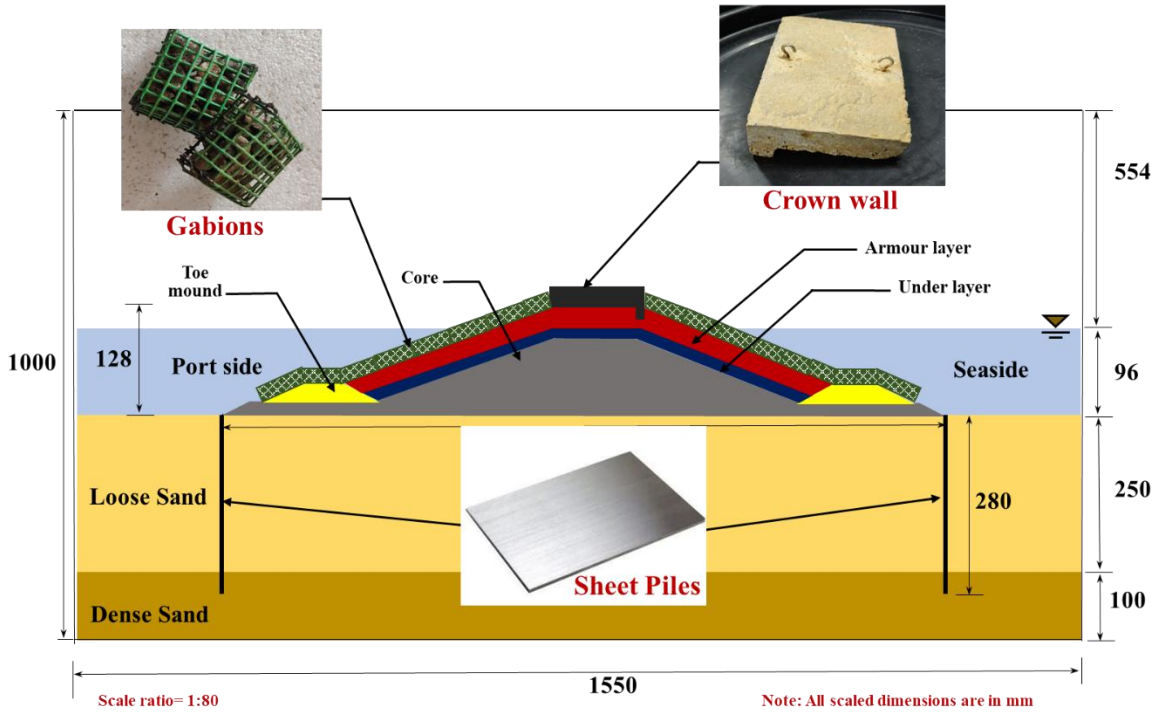

Fig. 7.8 Schematic representation of reinforced model

Lateral flow of foundation soils beneath breakwater is one of the major reasons for settlement and horizontal displacement of breakwater during earthquake. Sheet piles can restrict such lateral flow of foundation soils during an earthquake due to their bending characteristics. In the foundation soils, two Galvanized Iron (GI) sheet piles with a thickness of 2.5 mm were utilized. These sheet piles were embedded at a depth of 280 mm, comprising 250 mm within the loose sand layer and 30 mm within the dense sand layer. The construction process involved initially building the dense sand layer, followed by the insertion of the sheet piles into this compacted dense sand. Subsequently, the loose soil layer was constructed using the air pluviation method. The sheet piles were introduced mainly to overcome the lateral deformation of the seabed soils, inserted from the ends of upper seabed layer to the dense layer up to 3 cm embedment. The introduction of sheet piles in the foundation soils increases the shear stiffness and bearing capacity of the foundation soils. Due to which, the lateral displacement (and deformation) of the breakwater materials can be reduced during the earthquake loadings. In this study, the utilization of crown wall is proposed (which is absent in the existing prototype breakwater) due to its numerous advantageous. The crown wall is made of concrete is proposed to place on top of armour units, exactly at the centre of the model. In the experimental study, the concrete crown wall made of M40 grade was placed on armour stones and it was firmly fixed using shear key of 9 mm (Akarsh et al. 2024c). Three crown walls were used in longitudinal direction; and settlement and horizontal displacement are measured with reference to the centre one.

Gabions are also adopted to cover the entire rubble mound. Due to friction between the gabions and rubble mound, they can resist the lateral movement of the breakwater during earthquake, and thus they can reduce horizontal displacement of breakwater. The miniature gabions made of stones (rubbles) encased within the box type steel mesh and the size of gabions used were 40mm (L) x 40mm (B) x 20mm (H). In this way, the adoption of these countermeasures can reduce bearing capacity failures of foundation soils and the settlement and horizontal displacement of breakwater during the earthquakes. Also, it is expected that these reinforcing measures can perform well during tsunami.

The earthquake input waves are applied at the model's base as sinusoidal acceleration waves. In the study, two foreshocks and a main shock were used as earthquake loadings. For both foreshocks and main shock, the frequency and time duration were kept constant as 8 Hz and 8 sec respectively. The acceleration amplitude of the first foreshock was 0.1g (0.1g in prototype), and the second foreshock was 0.2g (0.2g in prototype). The main shock adopted was 0.4g (0.4g in prototype) in acceleration amplitude. The behaviour of RM breakwater was studied for medium to very strong earthquake and the effectiveness of countermeasures developed was determined for such strong earthquakes. After every earthquake loading, a sufficient time gap was given to dissipate the excess pore water pressure. The earthquake loadings are shown in Table 7.3.

Table 7.3 Earthquake load parameters

Input sinusoidal wave	Acceleration amplitude (a)	Frequency (f)	Duration (t)
First foreshock	0.1 g	8 Hz	8 Secs
Second foreshock	0.2 g	8 Hz	8 Secs
Main shock	0.4 g	8 Hz	8 Secs

7.2.3 Tsunami Flume Setup

A new apparatus was developed in the Geo-Disaster Prevention Laboratory at the National Institute of Technology Karnataka, Surathkal, India, that can be used to generate tsunami overflow through continuous water recirculation. This apparatus is designed to generate tsunami overflow through continuous recirculation of water with the aim of simulating and studying the impact of tsunamis on breakwaters and other structures. The apparatus has a dimension: 2,400 mm in length, 500 mm in width, and 1,000 mm in height. It is made of acrylic plates and steel frames. In the apparatus, a chamber of dimensions 1,800 mm (L) × 500 mm (W) × 1,000 mm (H) is separated for creating physical models (see Figure 7.9). The physical

models are crucial for testing the behaviour of structures, such as breakwaters, under simulated tsunami conditions.

To simulate the overflowing tsunami, water is stored in a tank and continuously circulated in a flume. Continuous water flow is deemed necessary to accurately replicate the effects of a tsunami, as isolated waves may not capture the dynamics of a tsunami adequately. The overflow condition, where the height of the tsunami surpasses the designed wave height of breakwaters, is simulated using submersible pumps to ensure continuous overflow and recirculation of water. One important aspect is maintaining continuous recirculation to prevent the reflection of overflowing tsunami water on the structure. The experimental setup involves controlling the velocity and overflowing depth over the crest using control valves. The tsunami flows at a depth of 100 mm above the withdrawn sea level of 50 mm. The study mentions that this specific tsunami flow depth represents a worst-case scenario, and it is consistent across cases involving both unreinforced and reinforced breakwater models. The continuous overflow tests were conducted for 30 minutes

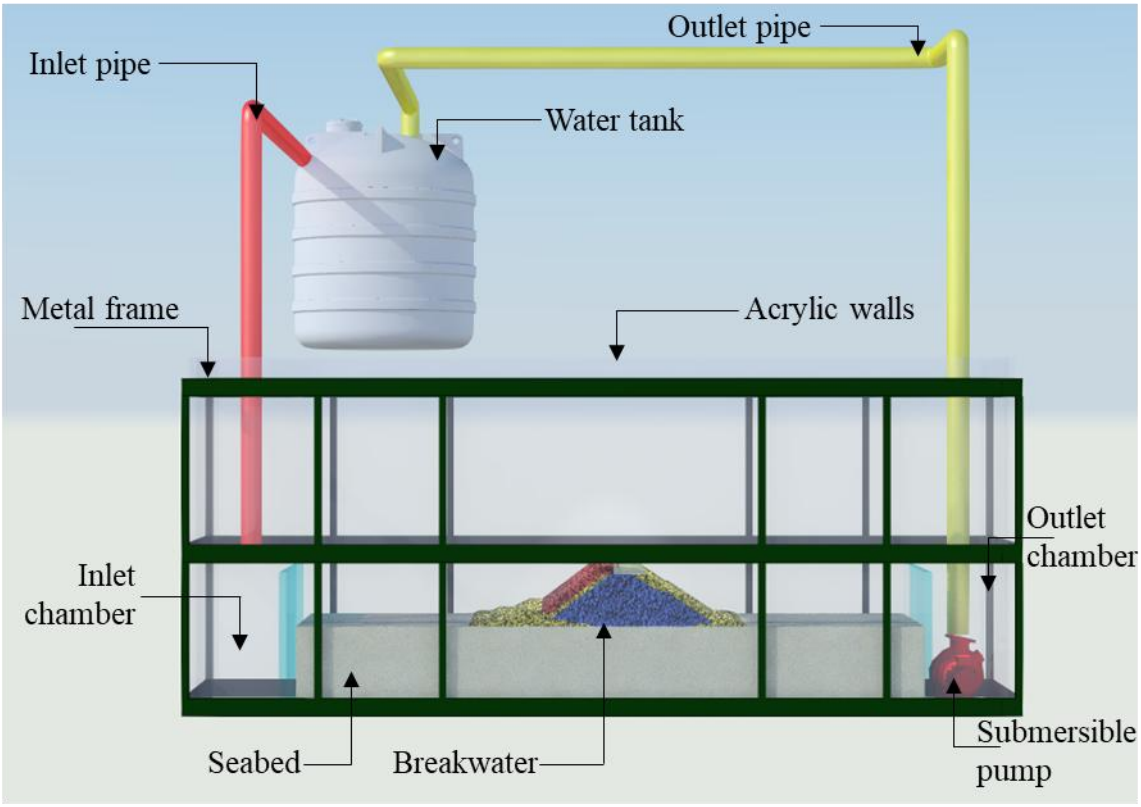

Fig. 7.9 Experimental apparatus developed for tsunami overflow (Sajan et al. 2024a)

7.2.4 Development of Breakwater Models for Tsunami Overflow Tests

(a) Modelling details

Similar to the previous tests for earthquake loadings, the physical model of the prototype breakwater was constructed over a seabed composed of river sand. The seabed consisted of two distinct layers. The lower layer, representing dense soil or bedrock, had a relative density of 90%. Above it, the upper layer (with a relative density of 60%) was filled using the pluviation method. The conventional model diagram used for tsunami overflow tests is shown in Figure 7.10. In the case of the reinforced model, the sheet piles were deployed in the foundation soils near both the ends of the breakwater. The sheet piles were made of steel plates that can act as a cut-off fall to prevent seepage through the seabed soils under tsunami overflow. Once seabed construction is done, the reinforced breakwater is constructed. This breakwater has a crown wall with shear keys and gabions. The crown wall with the shear key was placed on top of the breakwater to protect the crest from scouring and lateral force/sliding caused due to tsunami overflow. The presence of shear keys beneath the crown wall functions to reduce the lateral displacement of the crown wall under tsunami overflow. The gabions were placed over the armour layer of the rubble mound breakwater. The schematic representation of reinforced model is shown in Figure 7.11.

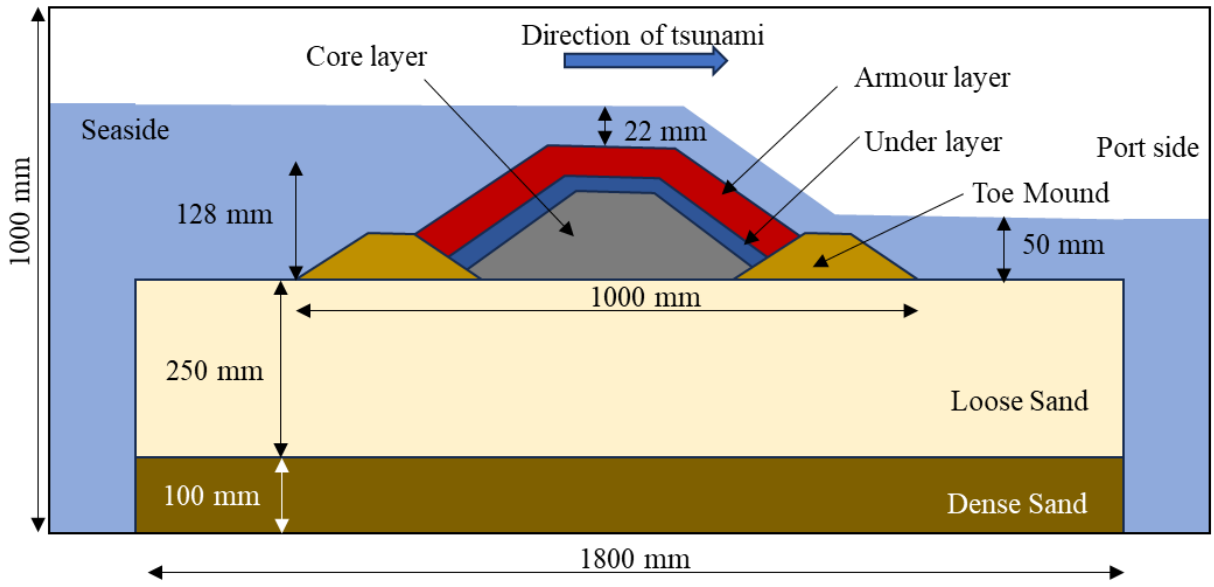

Fig. 7.10 Physical modelling of the conventional model without crown wall

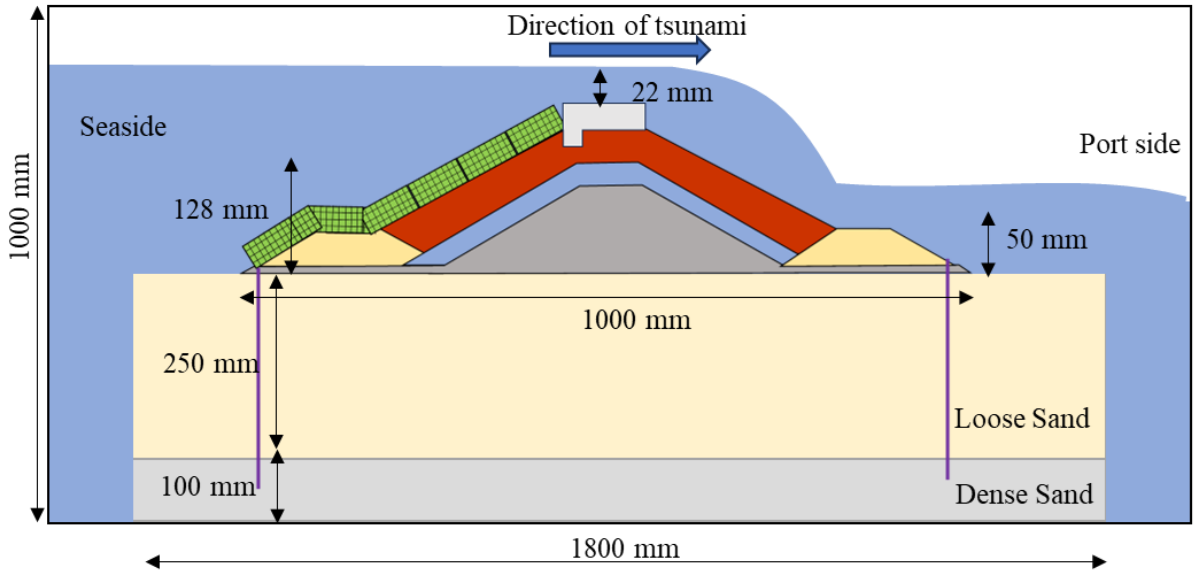

Fig. 7.11 Physical modelling of the reinforced model for tsunami overflow tests

(b) Seawater levels for the Tsunami Overflow tests:

Table 7.4 Seawater levels during the tsunami overflow tests

Items	**Values**	
	Model (mm)	**Prototype (m)**
Before Tsunami		
Initial withdrawn sea water level	50	4
During Tsunami		
Height of tsunami wave	100	8
Seawater level on the seaside	150	12
Seawater level on the port side	50	4

In studying tsunamis' influence on coastal infrastructure, it is essential to acknowledge that tsunamis often follow seismic activity. To recreate this scenario in laboratory experiments, researchers conduct the tsunami overflow test. During the test, water pumps are strategically positioned on both the seaside and port side of the breakwater. Their purpose is to maintain the seawater level. The simulated tsunami wave's height is set at 100 mm above the seawater level on the seaside. Prior to initiating the tsunami overflow test, meticulous control ensures that the seawater levels on both sides of the breakwater remain at mean sea level above the seabed.

Table 7.4 details the sea water levels during tsunami overflow tests. The tsunami overflow was conducted intentionally for a prolonged duration to evaluate the performance of the reinforced breakwater model against the tsunami-induced seepage through the breakwater and seabed soils. The generated tsunami had a height of 100 mm above mean sea level, with the mean sea level at 96 mm (equivalent to 7.68 m in the prototype). Considering the common withdrawal of sea level before a tsunami, a 50 mm water depth (equivalent to 4 m in the prototype) was incorporated. The tsunami overflowed the breakwater at a depth of 22 mm (1.76 m in the prototype) for 30 minutes. The estimated height of the tsunami in this study corresponds to a level 1 tsunami (100 mm or 8 m in the prototype).

7.2.5 Instrumentations

For instrumentations, different types of transducers (see Fig. 2) were used in order to measure the various parameters during the experimentations:

(i) *Pore pressure transducers:* Pore pressure transducers are specialized sensors those are used to measure the pressure of water within soil pores. They are particularly very useful in the study of earthquakes related research, as they can record the variation in pore water pressure that occurs during seismic activity. The transducers have a measurement range of 0 to 600mbar (0 to 60kPa), allowing them to monitor changes in pore water pressure over a wide range. These transducers work on the principle of piezometry, which measures the height of water movement against gravity (h_w). The transducer can accurately determine the pore water pressure by measuring the height of water in the pores. The pore water pressure is determined using the following equation,

$$P = \rho_w g h_w \qquad \textbf{(1)}$$

Where, p = Saturated pore water pressure in kPa,

ρ_w *= unit weight of water (kN/m^3)*

h_w *= Rise in water level*

(ii) *Accelerometers:* Accelerometers are special type of sensors which measure accelerations and vibrations. They are highly sensitive to even small changes in strain and acceleration, which makes them useful in detecting earthquakes and soil movements. The available sensors have a wide range of measurement capabilities, with a maximum measurement of ±1g and a sensitivity of 300mV/g (Akarsh et al. 2024c). The sensitivity of the accelerometer allows it to detect even the smallest vibrations and movements accurately. To ensure accurate measurements, accelerometers are calibrated by the manufacturer or provider

before they are used. This calibration process helps to eliminate any discrepancies in the sensor's readings, ensuring that the output accurately reflects the actual acceleration and vibrations.

(a) LVDT

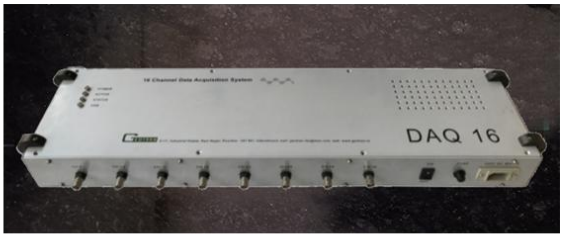

(b) Data Acquisition (DAQ) system

(c) Digital Amplifier

(d) Pore Pressure Transducers

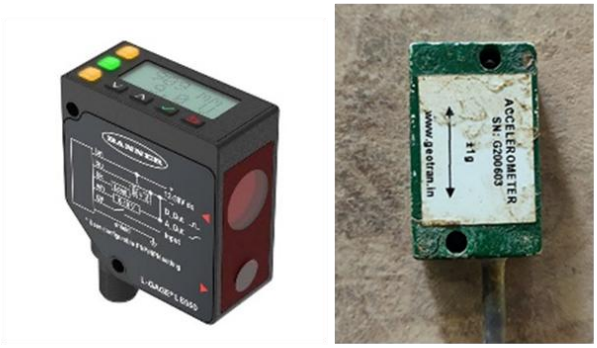

(e) Laser displacement gauge (f) Accelerometer

Fig. 7.12 Details of instrumentation for physical model tests

(iii) *Linear Variable Deformation Transform (LVDT):* An electromechanical transducer measures local small strain /deformation up to 100mm. It consists of an extended tip and an operated spring-mounted shaft. The LVDT is highly accurate and reliable, with a low temperature sensitivity and good linearity. The output of the LVDT can be easily interpreted using an amplifier and can be used for a variety of control and monitoring applications. The transducer senses the variation in the movement of the spring-attached shaft and transmits the signals to the DAQ system.

(iv) *Laser Displacement Gauge:* It is a highly sensitive distance-measuring transducer. It can be used to measure horizontal displacement or settlement of the breakwater during the earthquake loadings. The laser displacement gauge is an efficient and effective solution for precisely measuring displacements. It comes in a standard rectangular housing and has a wide range of detection capabilities, from 50mm to 5m.

7.2.5.1 Instrumentation layout for shake table tests

For the shake table experiment, a soil box with a modelling chamber measuring 1550 mm in length and 1000 mm in height, constructed from acrylic plates and steel frames, is employed. The shake table tests are conducted on a physical model situated within this soil box. Various transducers, such as pore water pressure transducers, accelerometers, displacement transducers, and laser displacement gauges, are strategically positioned at different locations. For the conventional model without a crown wall, the instrumentation layout is shown in Figure 7.13(a). The laser displacement transducers are utilized to measure the settlement and horizontal displacement of the breakwater (referred to as crest). One laser displacement transducer was used to measure the settlement as V at the centre of the crest. In order to measure the horizontal displacement, the movement of the aluminium sheet placed on the crest of the breakwater was considered and recorded by another laser displacement, and it was labelled as H. Five accelerations are meticulously recorded at multiple sites (A1 to A5) within the seabed layers and the breakwater by the accelerometers. Specifically, accelerometers A1, A2, and A3 are affixed at the top of the dense sand layer, within the loose sand layers, and on top of the loose sand layer of the foundation system, respectively. Accelerometers A4 and A5 are situated at the core and the crest of the RM breakwater. Furthermore, the four excess pore water pressures are observed at four distinct locations (P1 to P4) via pore water pressure gauges. Pore water pressure gauges P2, P3, and P4 are positioned within the loose sand layer, while P1 is precisely placed within the core.

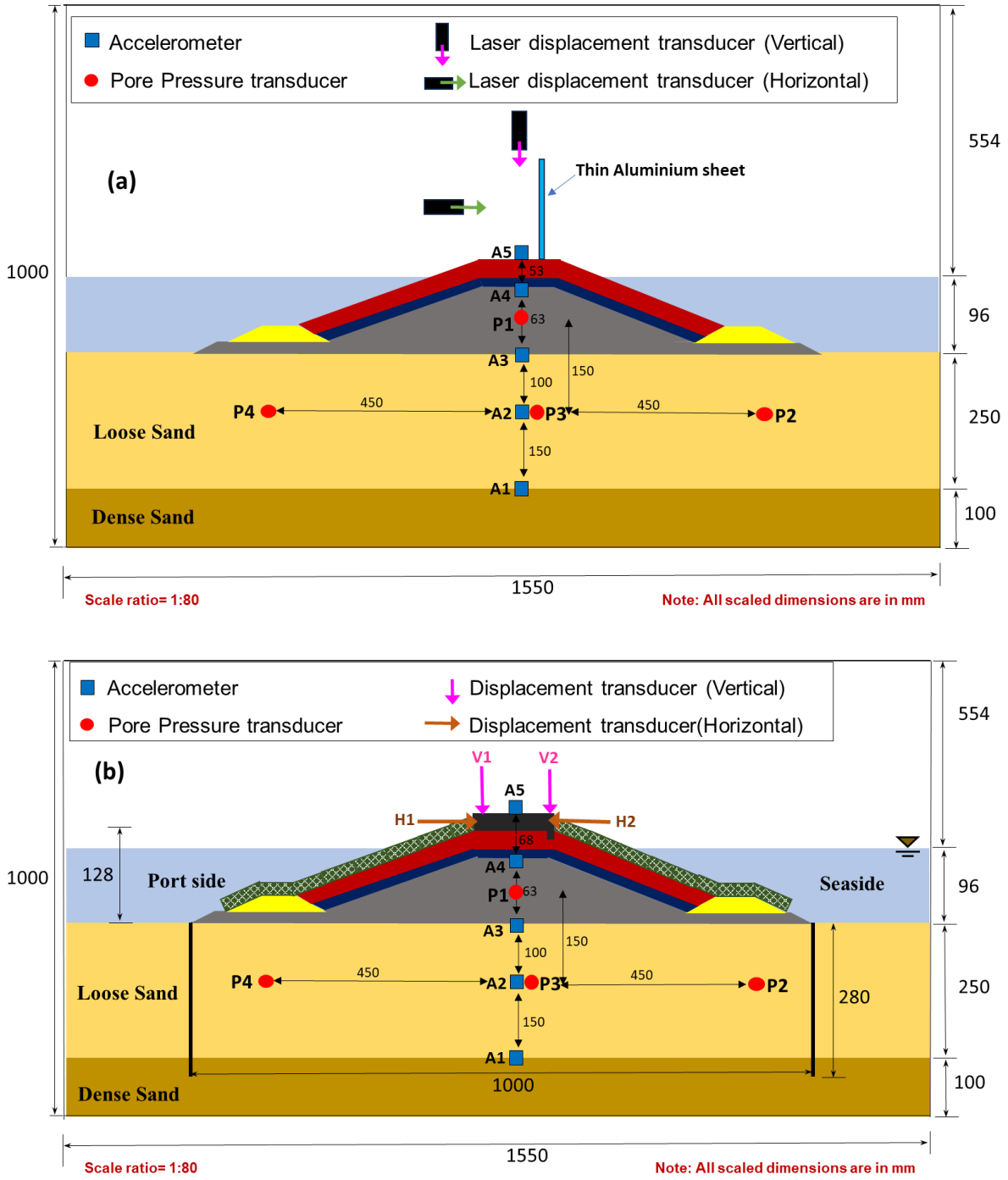

Fig. 7.13 Instrumentation: (a) Conventional model without crown wall and (b) Reinforced model

Figure 7.13(b) shows the reinforced model's instrumentation layout. To measure the settlement and horizontal displacement of the breakwater, measurements were taken at two specific points of the crown wall. Two displacement transducers were employed at V1 and V2 to measure the settlement of the crown wall. Additionally, the horizontal displacement of the crown wall was monitored using two displacement transducers at H1 and H2. The

crown wall, constructed from three segments of concrete blocks, had measurements for settlement and horizontal displacement explicitly taken for the middle concrete block. For the horizontal displacement values, a positive direction was assigned to signify leftward movement of the crown wall. The pore water pressure was measured at four locations, P1 to P4. Five accelerometers are used to record acceleration-time histories at 5 locations (A1 to A5) during the tests. All the transducers were connected to a dynamic amplifier and data acquisition system to obtain respective data.

7.2.5.2 Instrumentation layout for tsunami overflow tests

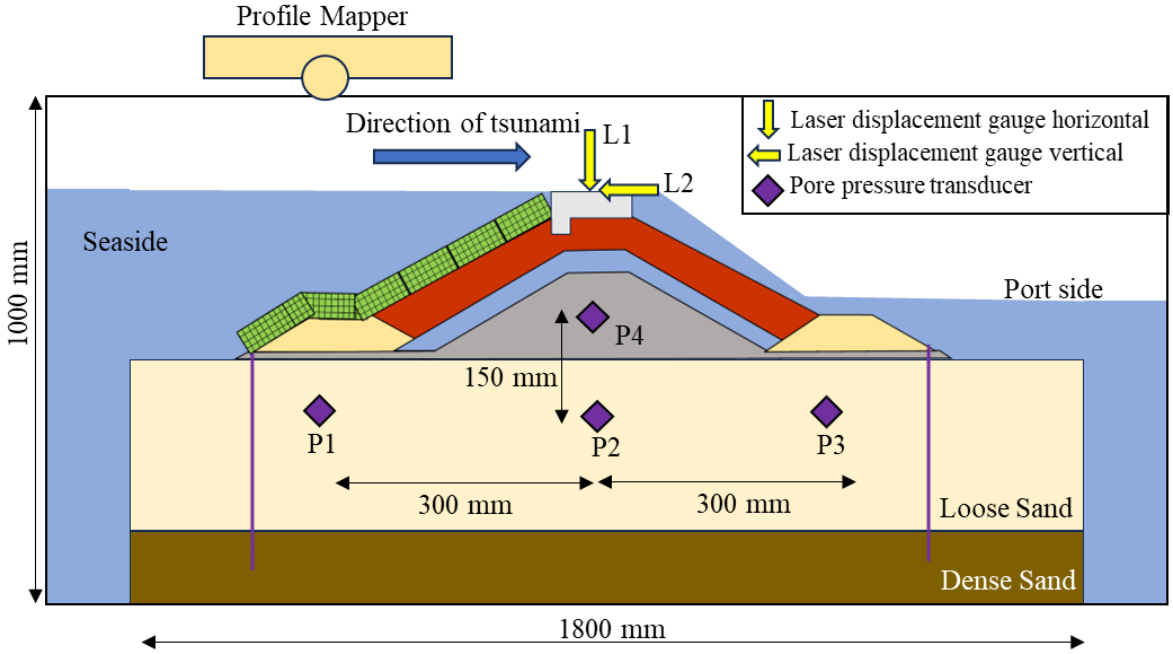

Fig. 7.14 Instrumentation for tsunami overflow test on the reinforced model

This section outlines the instrumentation setup used in the experimental investigation of tsunami resilience in rubble mound breakwaters. Sensors such as accelerometers, displacement transducers, laser displacement gauges, and pore water pressure transducers, were strategically deployed. Additionally, a profile mapping system facilitated the assessment of scouring effects during the tsunami overflow. The instrumentation employed in the experiments is represented in Figure 7.14. The horizontal displacement and vertical settlements of the rubble mound crest were monitored by using the displacement transducers and laser displacement gauges (L1 and L2). Four pore water pressure transducers (P1 to P4) were strategically deployed to monitor the pore water pressures within the seabed soils and the breakwater. Throughout the physical model tests, data from these sensors were continuously recorded. Additionally, a profile mapping system was utilised to quantify the

scouring on the conventional breakwater during the tsunami overflow. The breakwater was scanned both before and after the tsunami overflow, and the scanned profiles were then compared to determine the extent of damage incurred on the breakwater during the overflow. To collect the respective data, all transducers were connected to a dynamic amplifier and a data acquisition system.

7.2.5.3 Profile Mapper

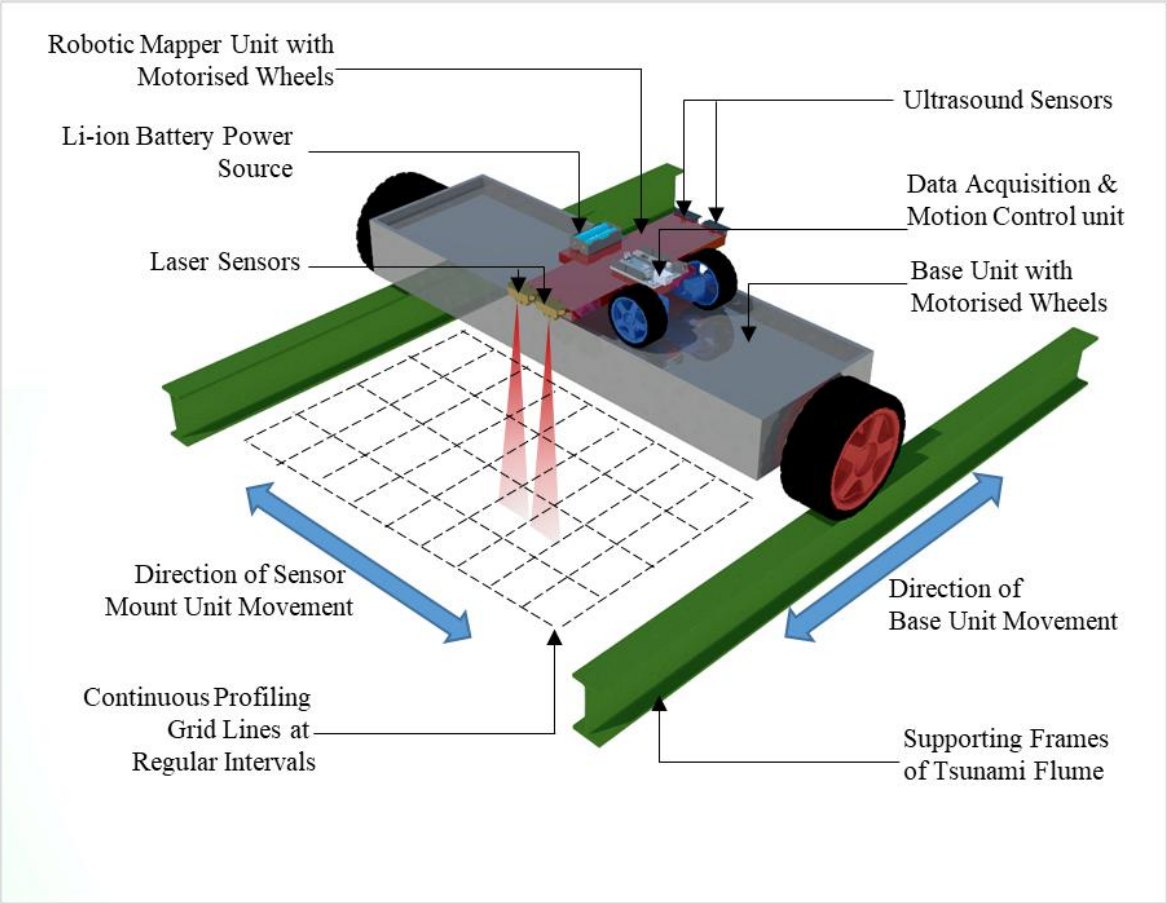

Fig. 7.15 Schematic representation of profile mapper (Sajan et al. 2024b)

The development of this specialized mapping device is aimed at providing a more accurate assessment of the damage caused to a RM breakwater by a tsunami. The device uses non-contact distance measuring gauges and advanced computational tools to compare the 3D profile of the RM before and after the tsunami. This significantly improves over the traditional semi-empirical equations used to estimate the damage, as the mapping device provides a much more precise evaluation. The device has two units capable of moving in both the X and Y planes, and each unit is fitted with motorized wheels for forward and backward movement, as shown in Figure 7.15. The base unit is positioned on top of a tsunami flume and moves

along the support frames to complete the scanning process. On the other hand, the sensor mount unit is placed on top of the base unit and is equipped with laser displacement and ultrasound distance measuring sensors. The scanning process involves moving the base unit along the length of the RM, and then shifting the sensor mount unit one grid length along the width of the RM. To ensure accurate measurements, the movement of the base unit is calibrated at a fixed speed, and the position coordinates of the sensors are calculated with precision. The data obtained is then exported in real-time through wireless communication and processed using 3D point cloud processing open-source software, CloudCompare. The use of this mapping device provides a more accurate assessment of the damage caused to the RM by the tsunami, as it takes into account the changes in the 3D profile of the RM before and after the tsunami (Sajan et al. 2024b; 2025).

8. RESULTS AND DISCUSSION

8.1 Performance of physical models against earthquake loadings

A comprehensive analysis was conducted to investigate the behaviour of the conventional breakwater model (without crown wall) subjected to earthquake loadings. Furthermore, a comparative analysis was carried out to assess the performance of the reinforced breakwater under the same earthquake loading conditions. The earthquake loadings include two foreshocks and one main shock. The primary focus of this evaluation was to examine the effectiveness of the reinforced foundation in mitigating excess pore water pressure, as well as reducing the settlement and horizontal displacement of the breakwater. The details about the deformation pattern studies are presented in subsequent sections.

8.1.1 Acceleration-time histories

The acceleration-time histories were recorded using five accelerometers positioned at different locations (A1 to A5) to monitor the propagation of seismic waves through the seabed soils and breakwater. Figure 8.1 represents the acceleration-time history observed during the first foreshock (acceleration amplitude= 0.1g, frequency = 8Hz, and duration =8s) for the conventional model (without a crown wall) and the reinforced model. The peak acceleration recorded in the dense sand layer (A1) is notably lower when compared to the peak acceleration in the loose sand layer (A3) and crest of the breakwater (A5). This was mainly due to the fact that the closely packed nature of the dense sand layer, characterized by a lesser void ratio, resulted in a dampening effect on the incoming seismic waves. In the case of the conventional model, the accelerations measured at A2 (0.06g) and A3 (0.08g) were relatively higher than

the acceleration measured at A1 (0.05g), which is shown in Figure 8.1(a). As seismic waves propagate from denser soil layers to loose soil layers, they undergo alterations in their velocity. The velocity slows down within the loose soil layers, leading to an increase in the amplitude of seismic waves. This amplification in amplitude, in turn, results in higher levels of acceleration. Additionally, within these loose soil layers, the energy dissipation mechanisms such as soil particle friction and pore fluid movement operate less efficiently compared to denser soils. This contributes to the reduced attenuation of seismic waves, allowing them to propagate with minimal energy loss, ultimately leading to amplification. Furthermore, an acceleration of 0.07g was recorded at A4 for the sinusoidal wave. This reduction in acceleration within the granular saturated coarse material is attributed to the generation of cyclic shear stresses, leading to fluctuations in effective stresses. Finally, the wave's acceleration increased to 0.09g at A5. Out of all the recorded accelerations, the highest value was recorded at A5, which corresponds to the crest of the breakwater. Comparatively, when examining the acceleration histories of the reinforced model in contrast to the conventional model, a noticeable reduction in peak acceleration was evident across all five accelerometers as shown in Figure 8.1(b). There was no significant change in the acceleration-time histories at A1 in the reinforced model. Meanwhile, the acceleration amplitude decreased by 20% and 33% at A3 (top of loose sand) and A5 (crest). This significant reduction in acceleration can be attributed to the presence of sheet piles in the foundation soils.

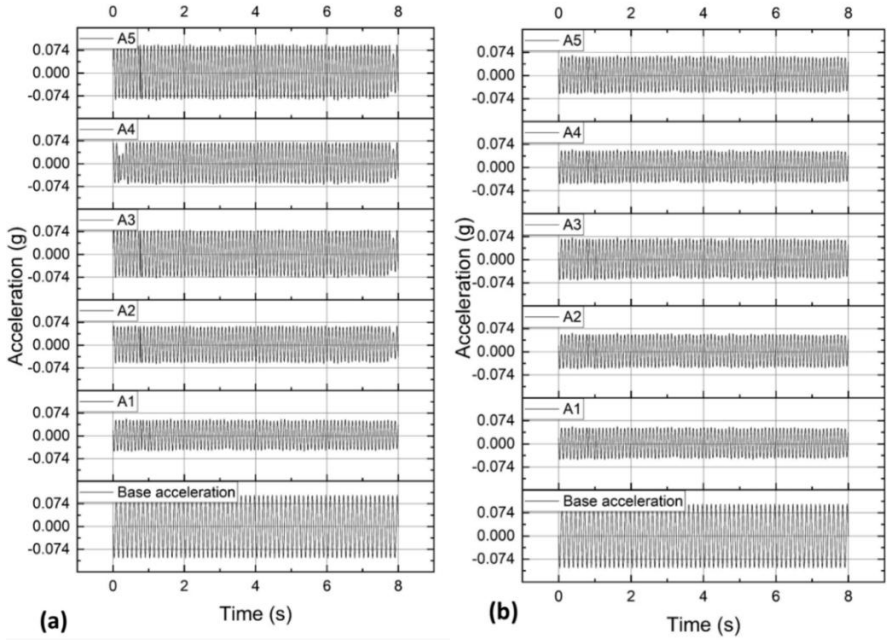

Fig. 8.1 Acceleration-Time histories for foreshock (0.1g): (a) Conventional model without crown wall and (b) Reinforced model

The acceleration-time history observed during the main shock (acceleration amplitude= 0.4g, frequency = 8Hz, and duration =8s) for conventional model without crown wall and reinforced model is presented in Figure 8.2. In conventional model, the peak acceleration recorded at A2, A3, A4 and A5 was 0.25g, 0.35g, 0.33g and 0.38g as shown in Figure 8.2(a). Whereas, the acceleration amplitude at locations A2, A3, A4, and A5 in the reinforced model was reduced by 16%, 28.5%, 33.3%, and 26.4% respectively, compared to the conventional model during the main shock (see Figure 8.2(b)). The reduction in acceleration amplitude at location A2 and A3 can be attributed to the presence of sheet piles in the foundation soils, which contribute to the reduction of acceleration amplification. Sheet piles provide lateral support to soil and resist horizontal forces induced by seismic shaking. By resisting soil movements and displacements, they help to limit the lateral deformations and reduce the potential for acceleration. Also, the use of sheet piles introduces energy dissipation mechanisms. The frictional resistance between the sheet piles and the surrounding soil contribute to energy dissipation during seismic shaking, thereby reducing the transmitted accelerations. In both the cases, the maximum acceleration amplitude was measured at A5 (crest of the breakwater).

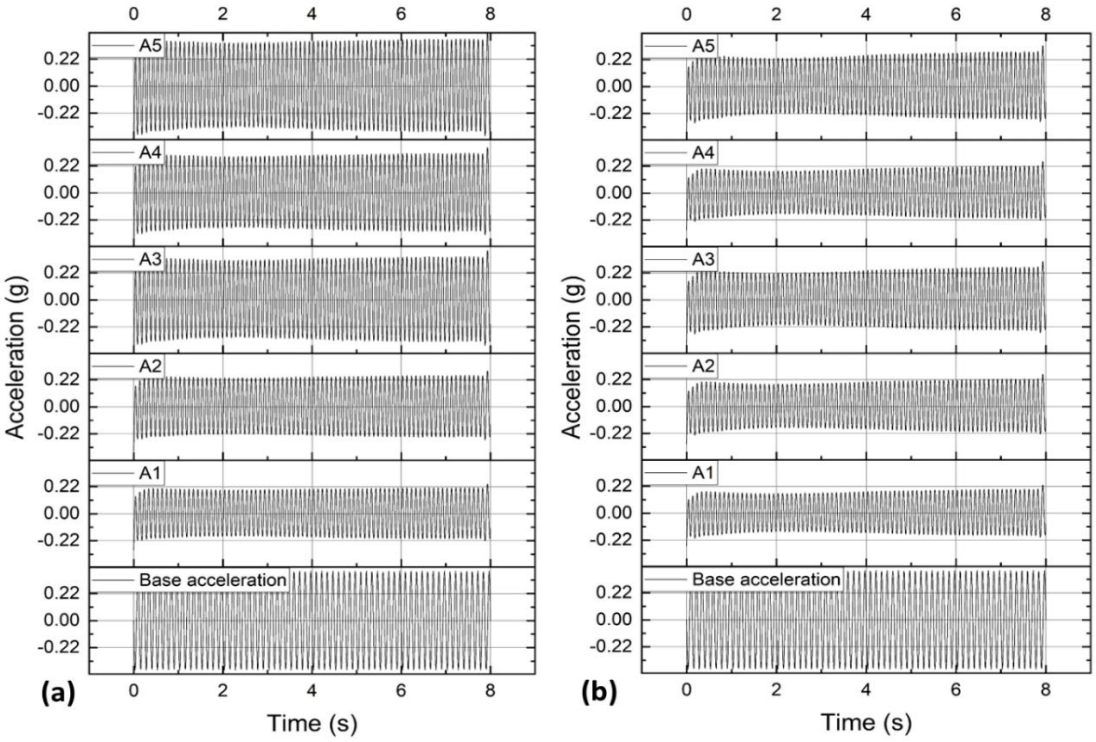

Fig. 8.2 Acceleration-Time histories for Mainshock: (a) Conventional model without crown wall and (b) Reinforced model

8.1.2 Effect of Acceleration Amplitude on Settlement

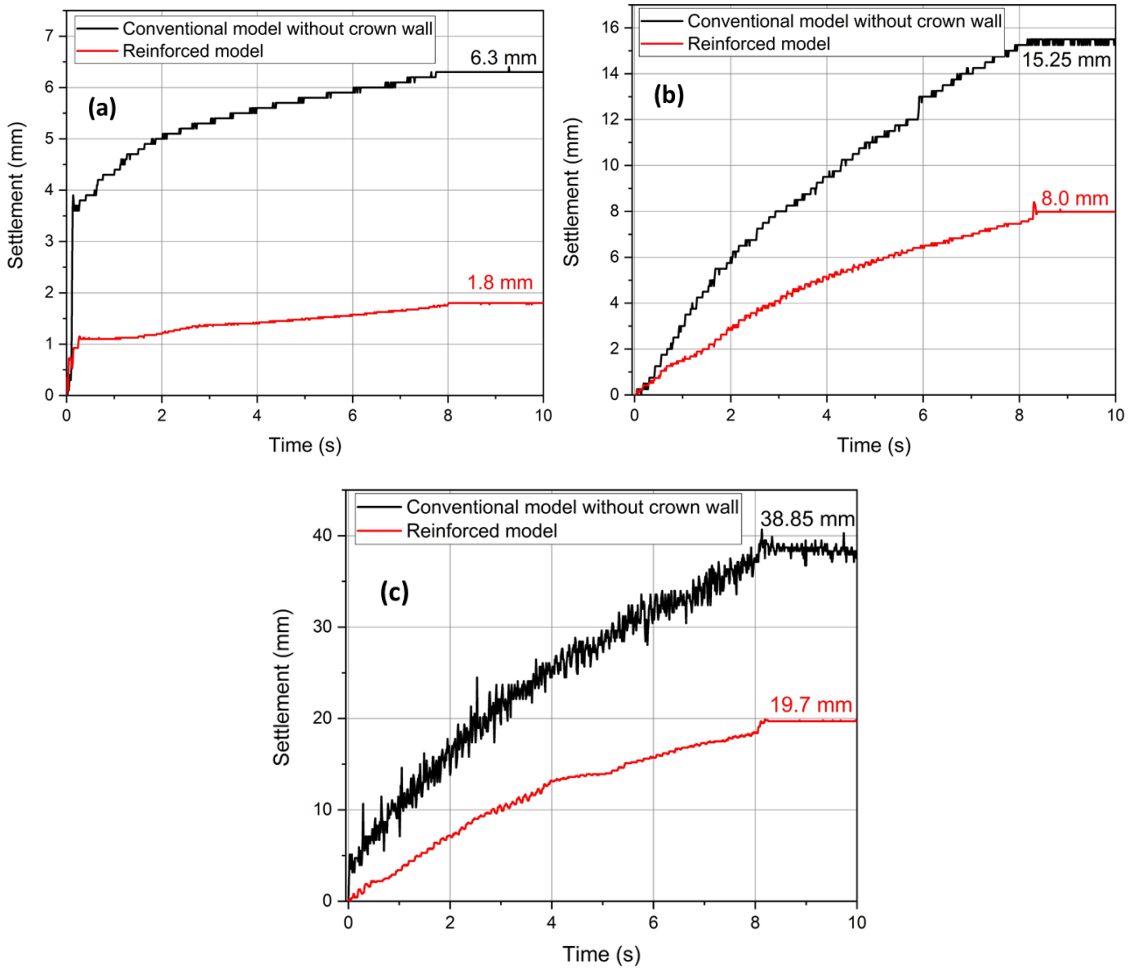

Fig. 8.3 Settlement of breakwater crest for conventional model and reinforced model: (a) first foreshock, a=0.1g, (b) second foreshock, a= 0.2g and (c) mainshock, a= 0.4g.

In the case of the conventional model (without a crown wall), settlement was measured using laser displacement transducers at the mid-location of the breakwater's crest (due to the absence of the crown wall). Whereas in the case of the reinforced model, the settlement was measured at the V1 and V2 locations of the crown wall (shown in Fig. 7.13(b)). Hence, to compare the effectiveness of the reinforced model, the average value of settlement measured at V1 and V2 was considered, and it is compared with the settlement measured for the conventional model. In the conventional model without a crown wall, the settlements observed during the first foreshock (0.1g), second foreshock (0.2g), and the main shock were 6.3 mm, 15.25 mm, and 38.85 mm, respectively, shown in Figure 8.3. Notably, during the main shock, the crest of the breakwater experienced a settlement that was 516.7% greater compared to the first foreshock. This significant settlement of the breakwater was attributed to the generation of higher excess pore water pressure during the main shock, leading to a decrease in the bearing capacity of the

foundation soils. Consequently, greater deformation and lateral movements of the seabed sand and stones comprising the breakwater body occurred when compared to the first foreshock. However, when the breakwater was reinforced with the sheet piles in the foundation soils, the settlements were reduced by 71.43%, 47.5%, and 49.3% during the first foreshock, second foreshock, and the main shock, respectively (ref. Figure 8.3(a) to Figure 8.3(c)) when compared to conventional breakwater. The introduction of sheet piles reduced the horizontal displacement of the seabed soils beneath the breakwater mound in the reinforced model, an element that is absent in conventional breakwater. This limitation in lateral movement was the reason for minimizing the excessive settlement. Consequently, the reinforcement notably minimized the vertical displacement of the breakwater material under input seismic loads.

8.1.3 Effect of Acceleration Amplitude on Horizontal Displacement

The horizontal displacement of the conventional breakwater was measured using a laser displacement transducer; and to measure the horizontal displacement, a thin aluminium sheet was placed on the crest to measure the same as shown in Figure 7.13(a)-instrumentation layout. The horizontal movement of the thin sheet represents the horizontal movement of the breakwater in the case of the conventional model (due to the absence of a crown wall, this arrangement has been made). However, in the case of reinforced breakwater, the horizontal displacement was measured at the H1 and H2 locations of the crown wall. For comparing the effectiveness of reinforcement, the average value of H1 and H2 observed during various earthquake loadings in the reinforced model was compared with the horizontal displacement of the crest of the conventional breakwater. Figure 8.4 shows the horizontal displacements of the breakwater for foreshocks and the mainshock. The conventional breakwater without a crown wall witnessed a horizontal displacement of 2.7 mm, 6.0 mm and 11.0 mm during the first foreshock, second foreshock and the main shock. Notably, the effect of acceleration amplitude is significant, with the conventional model experiencing a displacement increase of over 300% during the main shock compared to the first foreshock. As acceleration amplitude increased, along with seismic inertial forces, hydrodynamic forces acted on the breakwater slopes, leading to lateral movement of the rubble within the breakwater body. However, with the help of reinforcing elements, there was a reduction in the horizontal displacement of the breakwater by 63%, 28.3% and 37.3% during the first foreshock, second foreshock and the main shock, respectively, comparable to the conventional model (ref. Fig. 8.4(a) to Fig. 8.4(b)). The main reason behind such reduction is the use of sheet piles in the foundation sea bed. These sheet piles imparted lateral confinement within the seabed beneath the rubble mound body,

which reduced the mound's lateral displacement under the earthquake loadings. In addition to this, the stone-filled gabions surrounding the outer slopes of the breakwater have added extra stability to the mound by imparting higher frictional contact areas and additional weight that resisted the lateral displacement of the breakwater. Hence, the proposed model could help resist the impacts of earthquake loadings effectively.

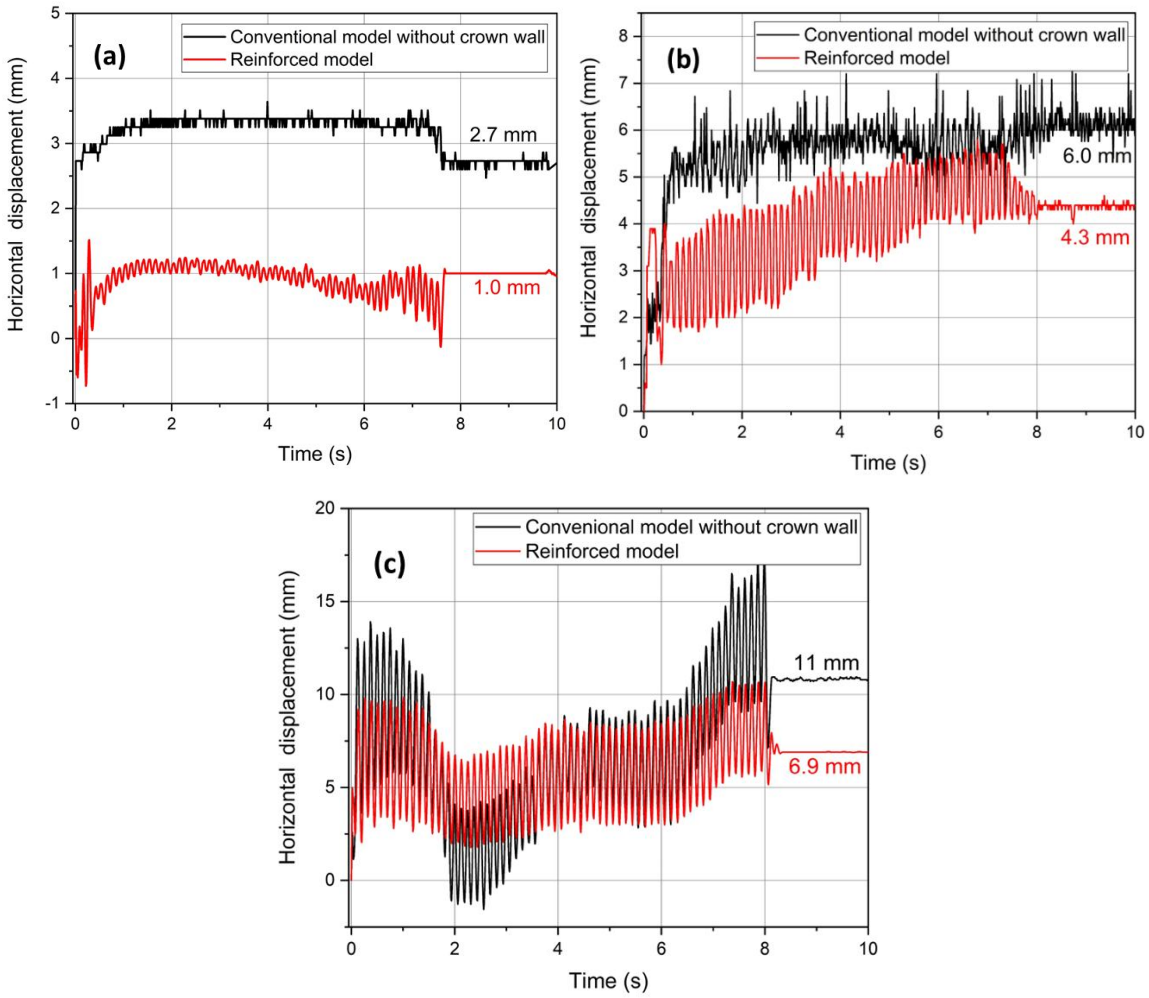

Fig. 8.4 Horizontal displacement of breakwater crest for the conventional model and reinforced model: (a) first foreshock (0.1g), (b) second foreshock (0.2g) and (c) mainshock (0.4g)

8.1.4 Generation of Excess Pore Water Pressure (EPWP)

The excess pore water pressure (EPWPs) developed during the earthquake loadings, and the same were analysed at four different locations, as shown in Fig. 7.13. To know the effects of the earthquake on EPWP inside the breakwater body, a transducer was placed at the centre of the breakwater body (P1). Pore water pressure transducers (P2, P3, P4) were also placed in the seabed foundation soils to see the effects of the earthquake loadings of EPWP. During the first foreshock, the maximum EPWP of 0.25 kPa was observed at P1, and it was increased by 1.14

kPa during the main shock loading in the conventional model without crown wall (see Figure 8.5). However, in the case of the reinforced model, the maximum EPWP developed was reduced to 0.11 kPa and 0.69 kPa during the foreshock (0.1g) and the main shock (0.4g) respectively, due to an increase in the stiffness of foundation soil, thereby a reduction in the deformation of the breakwater. Also, the presence of gabion along the slopes reduced the horizontal displacement of the breakwater, thereby increasing the stability of the breakwater during earthquake loadings. Due to lesser shear strains in the breakwater, the EPWP generated was less in the case of the reinforced model than the conventional model without a crown wall.

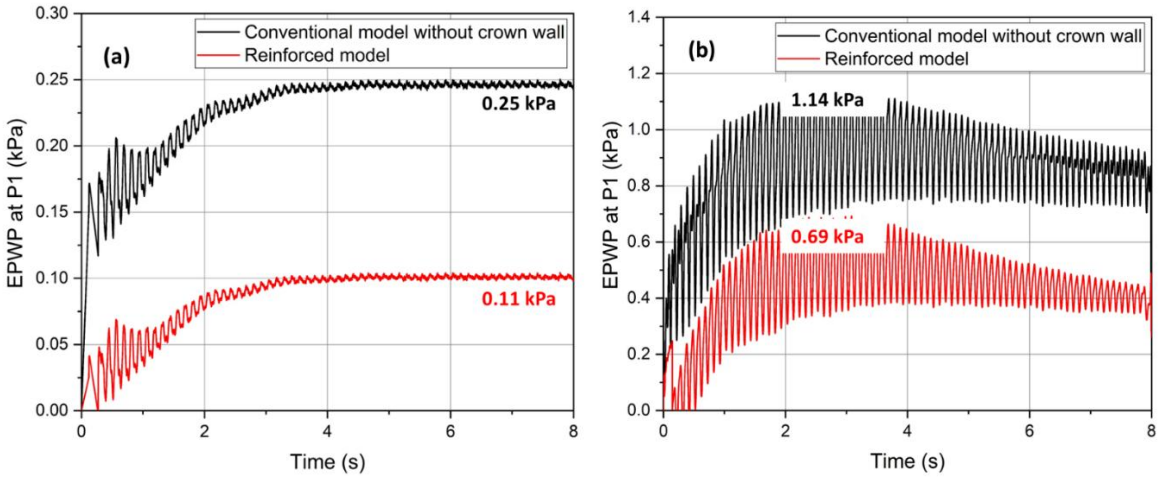

Fig. 8.5 EPWP measured at P1 for breakwater: (a) foreshock (0.1g) and (b) main shock (0.4g)

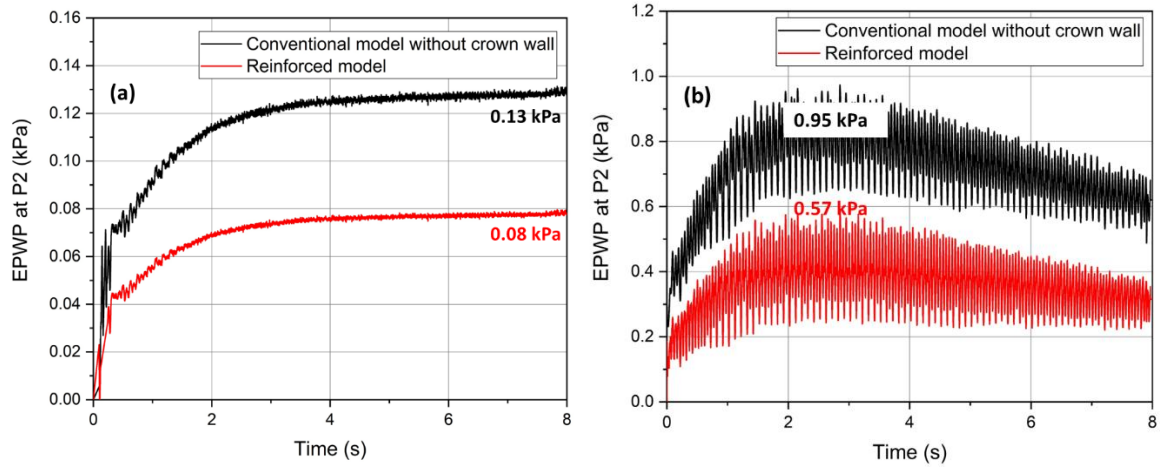

Fig. 8.6 EPWP measured at P2 for breakwater: (a) foreshock (0.1g) and (b) main shock (0.4g)

The EPWP observed during the foreshock (0.1g) and the mainshock (0.4g) at P2 and P4 are shown in Figure 8.6 and Figure 8.7, respectively. It was observed that maximum EPWP developed at P2 was 0.13 kPa, and it was increased by 0.95 kPa during the main shock in the

conventional model without a crown wall. Whereas in the case of the reinforced model, the maximum EPWP was reduced by 38.5% and 40% during the first foreshock and the main shock, respectively. Also, at P4, the maximum EPWP developed was 0.16 kPa, and it was increased by 0.85 kPa during the main shock in the conventional model (without a crown wall). But in the reinforced model, maximum EPWP developed was reduced by 43.8% and 40% during the first foreshock and the main shock respectively. These two locations in foundation soils are very near to the sheet piles. Due to increase in confinement of foundation soil, stiffness of soils increases and which attributed to reduction in EPWP generation at this location of reinforced model.

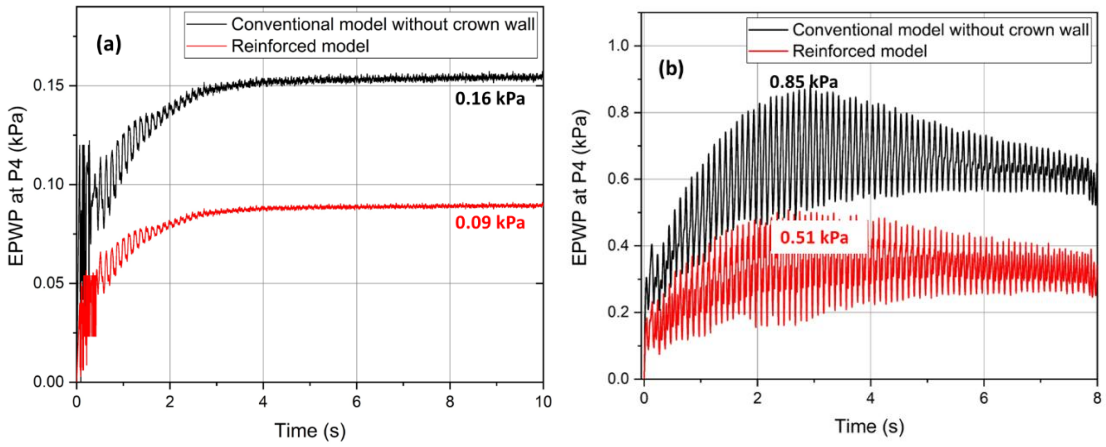

Fig. 8.7 EPWP measured at P4 for breakwater: (a) foreshock (0.1g) and (b) main shock (0.4g)

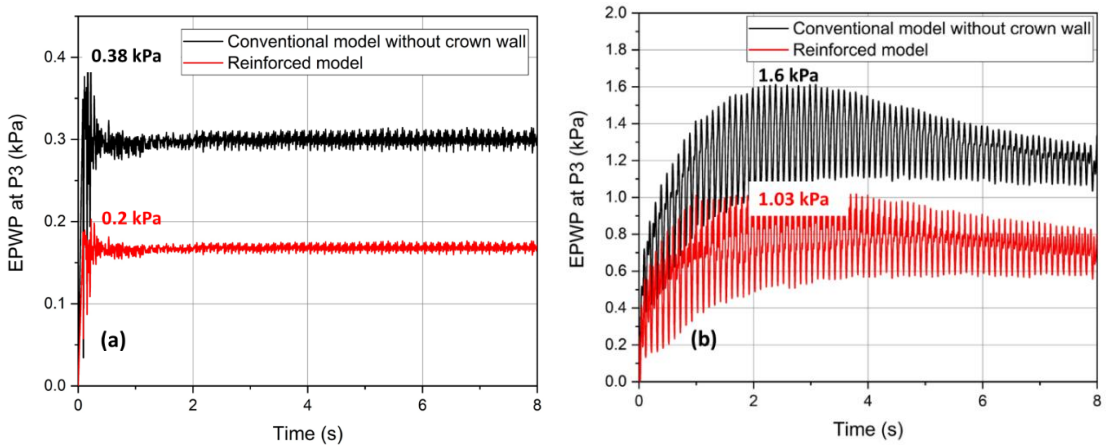

Fig. 8.8 EPWP measured at P3 for breakwater: (a) foreshock (0.1g) and (b) main shock (0.4g)

At the P3 location (beneath the breakwater), the maximum EPWP developed was 0.38 kPa and 1.6 kPa during the first foreshock and the mainshock respectively for the conventional model

(without crown wall). During the mainshock, EPWP observed was 4.2 times more than that during the first foreshock as shown in Figure 8.8(a) and Figure 8.8(b). As P3 lies beneath the breakwater body, the concentration of static weight would be larger, and due to seismic action, the settlement of the foundation would be more significant. Hence, the effect of the main shock on the increase in EPWP was significantly greater in the case of the P3 location comparable to other points. Also, the earthquake intensity plays a major role in the increase of EPWP, as one can observe from Figure 8.5 to Figure 8.8, and the main shock imparts a larger elevation in EPWP value at all the locations. The increase in EPWP could cause larger cyclic shear stresses and shear strain in the foundation of the rubble mound, and the bearing capacity of the soil could decrease. Ultimately, the soil starts to settle, allowing the breakwater to deform in all directions and affecting the stability of the breakwater, which was observed in the conventional breakwater model. At the P3 location of the reinforced breakwater, the model exhibited a substantial reduction in excess pore water pressures (EPWPs) compared to the unreinforced breakwater. The maximum EPWP developed was reduced by 47.4% and 35.6% during the first foreshock and the main shock compared to the unreinforced case (see Figure 8.8). This reduction was primarily attributed to the implementation of sheet piles in the foundation, which resulted in a decrease in the peak acceleration of input loadings. Additionally, the sheet piles effectively resisted lateral deformation of the surrounding soils during the earthquake event. Furthermore, the presence of an improved seabed beneath the breakwater played a crucial role in limiting the downward deformation of the rubble mound. Consequently, this countermeasure contributed to a reduction in shear strain experienced by the foundation soils. These factors collectively contributed to a decrease in shear strain and subsequently led to lower EPWP values at all the locations of the reinforced foundation as compared to the unreinforced foundation.

8.1.5 Deformation Pattern Studies

The deformation behaviour of the RM breakwater was comprehensively analysed through the photographs and videos obtained from a specialized high-resolution camera. The earthquake input loadings were given in the form of fore shocks (a= 0.1g and a=0.2g), and the main shock (a=0.4g).

(a) Conventional model without crown wall

The deformation patterns observed before and after earthquake loadings for the conventional model without a crown wall is shown in Figure 8.9(a) and Figure 8.9(b), respectively. The breakwater components were differentiated with different colours of variable-sized rubbles to observe changes during the earthquake loadings. In the foundation soil layers (especially loose sand), the soil deformation can be seen by the displacement of red-coloured sand. The white dotted lines were marked on the soil box to represent the model outline. During the first foreshock (a=0.1g), the breakwater exhibited minor changes, such as distortion in the arrangement of the armour rubbles. However, when the second foreshock (a=0.2g) occurred, noticeable changes were observed in the position of breakwater components. These included a reduction in crest height due to compaction of the core material and distortion in the shape of armour layer and underlayer. Also, there was lateral spreading of the armour rubbles on both the seaside and port side. The seismic loadings at the base of the model induce inertial forces and hydrodynamic forces.

Later, the input acceleration amplitude was increased to 0.4g (main shock). During the main shock (a=0.4g), the maximum EPWP within the breakwater (measured at P1) exhibited an increase from 0.25 kPa to 1.14 kPa, while in the foundation soils beneath the mound (measured at P3), it increased from 0.38 kPa to 1.6 kPa, as observed in comparison to the first foreshock (a=0.1g). It was seen that, the increase in the acceleration amplitude increased the magnitude of EPWP. This increase in EPWP had a direct impact on the settlement behaviour of the soil. Under earthquake loading conditions, the presence of water in the void spaces of the soil exerted pressure on the sand particles. The magnitude of this pressure was directly proportional to the applied load. Upon the release of this pressure, i.e., when the excess pore water is expelled from the voids, the sand particles rearrange themselves, resulting in a decrease in volume. Ultimately, this volume reduction can result in a settlement. Hence, the sand experienced a loss of shear strength during the particle rearrangement. Thus, the bearing capacity of the soil decreases significantly. Ultimately, the seabed soils start to settle, allowing the breakwater to deform in all directions. As depicted in Figure 8.9(b), it was evident that the foundation soils exhibited settling, lateral spreading, and intrusion into the underlying lower layers (indicated by the red-coloured sand). Notably, the deformation of the seabed soils is primarily concentrated along the model's central axis, particularly beneath the core region. This deformation gradually decreased as one moved towards the toe region of the model. In the

vicinity of the toe area, distinctive seabed bulges were observed. The deformation was notably pronounced in the loose sand layers and gradually tapered off as it extended into the denser sand layers. Additionally, the seismic input motion had the potential to induce liquefaction in the foundation soils.

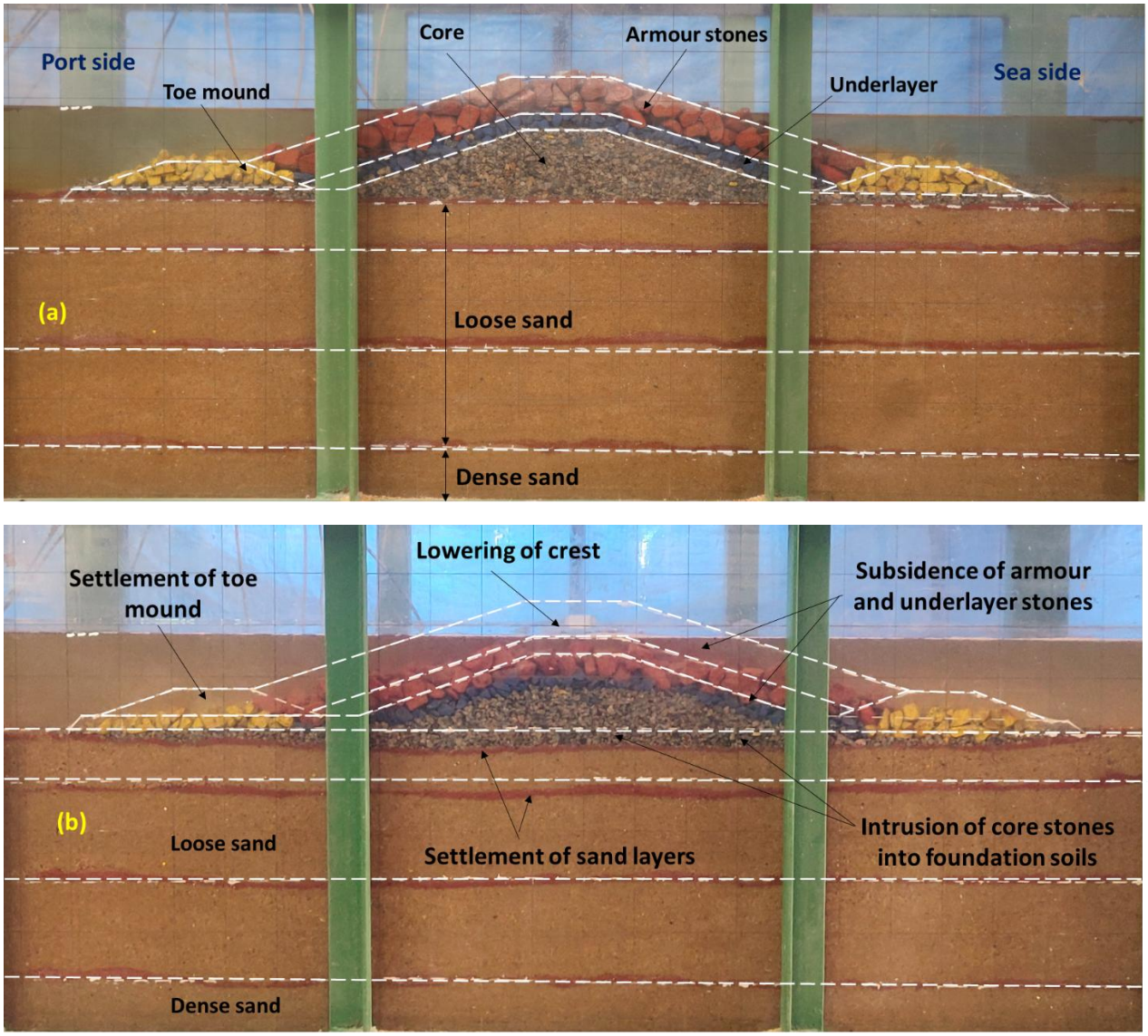

Fig. 8.9 Deformation of the conventional model: (a) before earthquake loadings and (b) after earthquake loadings

The deformation of foundation soils caused the constituent components of breakwater to deform in various directions. The development of shear strains during the earthquake loadings initiated the shear deformation and the slumping of core materials. As a consequence, during the main shock, the breakwater crest was settled by 38.85 mm (equivalent to 3.1 m in the prototype) and horizontally moved by 11 mm (equivalent to 0.9 m in the prototype). These observed settlement and horizontal displacement phenomena appeared to be influenced by the

volumetric strains developed within the breakwater. The deformations in the inner layers also induced various effects on the outer layers of the breakwater. On the both sides, the armour stones and underlayer stones vertically displaced and settled below the water level, forming heaps as they slumped and mixed. There was complete subsidence of breakwater components (amor, underlayer, toe mound, core stones) due to the impact of the main shock. During the main shock, the breakwater suffered a complete collapse, with sea waves overtopping it. In such a scenario, if a subsequent tsunami following the earthquake were to impact this already collapsed breakwater, critical questions about the effectiveness of this breakwater in safeguarding the port and harbour area would arise. Furthermore, the safety of coastal residents would also be a matter of concern. Hence, the breakwater should be reinforced with suitable reinforcing elements to make it resilient against earthquakes. Also, there is very much need for a crown wall for the existing conventional breakwater.

(b) Reinforced Breakwater model

The reinforced breakwater model before and after the earthquake loadings are depicted in Figure 8.10(a) and 8.10(b). During the first foreshock (0.1g), the countermeasure model remained unchanged. In the second foreshock (0.2g), minor alterations were observed, such as a slight tilt of the crown wall towards the port side. Subsequently, as the acceleration amplitude increased to 0.4g (main shock), substantial changes were observed in the reinforced model. These included slumping and shear deformation of the core material, sliding of the gabions on both sides of the breakwater, subsidence of armour and underlayer, settlement of crown wall and settlement and lateral spreading of the loose sand (indicated by the red-coloured sand in Figure 8.10(b)). Nevertheless, the addition of reinforcement led to an enhancement in the performance of the RM breakwater, reducing settlement by 47% and horizontal displacement by 37.3% compared to the conventional model without crown walls. Using gabions has reduced the rolling down of the amours on the slopes of breakwater and horizontal displacement. The reason might be the added weight, larger interface friction area, arrangement of gabions, etc. Also, including sheet piles at the extreme sides mitigated the lateral movement of the seabed. This restriction, in turn, resulted in a reduction in the settlement of the breakwater. The use of sheet piles running along the breakwater length serves as a cutoff wall or barrier, impeding the movement of sand and water. This effect led to a diminished loss in bearing capacity compared to the conventional breakwater. This is evident through the 35.6% reduction in excess pore water pressure (EPWP) observed in the countermeasure breakwater compared to the conventional model. The significant EPWP reductions observed across different locations

beneath the breakwater validate the importance of implementing such measures to enhance the stability and resilience of coastal structures exposed to seismic events.

Also, the provision of crown wall comes to play its role after the earthquake loadings. In case of reinforced model, the crown wall placed above the armour stones remained above the sea level, in contrast to the conventional model where the crest of the breakwater was completely sunk. This highlights the loss of stability in the conventional model during the main shock earthquake. Hence, the utilization of the reinforced model stands as a viable solution for enhancing the breakwater's resilience against seismic activities.

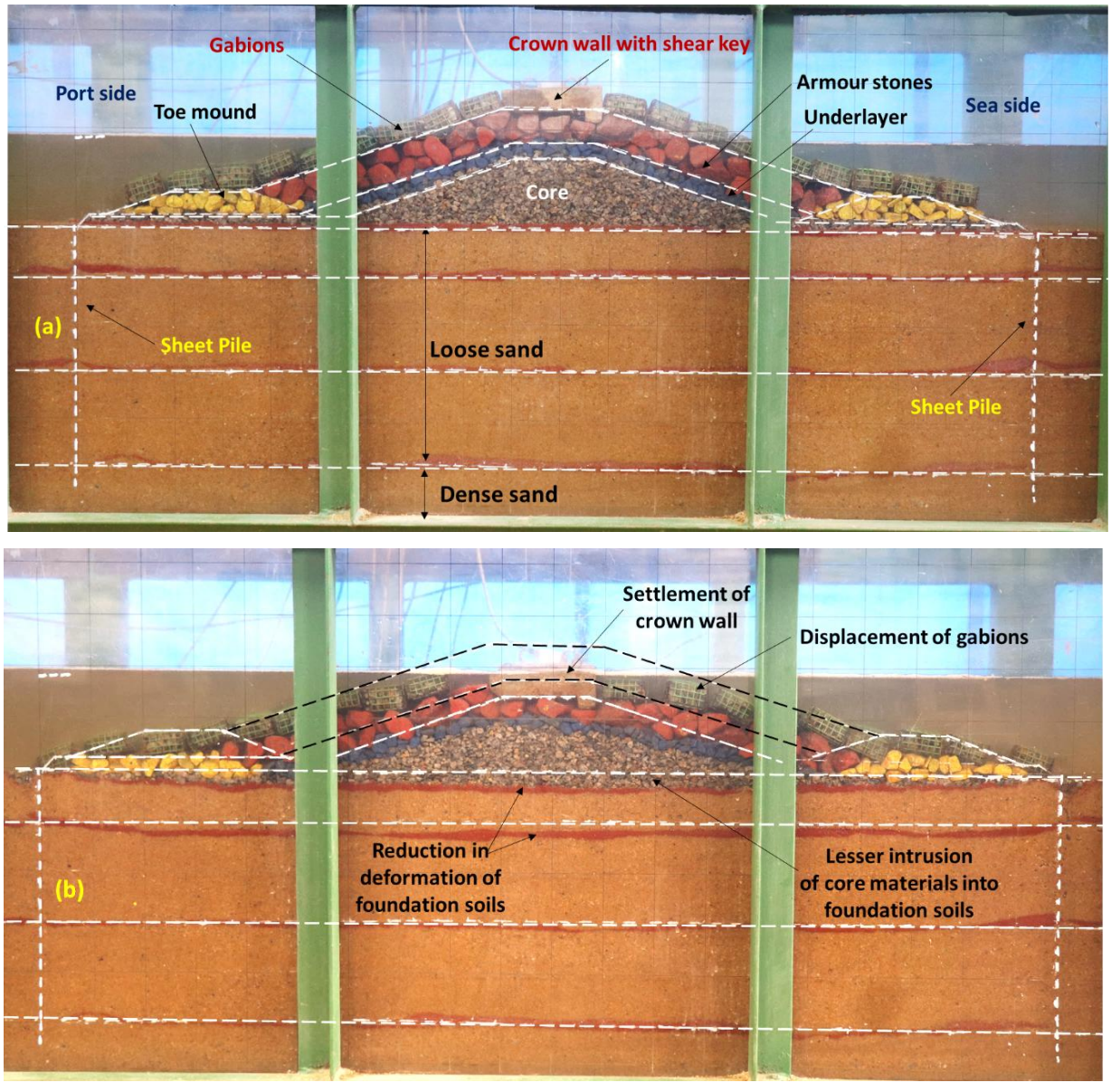

Fig. 8.10 Deformation of reinforced model: (a) before earthquake loadings and (b) after earthquake loadings

In summary, the combined reinforcing effects of these elements demonstrated exceptional effectiveness in substantially mitigating the deformations experienced by the reinforced RM breakwater. By reducing the settlement and horizontal displacement of the breakwater, the reinforcement measures showcased their capability to enhance the stability and structural integrity of the RM breakwater, particularly against high-amplitude earthquake loadings. These outcomes emphasize the importance of employing appropriate reinforcement strategies to fortify breakwaters, ensuring their resilience against potential seismic threats and safeguarding coastal regions from severe and life-threatening consequences.

8.2 Performance of Physical Models During Tsunami Overflow Tests

Numerous parameters were scrutinised during the tsunami overflow to assess the performance of the conventional breakwater. Key aspects included the settling of the crest, horizontal displacements, and the Incremental Pore Water Pressure (IPWP) that developed in the seabed soils. Additionally, the extent of scouring on the breakwater was thoroughly analysed through the utilisation of 3D profile mapping, comparing the breakwater's configuration before and after the tsunami overflow.

8.2.1 Settlement of the Crest

Emerged breakwaters are carefully engineered with a crest that extends above the freeboard level—an essential height threshold required to block tsunami overtopping. This elevated section serves as a physical barrier, preventing tsunamis from surging inland. However, when the breakwater height is compromised, it can allow tsunami waves to overtop the structure, significantly increasing the risk of coastal damage. This reduction in height is evaluated in terms of crest settlement during tsunami overflow tests, as illustrated in Figure 8.11.

In case of the conventional breakwater without a crown wall (scaled representation of the NMPT breakwater), crest settlement was measured at the midpoint using laser displacement transducers. To isolate the effect of tsunami-induced deformation, the initial settlement caused by the self-weight of the structure was excluded from the analysis. Thus, the presented values specifically reflect the settlement resulting from tsunami overflow. It was observed that the crest underwent a vertical settlement of 20.3 mm, which corresponds to 1.62 meters in the prototype scale. Additionally, approximately 67% of the armour layer depth was eroded during the tsunami event. During the overflow tests, the conventional rubble mound breakwater exhibited notable deformation, including lateral displacement of rubble units and vertical subsidence of the crest. A significant increase in settlement occurred within the first 90 seconds

of tsunami action, resulting in substantial structural damage. This deformation was primarily attributed to excessive seepage through the breakwater and the intense horizontal forces exerted by the tsunami.

Figure 8.11 compares the tsunami-induced settlement of the conventional breakwater with that of the reinforced model. Settlement in both models was measured at the crest using laser displacement sensors. To enhance clarity, the graph displays only the settlement caused by tsunami loading, excluding initial self-weight settlement. The conventional model suffered significant erosion—nearly 67% of the armour layer—while the reinforced model demonstrated markedly improved resilience. The addition of gabions on the armour layer, which increased both the weight and contact area, substantially enhanced structural stability. As a result, the reinforced configuration achieved a 94% reduction in crest settlement compared to the unreinforced counterpart.

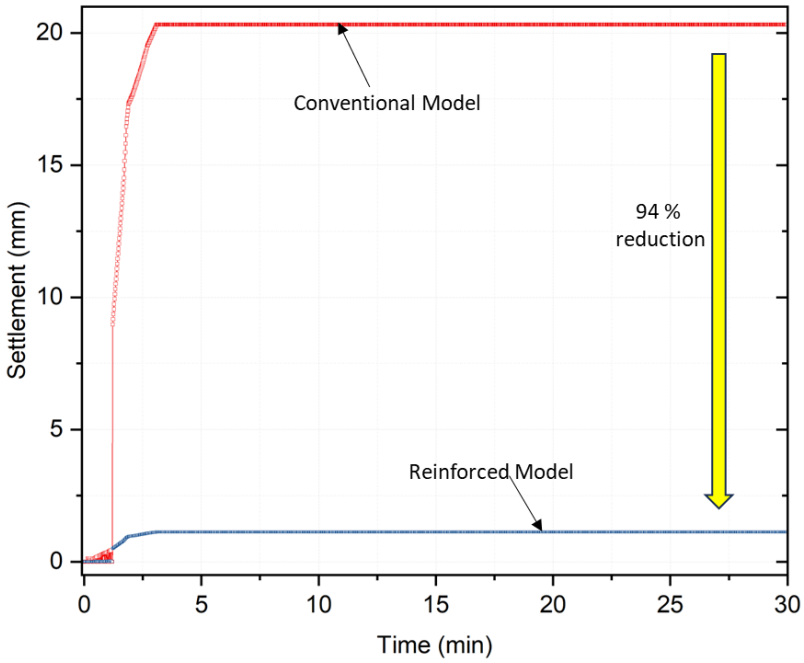

Fig. 8.11 Settlement of the crest for the conventional model

8.2.2 Horizontal Displacement of the Crest

Horizontal displacement at the crest of the conventional rubble mound breakwater presents a significant vulnerability during tsunami events, as it may expose the underlying core layer to direct impact. Given that the core is typically composed of lighter rubble, it is particularly susceptible to dislodgement under the dragging action of tsunami waves. Moreover, excessive seepage forces generated as seawater infiltrates the breakwater structure exacerbate this instability, contributing to lateral displacement of materials toward the harbour side. The

intense horizontal forces imparted by the tsunami further mobilize the armour stones, causing them to shift seaward, compromising the breakwater's structural integrity.

Minimizing or eliminating such horizontal displacements is critical to enhancing the resilience and effectiveness of coastal defence structures. Figure 8.12 illustrates the extent of crest displacement in a conventional breakwater during tsunami overflow, where the armour stones in the central crest region were displaced by 55.07 mm—equivalent to approximately 4.41 meters at prototype scale. This highlights the urgent need for targeted mitigation strategies.

To address this issue, integrating a crown wall equipped with a shear key has proven to be a highly effective reinforcement method. This structural enhancement significantly increases resistance to lateral forces, working synergistically with added gabions to counteract displacement. Adopting these design innovations has dramatically reduced crest displacement by as much as 98%, as shown in Figure 8.12. This outcome clearly demonstrates the effectiveness of combined structural reinforcements in fortifying breakwaters against tsunami-induced deformations. Such proactive and innovative measures are essential for improving coastal infrastructure's overall resilience and durability, particularly in regions prone to seismic and tsunami hazards.

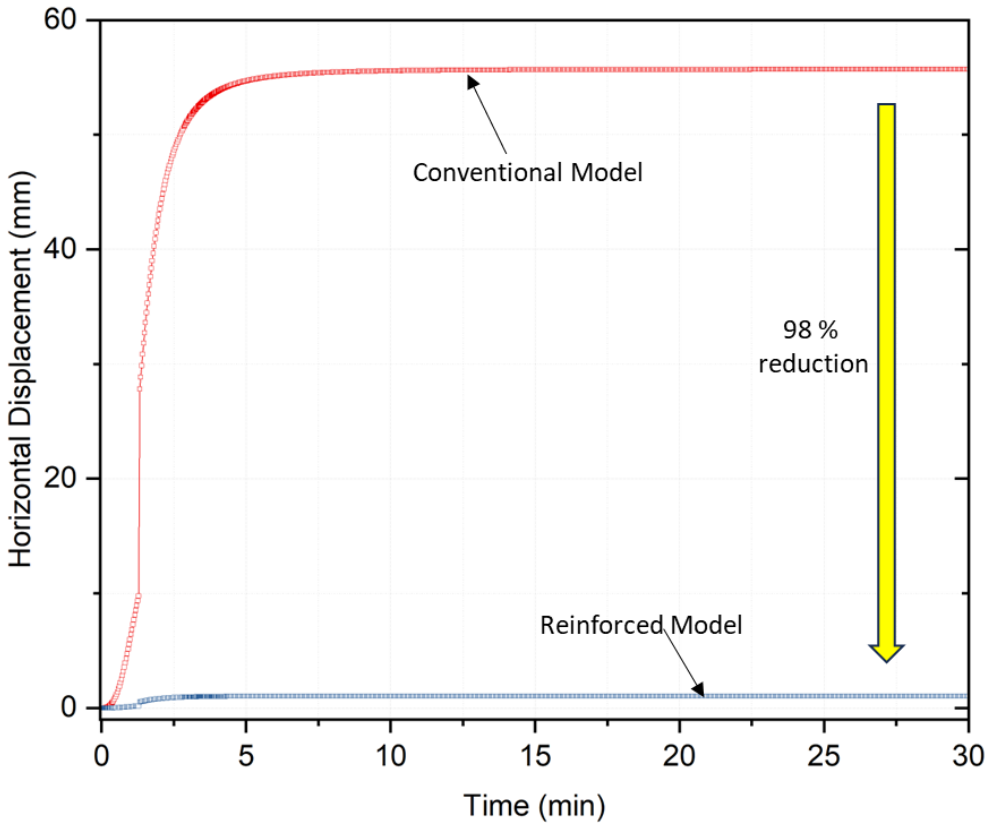

Fig. 8.12 Horizontal displacement of breakwater crest for the conventional model without crown wall during tsunami overflow

8.2.3 Incremental Pore Water Pressure (IPWP)

The stability of rubble mound breakwaters during tsunami events is critically influenced by the additional pore water pressure generated within both the seabed soils and the body of the breakwater. This pressure, known as Incremental Pore Water Pressure (IPWP), arises due to the rapid and intense loading conditions induced by tsunami overflow. To quantify IPWP, pore pressure sensors were installed and tared to zero prior to the commencement of overflow tests. This procedure eliminates the influence of the initial hydrostatic pressure corresponding to the still water level, ensuring that the recorded values accurately represent the excess pore pressure induced solely by tsunami action.

Test results indicate that IPWP is significantly higher on the seaward side of the breakwater compared to the port side. This disparity is attributed to the abrupt rise in water level on the seaward side during tsunami impact, which elevates pore pressure in the seabed soils beneath. In contrast, the presence of the breakwater structure acts as a barrier, resulting in a comparatively lower water level and, hence, lower IPWP on the port side. This pressure differential across the breakwater induces a pronounced hydraulic gradient, promoting horizontal seepage through the seabed soils. Such seepage can be detrimental, as it facilitates the migration of soil particles in the direction of flow, thereby reducing interparticle contact forces—i.e., the effective stress. A reduction in effective stress compromises the bearing capacity of the seabed, increasing the likelihood of settlement and instability of the overlying breakwater structure. Moreover, IPWP also affects the internal stability of the breakwater itself, where pressure gradients may trigger seepage paths that lead to the dislodgement of individual rubble elements.

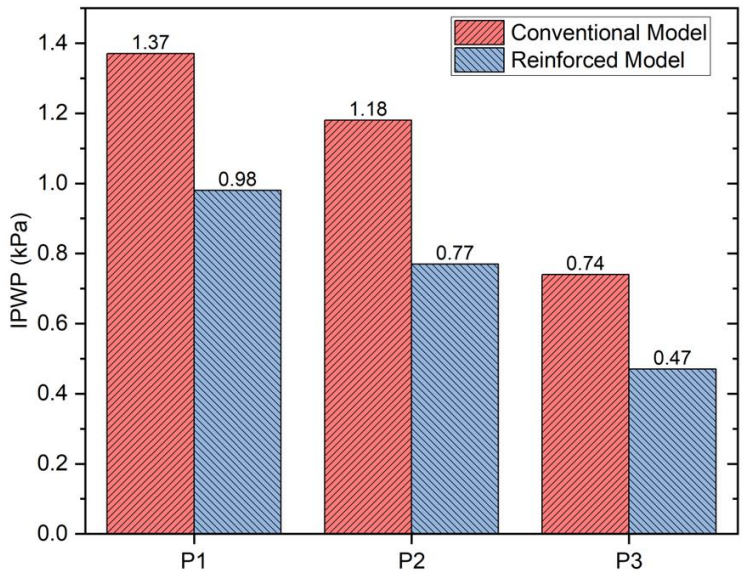

Fig. 8.14 IPWP measured at the seabed during tsunami overflow

In conventional breakwaters, the IPWP recorded in seabed soils on the port side was found to be 45.98% higher than that on the seaward side, highlighting the intensity of horizontal seepage during tsunami overflow (Figure 8.14). This substantial hydraulic gradient raises concerns over structural stability, particularly when reinforcement is absent. To mitigate these effects, reinforced breakwater models incorporate sheet piles beneath the structure, acting as effective cut-off walls that obstruct seepage flow paths. This reinforcement strategy led to a 35% (at P2) reduction in IPWP beneath the breakwater level compared to the conventional model, demonstrating its efficacy in enhancing foundation stability and overall performance during tsunami events.

In conclusion, incorporating countermeasures such as sheet piles is critical for reducing the adverse effects of IPWP. Considering these pore pressure dynamics in design practices is essential to ensure the long-term resilience and effectiveness of rubble mound breakwaters, particularly in seismically active and tsunami-prone regions.

8.2.4 Deformation Pattern Studies

The conventional model exhibited significant deformation during the overflow of the tsunami, as illustrated in Fig. 8.15. The combined effects of excess seepage and the intense horizontal forces exerted by the tsunami led to the dislodgment of rubbles, extending even to the primary armour layer. The onslaught of the overflowing tsunami initiated the scouring of the crest, with the armour layer on the port side slope eroding under the impact of the tsunami. This erosion resulted in the rolling down of both armour and core layer rubbles towards the harborside.

A significant quantity of 20.3 mm of scouring (1.62 m in the prototype) was observed in the conventional breakwater. This signified that 67% of the armour layer thickness was scoured off during the tsunami overflow. This substantial scouring compromised the breakwater's ability to effectively block overflowing, thereby heightening the risk of potential flooding in coastal areas. As evident in Figure 8.16, the scouring of the rubble mound occurred rapidly, indicating that the breakwater was rendered non-functional immediately after the impact of the tsunami. The observed deformations emphasise the critical need for enhanced resilience and robust design strategies in breakwaters to withstand the adverse effects of tsunami overflow.

The intrusion of the tsunami water through the body of the breakwater, coupled with the impact force of the overflowing tsunami on the port side slopes, has led to the scouring of armour rubbles. Consequently, the breakwater crest experienced settling by 20.3 mm (equivalent to 1.62 m in the prototype) and a horizontal displacement of 50.07 mm (equivalent to 4 m in the prototype). This substantial horizontal displacement is attributed to the rolling down of armour

rubbles from the crest towards the port side. Moreover, the reduction in the height of the breakwater opens the door for the tsunami to penetrate coastal regions. Therefore, reinforcing the breakwater with suitable elements is imperative to enhance its resilience against tsunamis. Additionally, there is a pressing need for a crown wall in the existing conventional breakwater to fortify its structure.

Fig. 8.16 provides a series of time frames, illustrating the evolution of the profile of the conventional breakwater during tsunami overflow. At t = 10 s, the tsunami waves reach the height of the breakwater and initiate overflow. Before the overflow commences, a significant volume of water seeps through the breakwater. The scouring of the crest begins, driven by the displacement of rubbles on the port side. After 1 minute of overflow, heavier primary armour units are observed to move with tsunami water, as depicted in the Fig. . The dislodged rubbles accumulate at the toe mound on the port side. The volume of piled rubbles increases, signifying continued rubble movement until the end of 20 minutes.

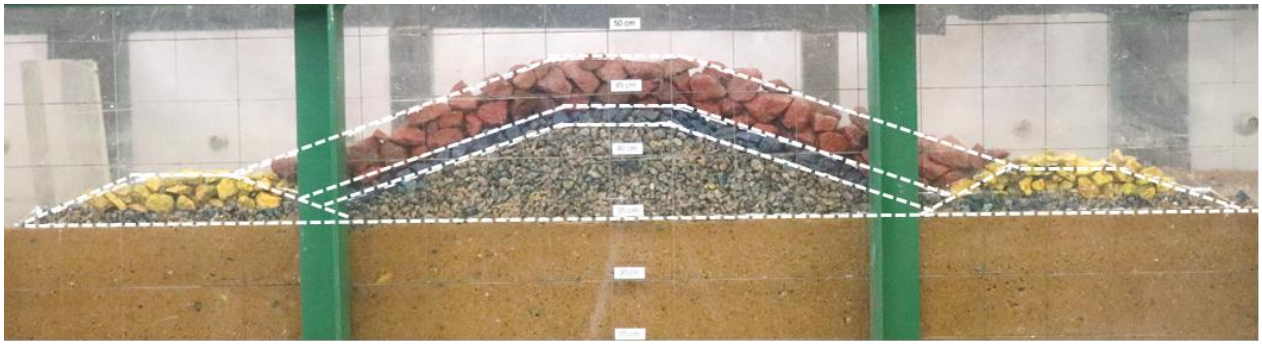

(a) Conventional model before tsunami overflow

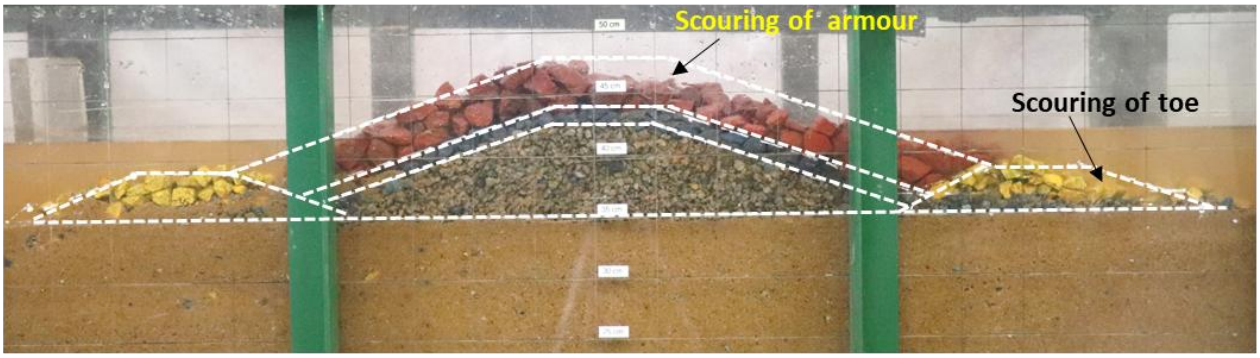

(b) Conventional model after tsunami overflow

Fig. 8.15 Deformation of the conventional model during the tsunami overflow flow

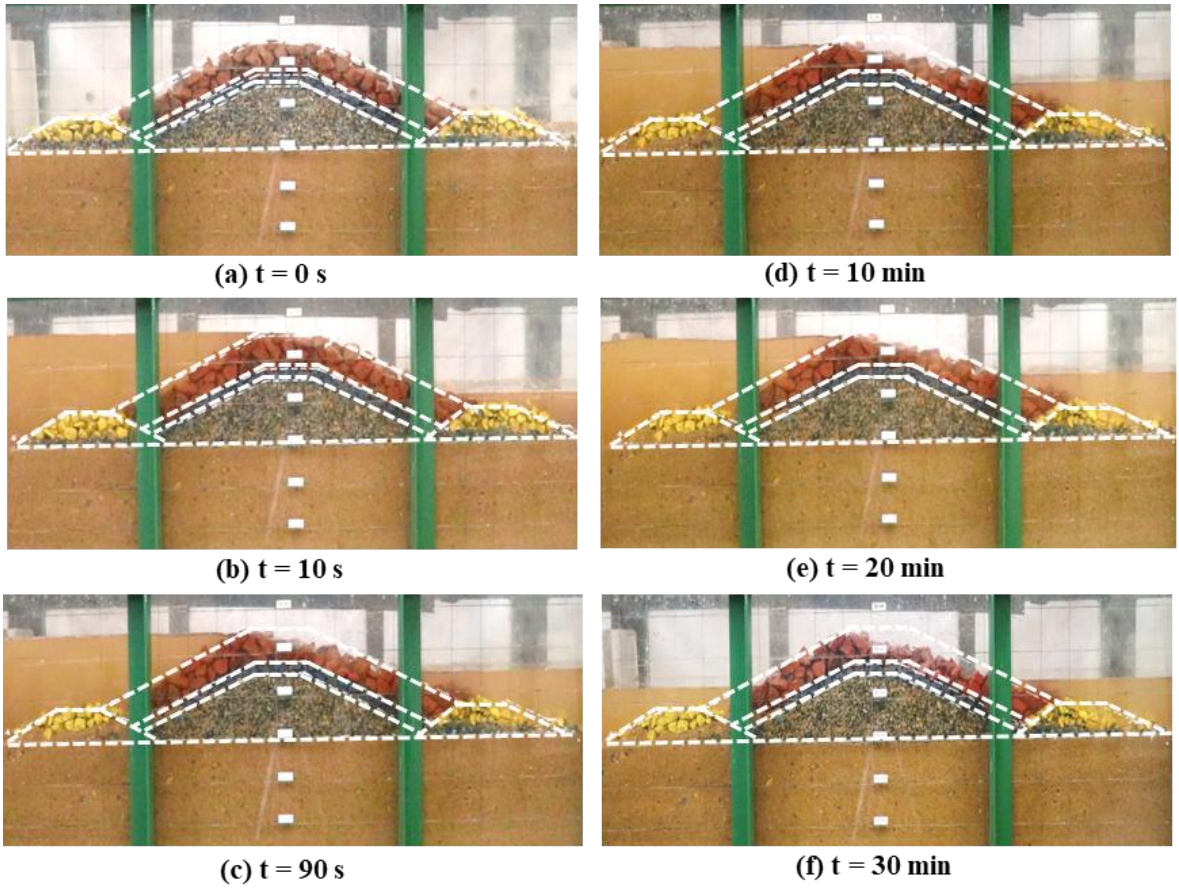

Fig. 8.16 Deformations of the conventional breakwater during the tsunami overflow

During the tsunami overflow, the reinforced model demonstrated remarkable stability, as depicted in Figure 8.17. The combined reinforcement of gabions, crown wall, and sheet piles contributed to its resilience, preventing any deformation. Additionally, the gabions protected the armour layer on the harbour side, mitigating the direct impact force of the overflowing tsunami. Notably, no scouring occurred in the reinforced breakwater, indicating the successful resistance of its armour layer to the tsunami overflow. This resilience is evident in Figure 8.17, where the reinforced model remained stable throughout the overflow, highlighting its ability to withstand tsunami impacts. The intactness observed in the reinforced models underscores the effectiveness of the countermeasure elements in mitigating the adverse effects of tsunami overflow.

The infiltration of the tsunami into the breakwater structure played a crucial role in dissipating energy within the reinforced models. This process helped to reduce the force exerted by the tsunami waves and mitigate potential damage to the breakwater. Furthermore, despite the force of the tsunami, the height of the breakwater remained constant, underscoring the effectiveness of reinforcing it with gabions without compromising its primary function of wave transmission.

The detailed sequence of events captured in Figure 8.18 provides insight into how the profile of the reinforced breakwater evolved during the tsunami overflow. At the 10-second mark (t = 10s), the tsunami waves reached the breakwater's crest, initiating overflow. Prior to this overflow, a substantial volume of water infiltrated through the breakwater structure, aiding in energy dissipation. Remarkably, this influx of water did not result in significant displacement of rubble within the breakwater. Instead, any dislodged rubble accumulated at the toe mound on the port side, indicating minimal disturbance to the breakwater's overall structure.

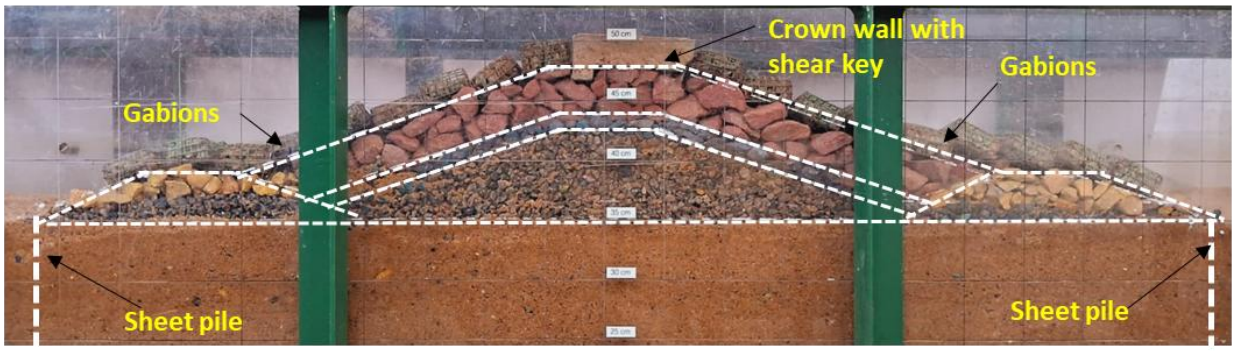

(a) Reinforced model before tsunami overflow

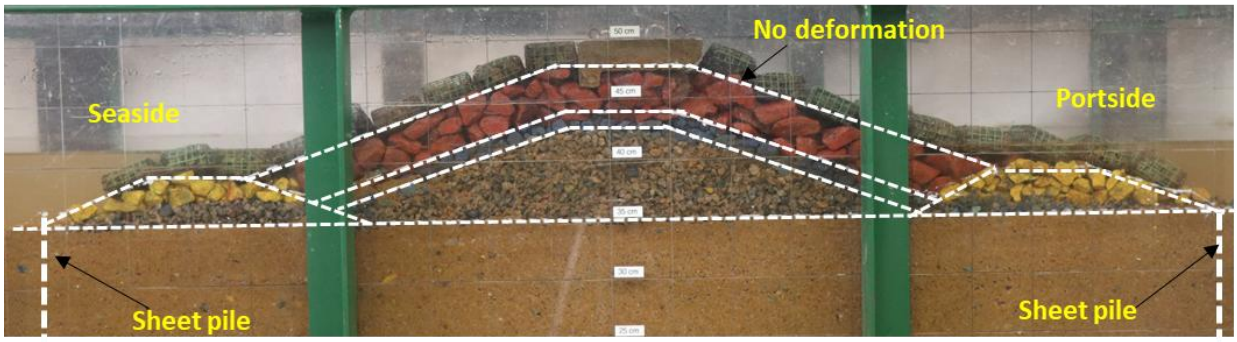

(b) Reinforced model after tsunami overflow

Fig. 8.17 Deformation of the reinforced model during the tsunami overflow

Throughout the tsunami overflow, the breakwater remained resilient and intact. This resilience underscores the effectiveness of the reinforcement measures, including gabions, in withstanding the forces exerted by the overflowing tsunami. Overall, the observed stability and performance of the reinforced breakwater highlight the importance of incorporating such countermeasure elements to effectively mitigate the adverse effects of tsunami overflow.

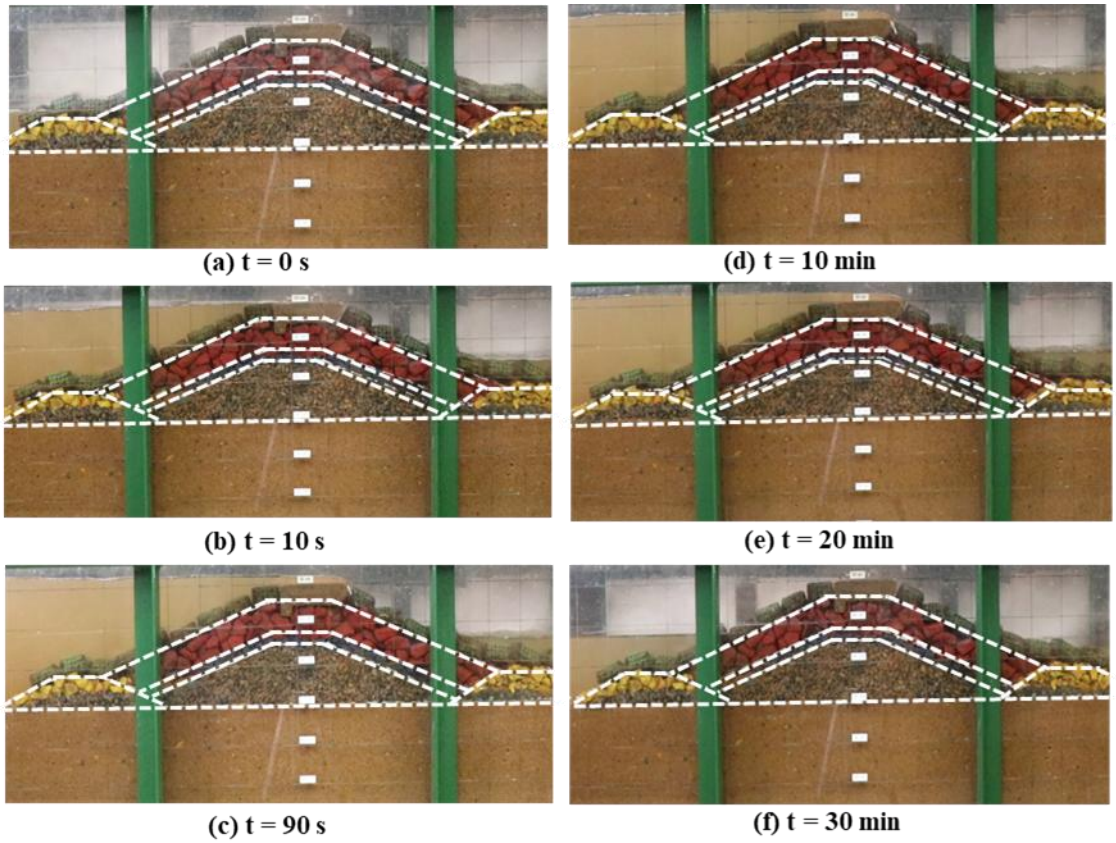

Fig. 8.11 Deformations of the reinforced breakwater during the tsunami overflow

8.2.5 3D Profile Comparison

A more precise analysis can be conducted by generating a 3D profile of the damaged breakwater and comparing it with its original structure (undamaged breakwater before tsunami). The GDP lab at the National Institute of Technology Karnataka, Surathkal, has devised a robotic mapper equipped with multiple distance-ranging sensors and wireless data transmitters operating on programmed commands. Laser displacement and ultrasound sensors mounted on the robotic mapper scan the entire breakwater profile both before and after the tsunami. Figure 8.19 presents the scanned profile of the conventional model before and after the tsunami overflow. The initial volume of the breakwater profile was 20,833 cc. The relative difference in elevation between each point of the initial and final breakwater profile during the tsunami overflow is depicted as a surface. Prominent scouring is evident toward the crest region, denoted by a depression in dark red banding at the centre of the surface. An upheaval is observed at the port side slopes due to the piling up of rolled-down armour rubbles, indicated by an upward bend in the comparative surface. The surface is undulated towards the port side and remains flat along the seaside, signifying that the breakwater profile has not changed after

the tsunami overflow. The seaside slope of the conventional model below sea level remained unaffected during the tsunami overflow.

Tsunami waves exert a substantial horizontal thrust on the rubble mound from the seaside to the port side direction. The net hydrostatic force acts from the seaside to the port side on the portion of the breakwater above sea level. However, in the submerged part of the breakwater, water is present on both the seaside and port side, cancelling out the hydraulic pressure below the mean sea level on both sides. This might contribute to the scouring of the breakwater portions above the mean sea level. In contrast, a significant portion of the armour layer rubble is scoured away. Moreover, the increased width of the breakwater towards the bottom contributes to better resistance against tsunami waves. Therefore, the armour rubbles in the crest region are crucial during a tsunami overflow. The side slopes of the mound are subjected to tsunami rundown, resulting in the dislocation of armour rubbles from the sides. The installation of a crown wall with shear keys can protect the crest of the breakwater from scouring during a tsunami overflow. Placing gabions on either slope of the breakwater can also reduce the movement of rubbles from the slopes.

Figure 8.20 illustrates the scanned profile of the reinforced model before and after the tsunami overflow. Remarkably, both the seaside slope and port side slope of the reinforced model remained unaffected during the tsunami event. Tsunami waves exert significant horizontal thrust on the rubble mound from the seaside to the port side direction. The resultant hydraulic force acts from the seaside to the port side on the breakwater section above sea level. However, the inclusion of shear keys in crown walls and the presence of gabions on either slope effectively resisted this hydraulic pressure.

Consequently, the armour rubbles in the crest region were shielded from the impact of the tsunami overflow. Furthermore, the gabions installed on the side slopes of the mound prevented the movement of armour rubbles from the sides by resisting tsunami rundown. Additionally, the installation of a crown wall with shear keys protected the crest of the breakwater from scouring during the tsunami overflow. Overall, the strategic placement of gabions on both slopes of the breakwater contributed to reducing the movement of rubbles from the slopes.

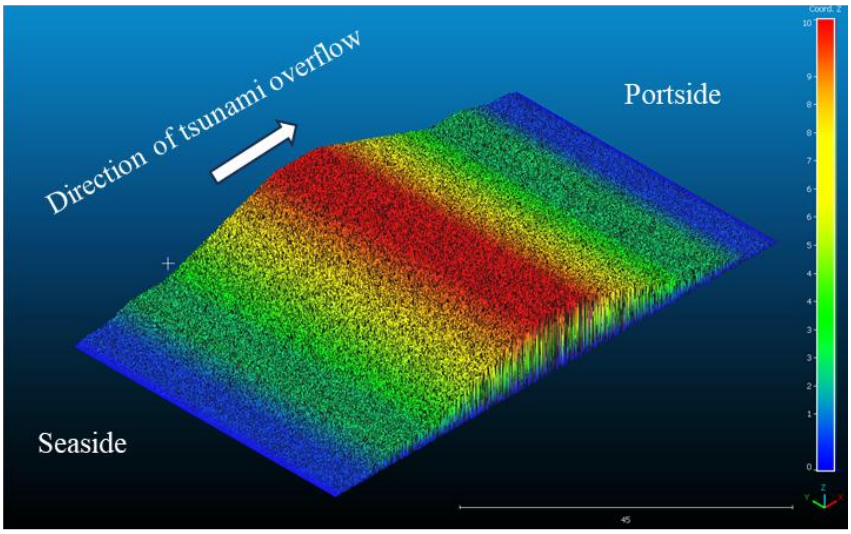

(a) Conventional model before tsunami overflow

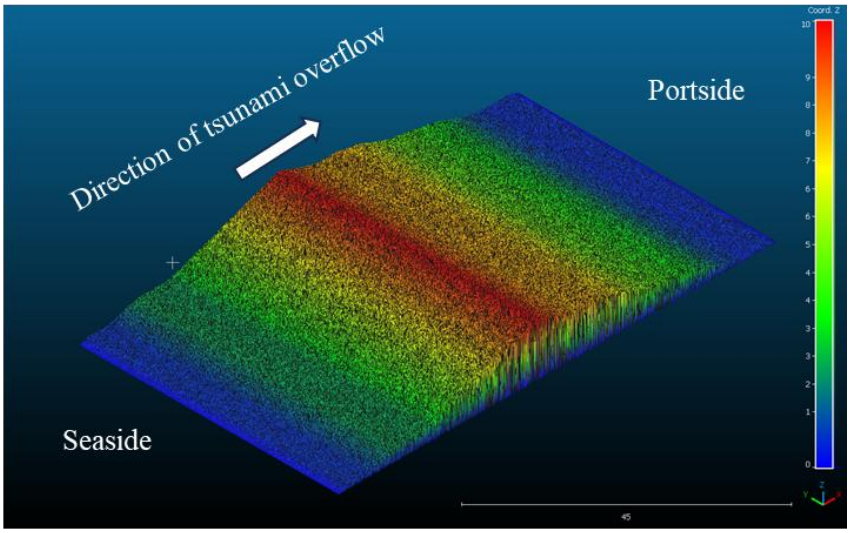

(b) Conventional model after tsunami overflow

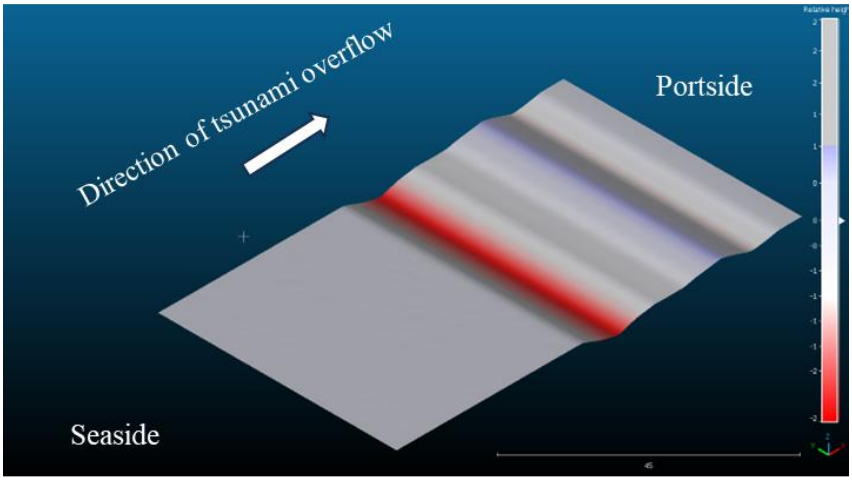

(c) Scoured Profile after tsunami overflow

Fig. 8.19 Profile of conventional model before and after tsunami overflow

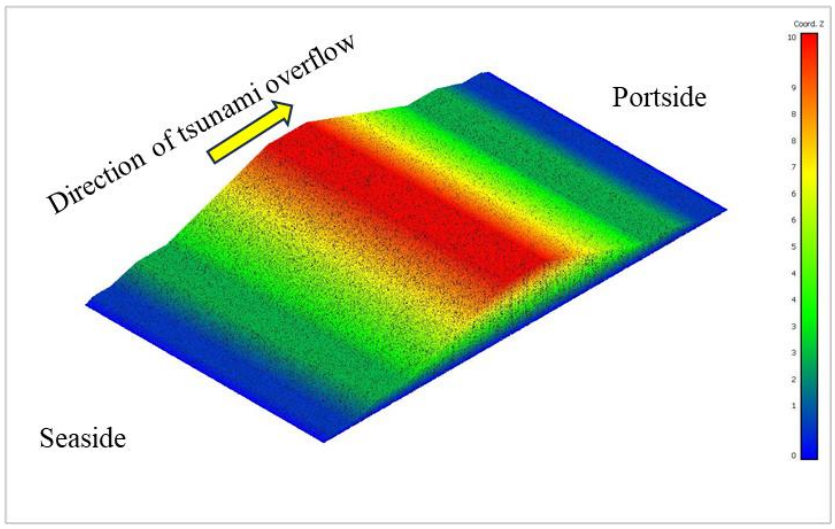

(a) Conventional model before tsunami overflow

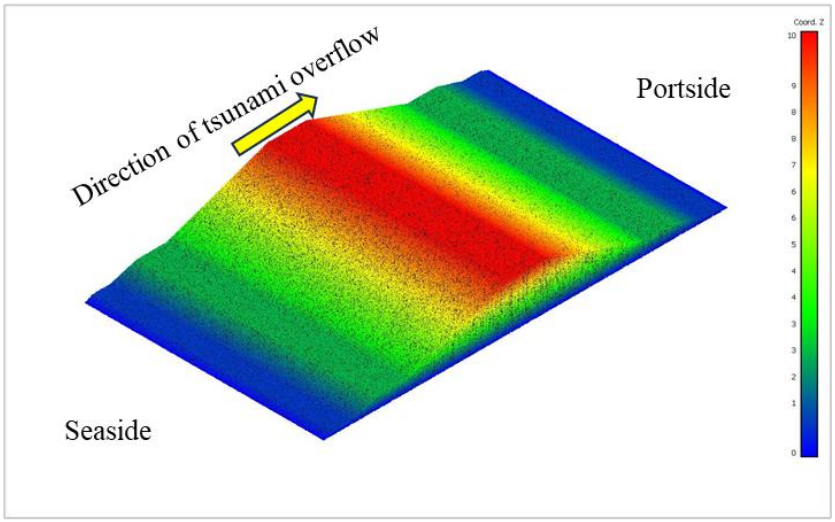

(b) Conventional model after tsunami overflow

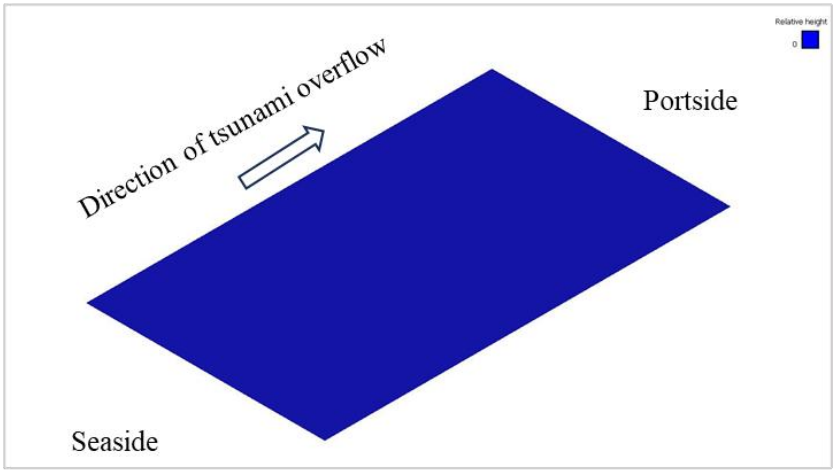

(c) Scoured Profile after tsunami overflow

Fig. 8.20 Profile of reinforced model before and after tsunami overflow

8.2.6 Damage Analysis

Damage parameters are used to quantify the degree of damage that occurred on the breakwater before and after the tsunami. The two damage parameters considered in the present study are: (i) Relative displacement of armour units (R_d) and (ii)dimensionless eroded area (S).

The displacement of armour units can be characterised by considering a fraction of the overall number of armour units. In this evaluation, the secondary armour units along the harborside slope, specifically the rubbles, are considered. The relative displacement of armour units (R_d) is calculated as the ratio of the number of dislodged armour rubbles in the layer ($N_{displaced}$) to the total number of armour rubbles in the layer (N_{total}), as expressed in the following equation (Hudson 1959).

$$R_d = \frac{N_{displaced}}{N_{total}} \times 100\% \quad \textbf{(2)}$$

This ratio provides insight into the proportion of armour units that have experienced displacement, offering a quantitative measure of the structural impact and vulnerability of the breakwater during the analysed events. A qualitative relation between relative displacement (R_d) and the degree of damage has been summarised in the Coastal Engineering Manual (United States Army Corps of Engineers 2002).

Table 8.1 Damage thresholds for various values of R_d

Thresholds	**R_d (%)**
Initiation of Damage	0-5
Intermediate Damage	5-10
Failure	20 and above

In the context of breakwater stability, a *lower value of R_d indicates a more stable structure.* The conventional breakwater experienced significant scouring, with nearly 16 % of the total armour units being displaced during the tsunami overflow, as demonstrated in Figure 8.21. Notably, not a single stone was displaced during the tsunami overflow, as evidenced in Figure 8.21.

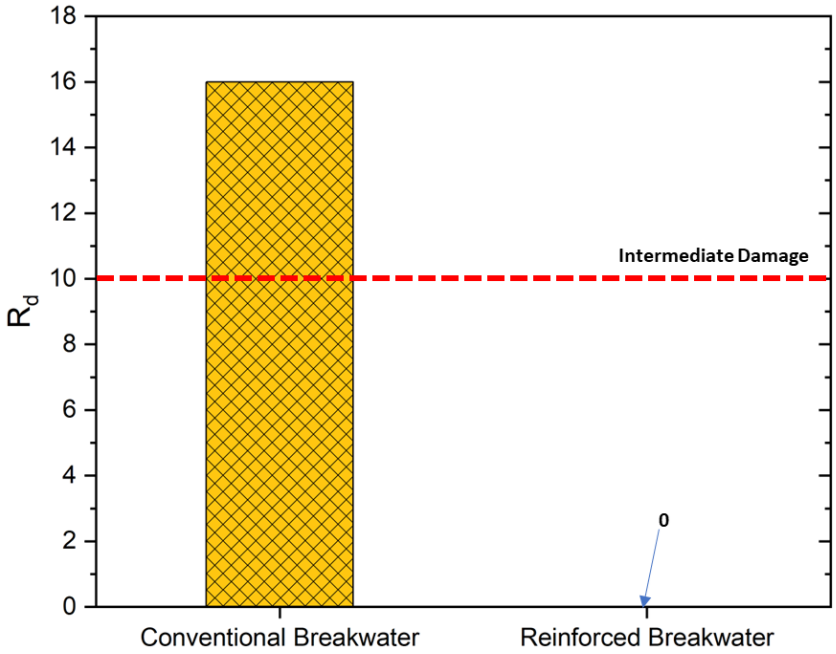

Fig. 8.21 Relative displacements of armour rubbles in the reinforced breakwater model

Dimensionless Eroded Area (S)

Broderick (1984) introduced another parameter known as the dimensionless eroded area (S). This parameter serves to quantify the extent of scouring that occurred on the mound due to wave action. It can be computed as follows:

$$S = \frac{A_e}{D_{n50}^2} \quad \textbf{(3)}$$

The limitations in the determination of average eroded area A_e using direct measurements were resolved through the below-mentioned equation) proposed by Vidal et al. (2004).

$$A_e = {}^{N_d D_{n50}^3}\Big/_{(1-n)B} \quad \textbf{(4)}$$

Therefore, by considering the number of eroded armour units (Nd), the nominal diameter of the armour stone (Dn50), and its bulk porosity (n), one can estimate the average area of the eroded mound. Additionally, the width of the model cross-section (B), which was set at 0.4 m for this study, plays a significant role in determining the average eroded area. Depending on the range of values obtained for S, with breakwater slope (cot α) varying from 1.5 to 4, the damages sustained by the breakwater can be classified according to Table 8.2 (Campos et al. 2020).

Table 8.2 Damage thresholds for various values of S

Thresholds	S
Initiation of Damage	1.5 - 3
Iribarren's Damage	2.5 - 4
Initiation of destruction	6.5 - 11
Destruction	12 – 18 and above

In the conventional breakwater, the relative eroded area was determined to be 9.25, as depicted in Figure 8.22. This value signifies that the rubble mound breakwater exceeded the threshold for the initiation of destruction by 42.3% during the tsunami overflow. Conversely, no movement was observed in the armour layer of the reinforced breakwater.

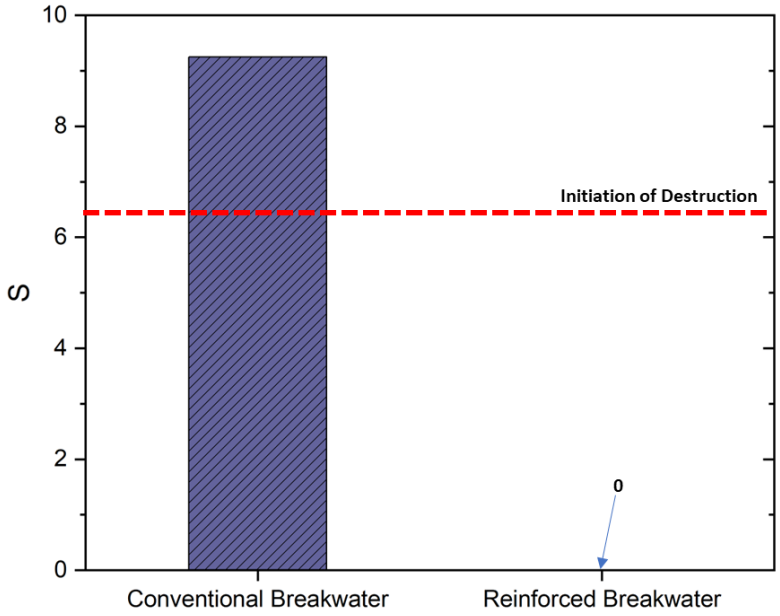

Fig. 8.22 Relative displacements of armour rubbles in the reinforced breakwater model

9. NUMERICAL ANALYSES

Numerical analysis is a critical component of this research, as it provides insights into the behaviour of breakwater structures under various loading conditions. By simulating different scenarios and parameters, we can predict the performance of both conventional and reinforced breakwaters and identify potential weaknesses and areas for improvement. This section focuses on the numerical analysis performed using PLAXIS 3D for conventional and reinforced breakwater models. PLAXIS 3D is a sophisticated finite element analysis (FEA) software developed by PLAXIS B.V., renowned for its capabilities in geotechnical engineering applications.

9.1 Numerical Modelling, Model Validation and Parametric Studies for Earthquake Loadings

Before conducting detailed numerical studies, it is essential to validate the numerical model against experimental data. This validation ensures that the model accurately represents the real-world behaviour of the breakwater structures. In this study, the numerical models were validated using data from shaking table tests conducted under varying seismic intensities, including foreshock levels of 0.1g and 0.2g and a main foreshock level of 0.4g. The successful validation provided a solid foundation for subsequent numerical analysis.

9.1.1 Methodology of the Numerical Model

The methodology for the numerical modelling of breakwater structures in this study involves several key steps, from the initial setup of the seabed and breakwater configurations to the selection and application of appropriate soil constitutive models.

Seabed Soil Modelling:

The seabed soils are modelled as two layers (loose and dense sand layers), consistent with the configurations used in the shake table tests. This approach ensures that the numerical model accurately reflects the experimental setup, facilitating direct comparisons between numerical and experimental results.

Loose Sand Layer: This layer represents the upper part of the seabed, characterized by low density and high compressibility. It is critical to model this layer accurately as it significantly influences the overall stability of the breakwater structure.

Dense Sand Layer: Situated beneath the loose sand layer, the dense sand layer has higher density and lower compressibility. This layer provides foundational support to the breakwater and reflects a hard stratum beneath the foundation seabed that affects its response to external loads. The seabed modelling in PLAXIS 3D is shown in Figure 9.1.

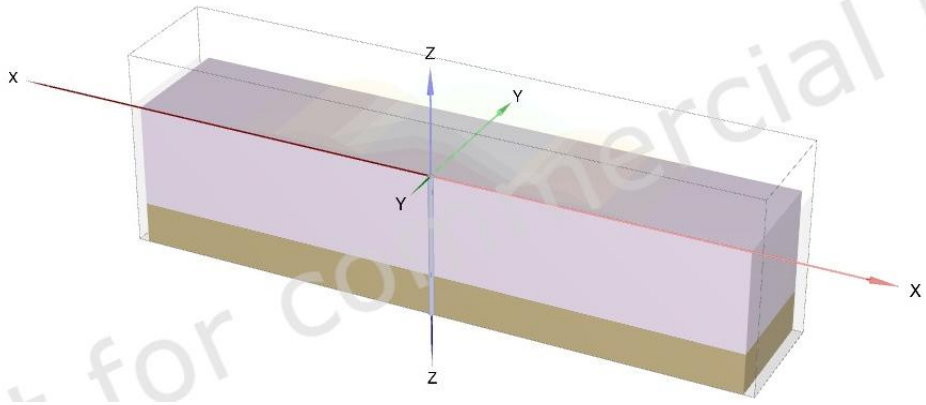

Fig. 9.1 Seabed layers modelled in the soil module

These layers are defined in the numerical model with specific properties that replicate their real-world behaviour, including parameters such as density, stiffness, and shear strength as detailed in Table 9.1. The UBC-3D (University of British Columbia 3-Dimensional) PLM (Plasticity Liquefaction Model) is used to model the seabed. This model is specifically designed to simulate the behaviour of sand under cyclic loading conditions, making it suitable for representing the dynamic response of loose and dense sand layers during seismic and tsunami events. The UBC-3D PLM model accounts for factors such as stress-strain relationships, cyclic mobility, and liquefaction potential, providing a comprehensive simulation of seabed behaviour under varying conditions.

Table 9.1 Properties of the seabed for numerical modelling

Parameters	**Loose Sand**	**Dense Sand**
Model	UBC-3D PLM	UBC-3D PLM
Unsaturated Unit Weight (kN/m^3)	17	17.5
Saturated Unit Weight (kN/m^3)	17.5	18
Cohesion	0	0
Angle of Friction	36º	42º
Dilatancy Angle	6º	12º
Poisson's Ratio	0.2	0.2
Relative Density	60%	90%

Breakwater Modelling

The breakwater itself is modelled on top of the seabed using soil constitutive models that account for the distinct properties of different layers within the breakwater structure (see Figure

9.2). This step involves the creation of a multi-layered breakwater model that simulates the actual construction and material composition of the breakwater.

Core Layer: Typically composed of coarse material, the core layer provides the main structural integrity of the breakwater. Its properties include high strength and stiffness.

Filter Layer or Underlayer: This layer, placed around the core, consists of finer materials that prevent the migration of the core material while allowing water to pass through. Its properties are defined to reflect its filtration function.

Armour Layer: The outermost layer, usually made of large stones or concrete units, protects the breakwater from direct wave impacts and erosion. Its properties are defined to ensure high resistance to wave action and impact forces.

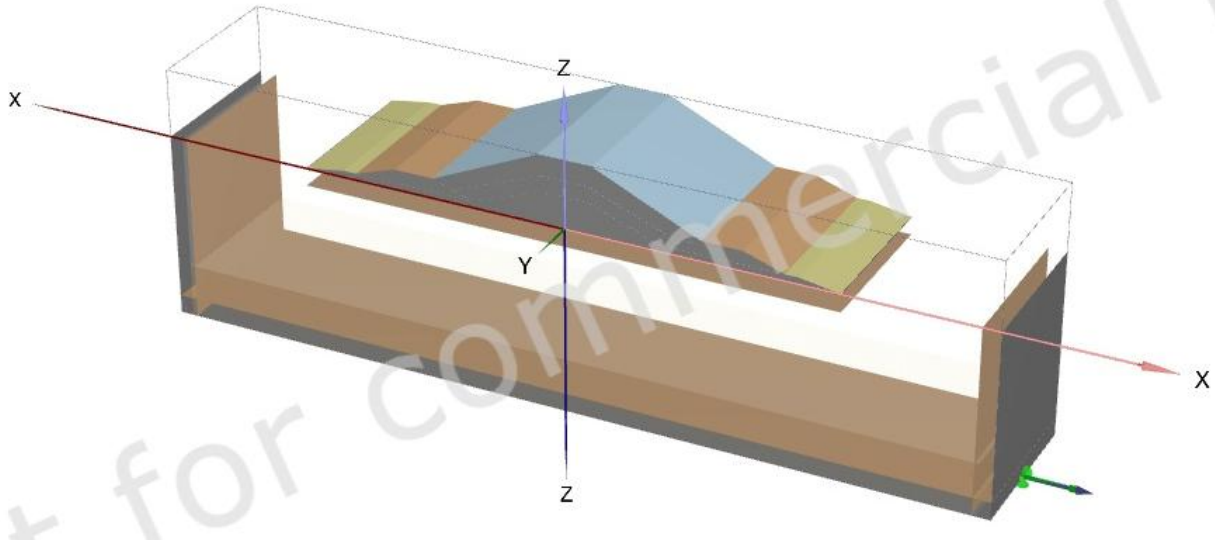

Fig. 9.2 Breakwater modelled in the structure module

Each layer is assigned specific mechanical properties, including Young's modulus, Poisson's ratio, and internal friction angle, to accurately simulate their individual and collective behaviour under loading conditions, as detailed in Table 9.2. The Hardening Soil (HS) Small model is employed to model the breakwater rubbles. This advanced soil model captures the non-linear behaviour of soils with small-strain stiffness. It is particularly effective for simulating the breakwater's response to small cyclic deformations and dynamic loading. The HS Small model includes parameters such as stiffness modulus, unloading/reloading stiffness, and small-strain shear modulus, ensuring an accurate representation of the breakwater material's mechanical behaviour.

Table 9.2 Properties of the breakwater for numerical modelling

Parameters	Core	Under Layer	Toe Mound	Armour Layer
Model	HS Small	HS Small	HS Small	HS Small
Unsaturated Unit Weight (kN/m^3)	16	17	17	18
Saturated Unit Weight (kN/m^3)	17	18	17.5	18.5
Cohesion (kPa)	0	0	0	0
Angle of Friction	41º	42º	42º	44º
Dilatancy Angle	10º	6º	6º	8º
Poisson's Ratio	0.2	0.2	0.2	0.2

Material Properties Assignment: The specific material properties for each layer of the seabed and breakwater are assigned based on experimental data and available literatures. This includes defining each material layer's density, stiffness, strength, and other relevant parameters. The model of the breakwater and seabed after assigning the material properties is shown in Figure 9.3.

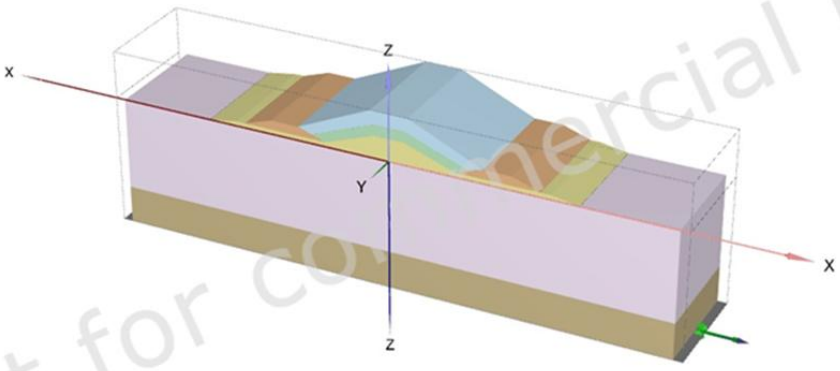

Fig. 9.3 Breakwater and seabed with material properties assigned

Meshing: A finite element mesh is generated for the entire model, ensuring that the mesh is sufficiently refined to capture the detailed behaviour of the structures. Special attention is given to areas with high gradients in material properties or expected stress concentrations. Finer meshing was utilised to discretise the model into tetrahedrons of 12 nodes.

Boundary Conditions and Loading: Appropriate boundary conditions are applied to simulate the physical constraints and external forces acting on the model. The earthquake loading was applied as a surface displacement at the bottom of the soil domain with a sinusoidal input that varies in amplitude with a frequency of 8 Hz as shown in Figure 9.4. The input motion was selected to replicate the input motion given at the base of the model in the shake table experiments. The boundary includes fixing the base and sides of the model to prevent unrealistic deformations and applying dynamic loads to simulate seismic and tsunami forces. During these propagation of input motions through soil, some of these waves can be reflected back from boundaries on either side as well as bottom. This reflection of input motion within soil domain has to be minimized to replicate the real-world scenario. Therefore, absorbing type boundaries are defined around the soil medium. In PLAXIS, the absorbing type boundaries are of three types,

- Viscous boundaries
- Free-Field boundaries
- Compliant base boundaries

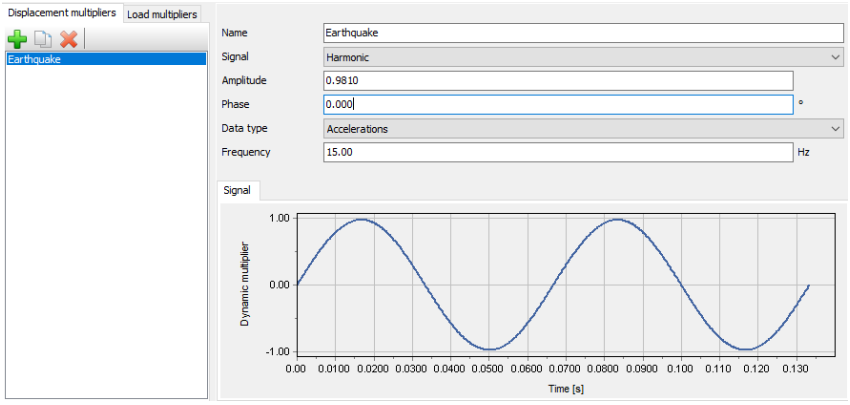

Fig. 9.4 Sinusoidal input motion defined at the base of the model

The viscous boundaries are generally used when the vibrating source is within the soil domain. For example, pile driving through soil, machine foundation on top of soil etc. Whereas, when the source of vibration is outside the soil domain, such as that of earthquake loadings, the free-field boundaries are defined. When free-field boundaries are assigned for lateral boundaries of a soil domain, compliant base boundaries have to be defined at the bottom. The compliant base

boundary would ensure both the transmission of input waves into the soil and any reflected waves away from the soil.

Simulation and Analysis: The numerical simulations are conducted using Plaxis 3D, running multiple scenarios to assess the stability and performance of the breakwater under different loading conditions. The results are then analysed to evaluate key performance indicators such as settlement, horizontal displacement, pore water pressure, and stress distribution.

9.1.2 Validation

The validation of the numerical model is a crucial step in ensuring that the simulations accurately represent the physical behaviour of the breakwater structures under dynamic loading conditions. In this study, the validation was performed by comparing the numerical results with experimental data obtained from shaking table tests. These tests involved subjecting both conventional and reinforced breakwater models to varying seismic intensities, specifically foreshocks of 0.1g and 0.2g, and a main foreshock of 0.4g. The primary metric for validation was the settlement of the breakwater crest, a critical indicator of structural stability and performance.

The results from the numerical simulations were compared with the experimental data to validate the accuracy of the numerical model. The validation process involved the following steps:

Data Comparison: The settlement of the breakwater crest observed in the numerical simulations was compared with the experimental measurements for each seismic loading condition. This comparison was made in terms of both magnitude and trend of settlement.

Parameter Tuning: If significant discrepancies were observed, the material properties and model parameters in the numerical simulations were adjusted to better match the experimental results. This iterative process involved fine-tuning parameters such as soil stiffness, damping coefficients, and interface properties.

Validation Metrics: Key validation metrics included the maximum settlement of the breakwater crest, the rate of settlement over time, and the distribution of settlement along the crest. These metrics provided a comprehensive assessment of the model's accuracy.

The validation results indicated a high degree of correlation between the numerical simulations and the experimental data. Key findings included:

Fore Shock (0.1 g): The numerical model accurately predicted the small settlement observed in the experimental tests. The response of the breakwater in the numerical model during the

foreshock was observed to follow the same trend as observed in the shake table tests as highlighted in Figure 9.5.

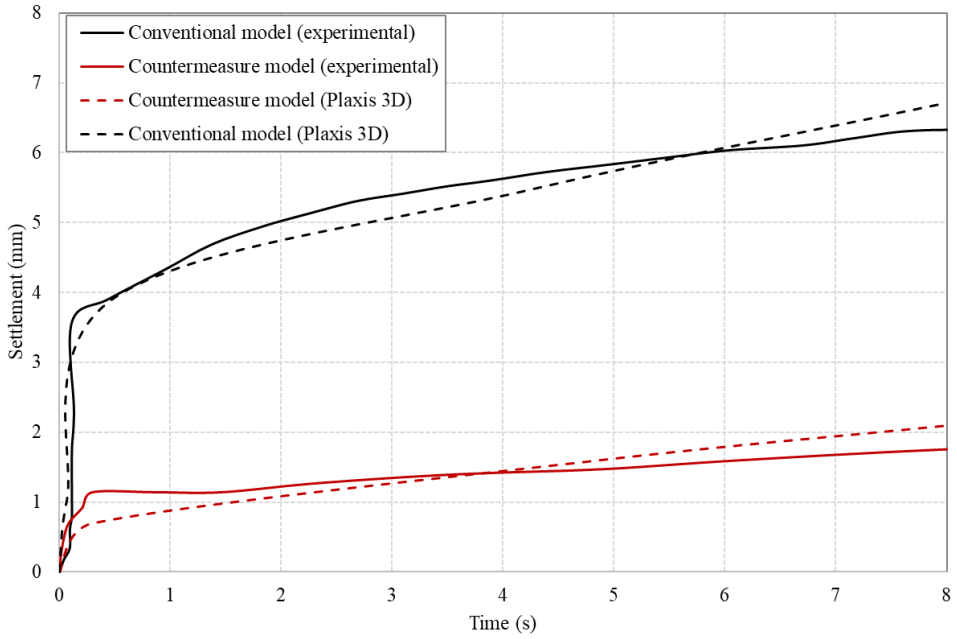

Fig. 9.5 Settlement of crest of the breakwater models during the foreshock (0.1g)

Fore Shock (0.2g): For the higher intensity foreshock, the numerical simulations again closely matched the experimental results. The trend of increasing settlement with higher seismic intensity was well captured by the model as shown in Figure 9.6.

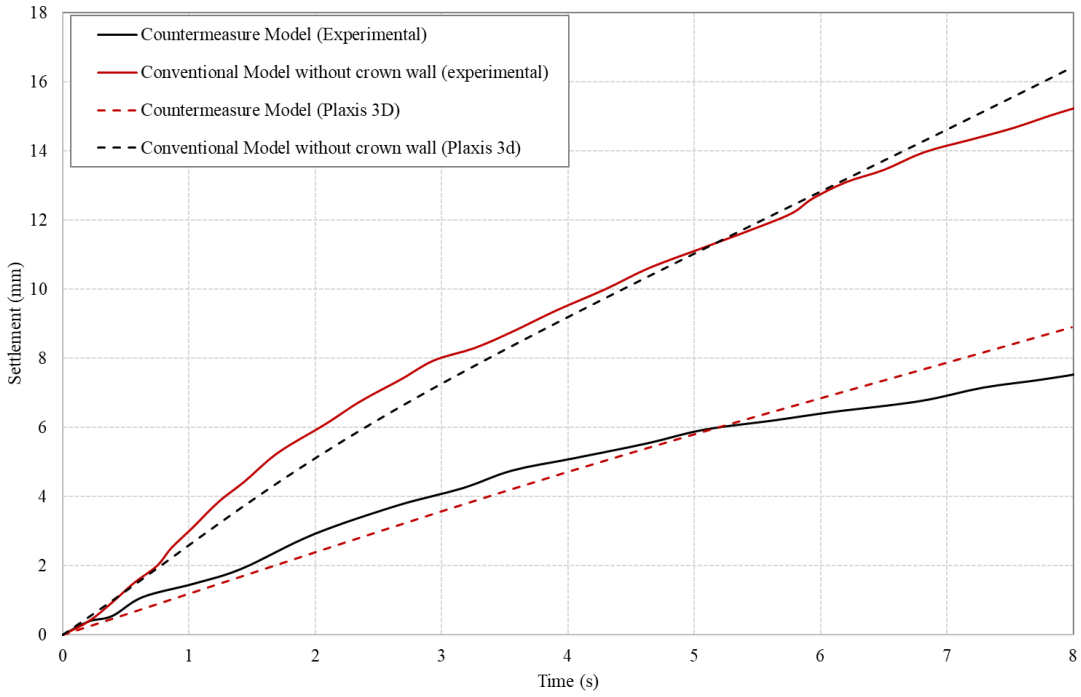

Fig. 9.6 Settlement of crest of the breakwater models during the second foreshock (0.2g)

Main Shock (0.4g): The main foreshock test, which represented the highest seismic intensity, showed a larger settlement in both the numerical and experimental results as shown in Figure 9.7. The numerical model predicted the maximum settlement, demonstrating its robustness in simulating high-intensity seismic events.

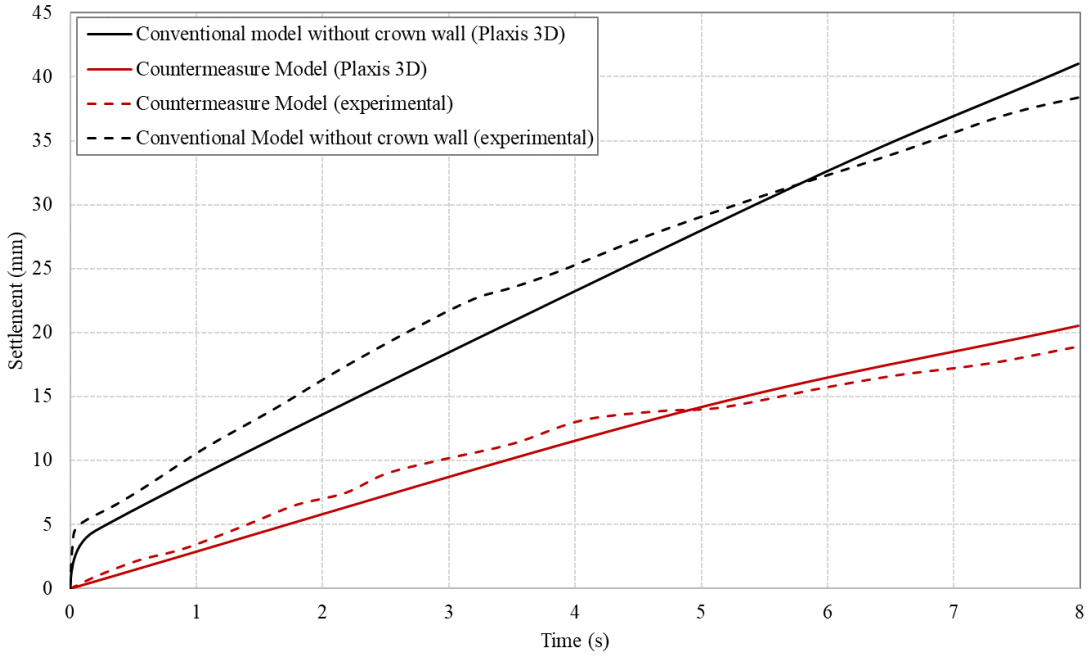

Fig. 9.7 Settlement of crest of the breakwater models during the mainshock 0.4g

9.1.3 Parametric Studies

The parametric study conducted in this research aims to investigate the influence of various factors on the performance and stability of both conventional and countermeasure breakwater models. The parametric study for the conventional breakwater model focuses on three main factors: the depth of the loose sand layer, the depth of water above the ground level, and the density of the loose sand. Each parameter is varied independently to assess its impact on the breakwater's performance. For the countermeasure model, the study explores additional factors specific to the reinforced design. These include the thickness and embedment depth of sheet piles, in addition to the parameters considered for the conventional model.

Effect of the Depth of Loose Sand Layer in the Conventional Model

The depth of the loose sand layer is a critical factor in determining the stability and settlement behaviour of breakwater structures. In this study, numerical simulations were performed to investigate how varying the loose sand layer's depth affects the breakwater crest's settlement over time. The attached graph illustrates the settlement of the breakwater crest (Y-axis) against

the duration of input motion (X-axis) for depths of 200 mm, 250 mm, and 300 mm. It is evident from the Fig. 9.8 that the settlement increases with increase in the depth of the loose sand layer. The analysis indicates that as the depth of the loose sand layer increases, the breakwater experiences greater settlement. This can be attributed to the fact that deeper loose sand layers provide less resistance to the applied loads, resulting in higher compressibility and greater deformation. For instance, when the depth of the loose sand layer is 200 mm, the settlement is relatively lower compared to when the depth is increased to 250 mm and 300 mm as shown in Figure 9.8. This trend is consistently observed throughout the duration of the input motion, highlighting the significant impact of loose sand layer depth on breakwater performance. Moreover, the rate of settlement also appears to be influenced by the depth of the loose sand layer. The initial settlement rate is higher for deeper loose sand layers, indicating a more pronounced immediate response to the applied loads. Over time, the difference in settlement between the various depths becomes more pronounced, with the 300 mm depth showing the highest overall settlement, followed by the 250 mm and 200 mm depths. This suggests that deeper loose sand layers not only result in greater total settlement but also exhibit a more rapid initial settlement response, which could be critical during seismic events.

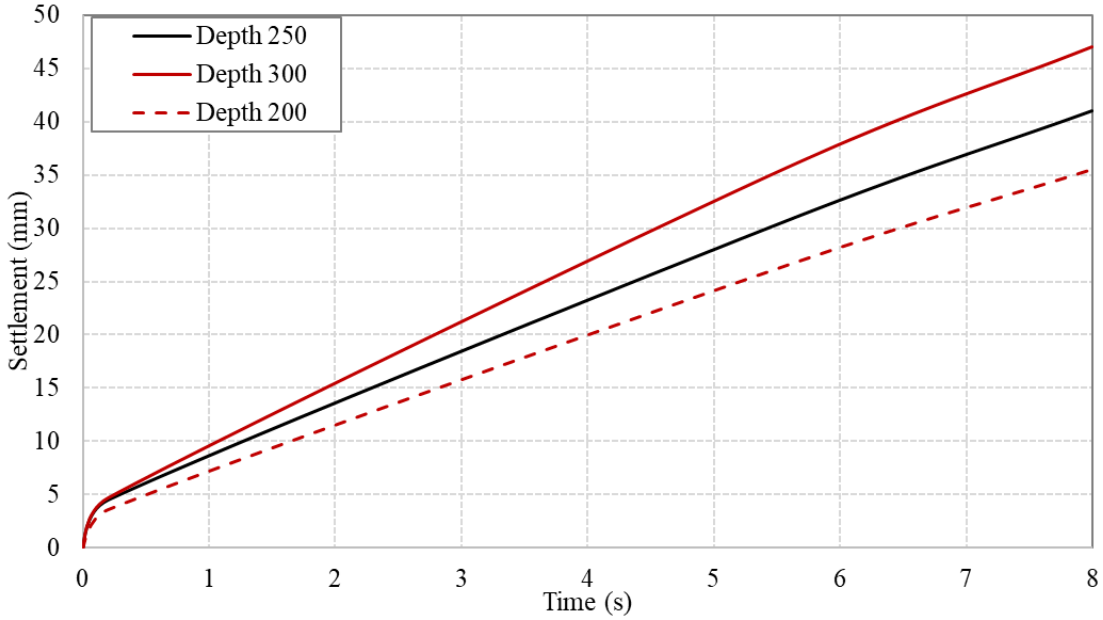

Fig. 9.8 Settlement of crest of the conventional model with various depths of loose sand layer

The parametric study on the depth of the loose sand layer reveals that deeper layers led to increased settlement of the breakwater crest. This finding underscores the importance of considering the depth of loose sand in the design and analysis of breakwater structures, particularly in regions susceptible to seismic activity. By understanding the relationship between loose sand layer depth and breakwater settlement, engineers can develop more

effective designs and mitigation strategies to enhance the stability and performance of breakwaters under dynamic loading conditions.

Effect of the Depth of Mean Sea Level in the Conventional Model

The depth of the mean sea level is another significant factor influencing the stability and settlement of breakwater structures. In this study, the numerical analysis was conducted to assess how varying the depth of the mean sea level affects the settlement of the breakwater crest over time. The attached graph illustrates the settlement of the breakwater crest (Y-axis) against the duration of the input motion (X-axis) for mean sea level depths of 90 mm, 96 mm, and 100 mm. It is clear from the graph shown in Figure 9.9 that the settlement increases with an increase in the mean sea level depth. The analysis shows that as the depth of the mean sea level increases, the breakwater experiences greater settlement. This can be attributed to the higher water pressure exerted on the breakwater structure with deeper sea levels, resulting in greater deformation and settlement. For instance, when the mean sea level depth is 90 mm, the settlement is relatively lower compared to when the depth is increased to 96 mm and 100 mm. This trend is consistently observed throughout the duration of the input motion, underscoring the substantial impact of mean sea level depth on breakwater performance.

Additionally, the rate of settlement also appears to be influenced by the depth of the mean sea level. The initial settlement rate is higher for deeper mean sea levels, indicating a more pronounced immediate response to the applied loads. Over time, the difference in settlement between the various depths becomes more significant, with the 100 mm depth showing the highest overall settlement, followed by the 96 mm and 90 mm depths. This suggests that deeper mean sea levels not only result in greater total settlement but also exhibit a more rapid initial settlement response, which could be critical during dynamic loading events such as tsunamis.

The parametric study on the depth of the mean sea level reveals that deeper sea levels lead to increased settlement of the breakwater crest. This finding highlights the importance of considering the depth of the mean sea level in the design and analysis of breakwater structures, particularly in regions prone to rising sea levels and dynamic loading conditions. By understanding the relationship between mean sea level depth and breakwater settlement, engineers can develop more effective designs and mitigation strategies to enhance the stability and performance of breakwaters under varying sea level conditions.

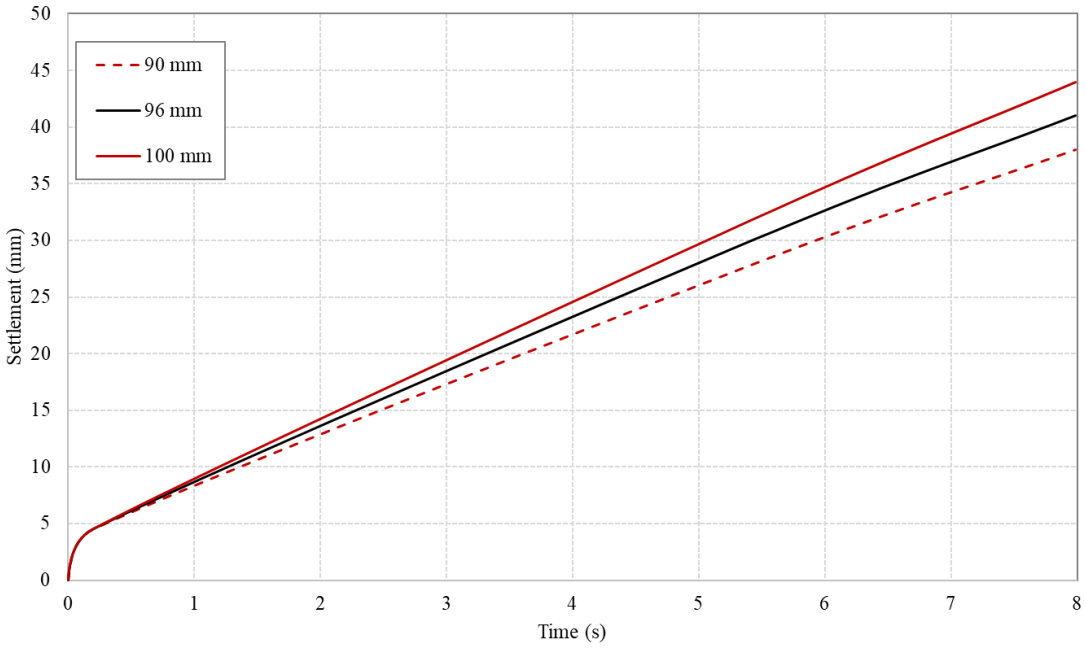

Fig. 9.9 Settlement of crest of the conventional model with various depths of mean sea level

Effect of Density of Loose Sand in the Conventional Model

The effect of the density of the loose sand layer on the settlement of the crest of a conventional rubble mound breakwater model subjected to earthquake loading is illustrated in Figure 9.10. The numerical model simulates the response of the breakwater during an 8-second earthquake, with settlement measured over time for three different sand densities: 16.5 kN/m³, 17.5 kN/m³, and 18.5 kN/m³. In the initial phase of the earthquake loading, all three density models exhibit rapid settlement within the first second. This indicates a quick response of the loose sand layer under seismic excitation, regardless of its density. As time progresses, the rate of settlement varies based on the density of the loose sand layer. The model with a sand density of 16.5 kN/m³, represented by the dashed red line, shows the highest settlement throughout the earthquake duration. This suggests that loose sand layers result in greater deformation under seismic loading. Conversely, the model with a sand density of 17.5 kN/m³, depicted by the solid black line, exhibits intermediate settlement values, indicating moderate deformation. The model with the highest sand density of 18.5 kN/m³, shown by the solid red line, displays the least settlement, highlighting the increased stability provided by denser sand layers.

The observed trend suggests a clear inverse relationship between the density of the loose sand layer and the settlement of the breakwater crest. Higher densities result in less settlement, implying better support and resistance to seismic forces. For the construction and maintenance of conventional rubble mound breakwaters in seismically active regions, the density of the underlying loose sand layer is a critical factor. Ensuring a higher density could significantly

enhance the structure's resilience to earthquake-induced settlements. Engineers should consider pre-compaction or the use of denser materials for the sand layer to mitigate settlement issues. The results underscore the importance of geotechnical properties in the overall seismic performance of coastal structures. Properly addressing the density of the foundational sand layer can reduce the risk of excessive settlement and potential structural failure during earthquakes. In conclusion, the numerical model's analysis highlights the crucial role of loose sand layer density in the settlement behaviour of conventional rubble mound breakwaters under seismic loading. Future designs should prioritize optimizing the density of foundation materials to enhance structural stability and performance during seismic events.

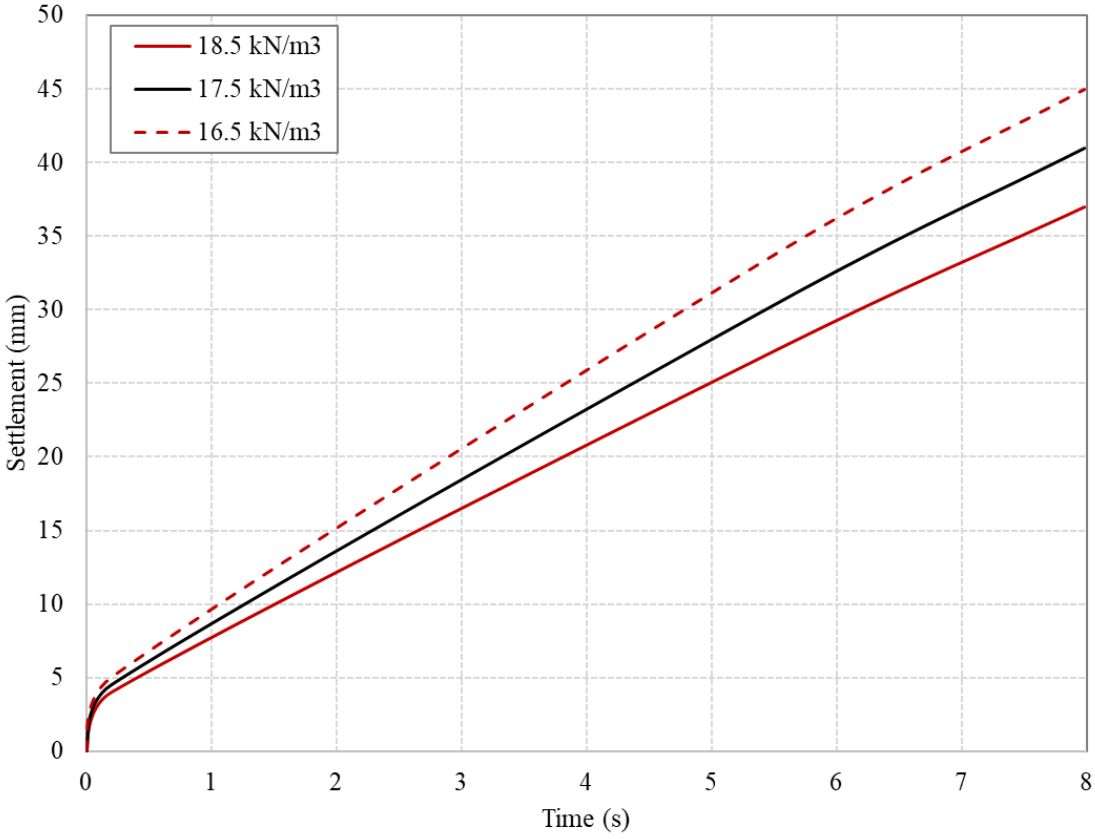

Fig. 9.10 Crest Settlement of the conventional breakwater model with various densities of loose sand layer

Effect of the Thickness of Sheet Pile in the Countermeasure Model

Figure 9.11 illustrates the effect of sheet pile thickness on the settlement of the crest of a breakwater model subjected to an 8-second earthquake loading. In this countermeasure model, sheet piles were inserted into the seabed beneath the breakwater, extending through the loose sand layer and embedding into the dense sand layer beneath. During earthquakes, these sheet piles act as lateral confinement in the foundation soil, thereby enhancing its bearing capacity

and reducing the settlement of the breakwater. The numerical study varied the thickness of these sheet piles to observe their influence on settlement reduction.

The settlement trends in the graph indicate that the thickness of the sheet piles significantly impacts the settlement behaviour of the breakwater. The model with the thinnest sheet piles, at 2 mm (represented by the solid black line), exhibits the highest settlement values over the duration of the earthquake. This suggests that thinner sheet piles provide less lateral confinement and bearing capacity, leading to greater deformation under seismic loading. In contrast, the models with thicker sheet piles demonstrate reduced settlement. The 2.5 mm thick sheet piles (shown by the solid red line) result in moderate settlement values, indicating improved performance compared to the 2 mm thick piles. The most substantial reduction in settlement is observed in the model with 3 mm thick sheet piles (represented by the dashed red line). This model shows the least settlement throughout the earthquake duration, highlighting the superior effectiveness of thicker sheet piles in enhancing soil stability and reducing settlement.

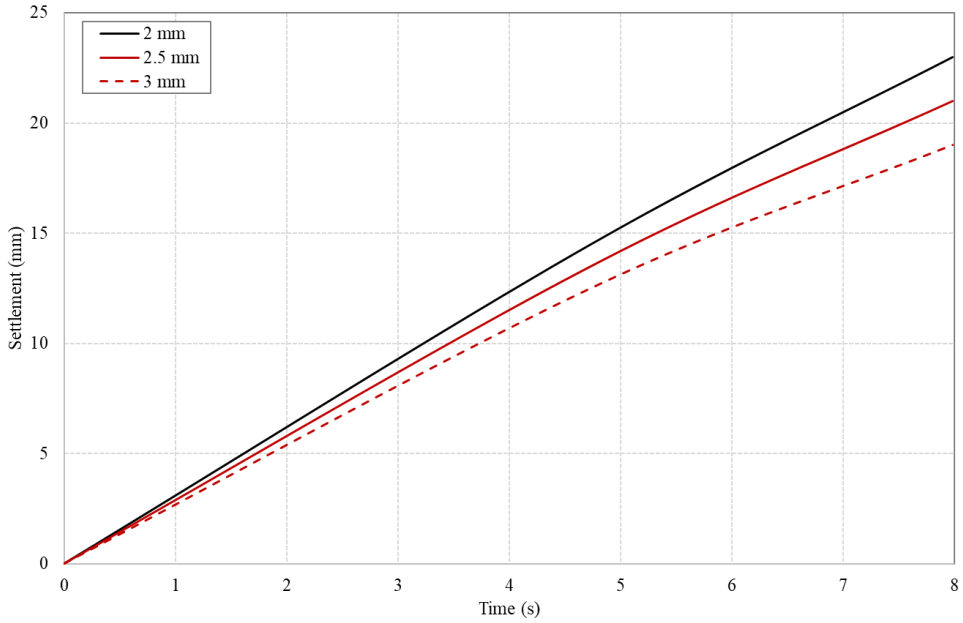

Fig. 9.11 Settlement of crest of the countermeasure model with various sheet pile thickness

These results clearly demonstrate that increasing the thickness of sheet piles enhances the lateral confinement of the foundation soil, thereby improving its bearing capacity and significantly reducing the settlement of the breakwater under seismic loading. For practical applications, this suggests that employing thicker sheet piles as a countermeasure can effectively mitigate settlement and enhance the seismic resilience of breakwater structures. Consequently, the design and construction of breakwaters in earthquake-prone regions should

consider the use of appropriately thick sheet piles to ensure optimal performance and structural stability.

Effect of the Embedment Depth of Sheet Pile in the Countermeasure Model

Figure 9.12 illustrates the effect of sheet pile embedment depth on the settlement of the crest of a breakwater model subjected to an 8-second earthquake loading. In this countermeasure model, sheet piles were embedded through the loose sand layer into the denser sand layer beneath. This configuration aims to improve the bearing capacity of the foundation soil by providing lateral confinement during seismic events, thus reducing the settlement of the breakwater. The numerical study varied the embedment depths of the sheet piles to observe their influence on settlement reduction.

The settlement trends depicted in the graph reveal that the embedment depth of the sheet piles significantly affects the settlement behaviour of the breakwater. The model with the shallowest embedment depth of 260 mm, represented by the dashed red line, exhibits the highest settlement values throughout the earthquake duration. This indicates that a shallower embedment depth provides less effective confinement and bearing capacity, resulting in greater deformation under seismic loading. As the embedment depth increases, the settlement values decrease. The model with an embedment depth of 280 mm, shown by the solid black line, demonstrates moderate settlement values, indicating an improvement in performance compared to the 260 mm depth. The model with the deepest embedment of 320 mm, represented by the solid red line, shows the least settlement throughout the earthquake duration. This illustrates that deeper embedment of sheet piles provides superior confinement and stability, effectively reducing settlement.

These results highlight the importance of embedment depth in enhancing the performance of sheet piles as a countermeasure for reducing settlement. Increasing the embedment depth improves the lateral confinement of the foundation soil, thus enhancing its bearing capacity and significantly reducing the settlement of the breakwater under seismic loading. For practical applications, this suggests that designing breakwaters with appropriately deep sheet pile embedment can effectively mitigate settlement and enhance the seismic resilience of these structures. Therefore, engineers should consider optimal embedment depths when implementing sheet piles as a countermeasure to ensure the stability and performance of breakwaters in earthquake-prone regions

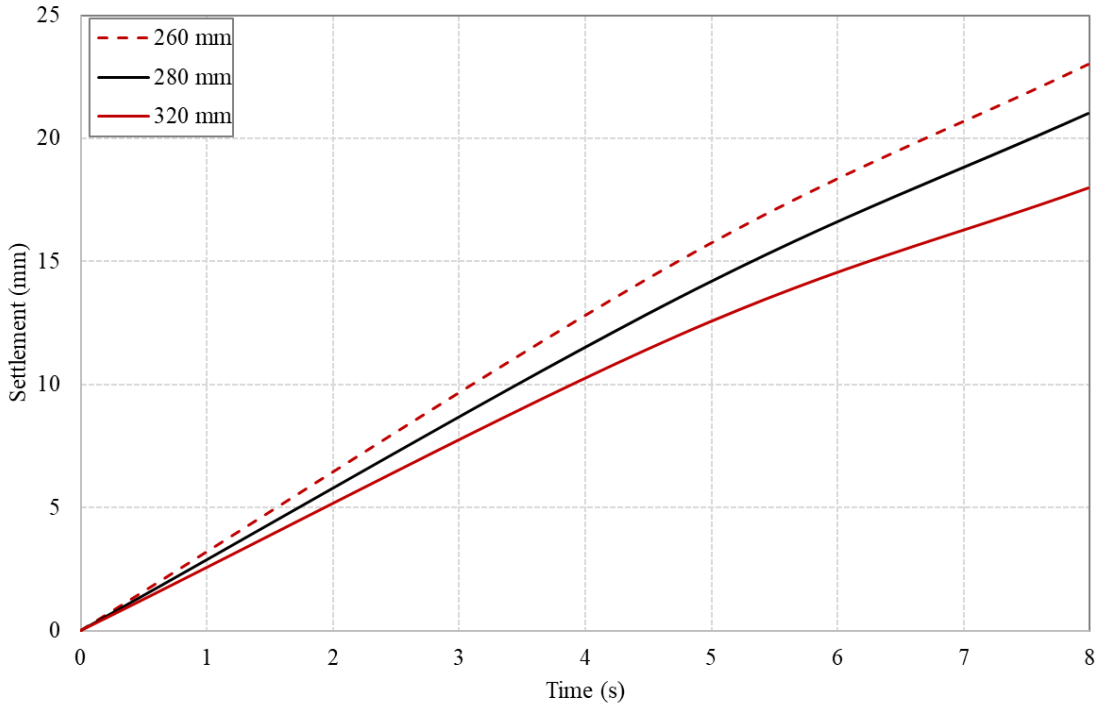

Fig. 9.12 Settlement of crest of the countermeasure model with various embedment depth of sheet pile

9.2 Numerical Modelling, Model Validation and Parametric Studies for Tsunami Flow Studies

In this section, stability analysis is performed in the finite element software Plaxis 3D for different scenarios of tsunami overflow. The height of the tsunami was varied to understand the change in stability of the rubble mound. The deformation of nodes along the crest, seaside slope, and harbour side slope were analysed to evaluate the degree of damage that occurred on the structure.

9.2.1 Numerical Modelling

In a similar way to experimental studies, the breakwater was modelled on top of a seabed layer which was divided into two layers. The top seabed layer was modelled as loose sandy soil and bottom as a hard layer. The geometry was then assigned with materials as per the properties mentioned in the material data set tabulated in Table 9.13. Previous research works by Cihan and Yuksel (2013) have accurately validated the numerical modelling of RM breakwaters using soil constitutive models in Plaxis (Cihan and Yuksel 2013). Therefore, the present study also adopts similar properties for numerical modelling the RM breakwater. A fifteen nodded triangular meshing was assigned to the whole model with finer meshing towards within the breakwater. The numerical model was discretized into 6485 nodes and 786 elements. The flow

conditions were then defined to simulate the raise of tsunami in the seaside. Tsunami was modelled as a reached level of water above withdrawn sea level. The water level during tsunami on either seaside and harbour side was plotted in the flow conditions module. Tsunami height was increased up to 15 m above the withdrawn sea level of 5 m by defining head functions. The analysis was performed using the staged construction module in PLAXIS, with the calculation type set to "fully coupled flow-deformation analysis." This method accounted for the interaction between hydraulic flow and structural deformation, providing comprehensive insights into the breakwater's response to tsunami-induced forces.

Table 9.13 Input parameters for numerical modelling

Material	**Armour**	**Core**	**Crown wall**	**Top Sand layer**	**Bottom Sand layer**
Model	Hardening Soil	Hardening Soil	Linear Elastic	Mohr-Coulomb	Mohr-Coulomb
Drainage Type	Drained	Drained	Non-porous	Drained	Drained
γ_u (kN/m^3)	18	16	50	17	17
γ_d (kN/m^3)	20	17	50	18	18
e_{int}	0.5	0.5	0.5	0.5	0.5
E_{50}^{ref} (kN/m^2)	130x10^3	110x10^3	30 x10^6	30 x10^3	55 x10^3
υ'	0.2	0.2	0.15	0.3	0.35
c'	0	0		1	1
ϕ'	45	41		35	42
ψ	5	10		0	0
K_0^{nc}	0.316	0.35			
Ground water Model	Standard	Standard		Standard	Standard
Soil Type	Coarse	Coarse		Coarse	Coarse
Permeability k_x(m/s)	1	0.8		8.25 x10^{-5}	8.25 x10^{-5}
Permeability k_y (m/s)	1	0.8		8.25 x10^{-5}	8.25 x10^{-5}

9.2.2 Numerical Model Validation for tsunami

Validation of the numerical model was carried out with the pore water pressure readings obtained from the experiment. The incremental porewater pressure (IPWP) as detailed in Figure 9.13 was measured as the difference in the peak pore pressure reading before and during the tsunami overflow. The location of sensors P1, P2, and P3 were marked in the numerical model as points of interest. Further, active pore water pressure for each case was determined from two calculation stages before and during the tsunami overflow. Figure 9.13 depicts the IPWP plotted across the length of the breakwater along the locations of the pore pressure transducers. It can be inferred from the figure that the developed numerical model can seemingly predict the behaviour of the RM breakwaters. Overall, the close agreement between the numerical model and experimental results validates the model's capability to simulate pore water pressure dynamics beneath a breakwater during tsunami overflow conditions. The slight differences observed at P2 and P3 could be attributed to inherent complexities in replicating exact field conditions in a controlled experimental environment. Nevertheless, the consistent trends and comparable magnitudes affirm the reliability of the numerical model in predicting the hydrodynamic behaviour of the structure.

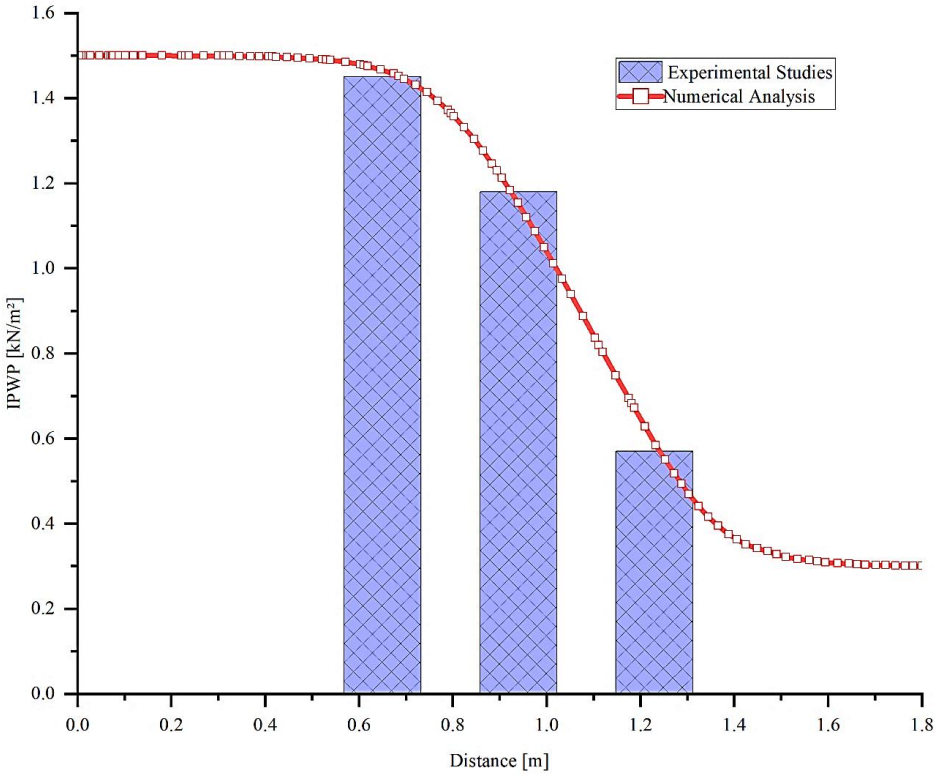

Fig. 9.13 Validation of numerical model with IPWP measured during the tsunami overflow test

9.2.3 Parametric Studies

The parametric study conducted in this research aims to investigate the influence of tsunami wave height on the performance and stability of the NMPA breakwater. By systematically varying the tsunami height, the study provides insights into how different tsunami overflow conditions affect the breakwater's response to dynamic loading, specifically in terms of settlement and overall stability.

Settlement of the Breakwater

The settlement of NMPA breakwater is a critical parameter in understanding its overall stability and response to varying tsunami loads. This study examines vertical settlement contours of the breakwater under different tsunami heights using a dimensionless parameter, h_t/H, where h_t represents the height of the tsunami, and H is the breakwater height, taken as 10 meters in this case. The analysis considers values of h_t/H ranging from 0.3 to 1.5, as shown in Figure 9.14(a)-(e). The observed settlement profiles provide essential insights into the structural performance of the breakwater when subjected to dynamic forces from tsunamis.

The settlement of a breakwater under tsunami conditions refers to the vertical displacement or subsidence of its structural body due to the dynamic forces exerted by the overflow of water. Settlement is a result of the interplay between hydrodynamic pressures from the tsunami wave and mechanical properties of the breakwater materials and foundation. As tsunami height increases, pressure exerted on the breakwater also increases, leading to higher stresses within the structure. This study analyses the effects of different tsunami heights on settlement and aims to quantify the impact of varying water inundation levels on the breakwater's stability.

In the case where the tsunami height is relatively small, with ht/H = 0.3, the settlement profile indicates a minimal impact on the breakwater. The contours in Figure 9.14(a) show a moderate concentration of vertical displacement around the center of the breakwater, with the highest settlement values occurring in a localized region. This indicates that the breakwater maintains overall stability under such small tsunami heights, experiencing only minor deformation. The relatively low settlement values in this case suggest that the breakwater is capable of withstanding this level of dynamic loading with negligible risk of failure or significant structural compromise.

As the tsunami height increases to $h_t/H = 0.6$, settlement contours (Figure 9.14(b)) reveal a more pronounced displacement pattern. The region of maximum settlement becomes more extensive, with higher vertical displacements observed across a larger portion of the breakwater. This indicates that increased tsunami height imposes greater hydrodynamic forces

& seepage, leading to more significant deformation. The settlement behaviour suggests that while the breakwater still retains a considerable degree of stability, the increased tsunami height results in noticeable structural responses, which could potentially lead to long-term issues if the breakwater were to experience repeated loading of this magnitude.

The deformation is still largely confined to the centre region of the breakwater, but the gradient between the settlement values is steeper than in the $h_t/H = 0.3$ case, suggesting that the structure is beginning to experience more substantial stress distribution.

With a further increase in the tsunami height to $h_t/H = 0.9$, the settlement contours in Figure 9.14(c) shows a significant rise in the extent and intensity of vertical displacement. The settlement is now more widespread, with the highest values extending across much of the breakwater structure. This indicates that hydrodynamic forces are now sufficiently large to cause substantial deformation in the breakwater materials and foundation.

The central part of the breakwater experiences higher settlement, with the contours showing higher intensity in this region. This suggests that the breakwater is approaching critical levels of deformation, where continued loading could lead to structural instability. The behaviour observed here emphasizes the importance of designing breakwaters to withstand not only small tsunamis but also larger events that may impose considerable dynamic forces.

When the tsunami height exceeds height of the breakwater, with $h_t/H = 1.2$, the settlement profile becomes even more pronounced, as shown in Figure 9.14(d). The contours depict a broad region of maximum settlement, with vertical displacement values reaching their peak. This indicates the breakwater experiencing near-failure conditions, where the hydrodynamic forces and seepage are causing severe stress concentrations within the structure.

At this stage, the structural integrity of the breakwater is significantly compromised, with large portions of the breakwater experiencing high levels of deformation. The settlement behaviour suggests that the breakwater's ability to withstand further tsunami loading without catastrophic failure is now severely diminished. The extent of settlement observed in this case indicates that the breakwater would require significant reinforcement or design modifications to prevent structural collapse in face of such extreme tsunami events.

In the most extreme case, where the tsunami height is 1.5 times the breakwater height $h_t/H = 1.5$, settlement contours (Figure 9.14(e)) show the most extensive and severe displacement. Vertical settlement values are the highest across the entire breakwater, indicating a near-total structural failure under this loading condition. The contours suggest that the breakwater cannot resist the overwhelming hydrodynamic forces, resulting in significant deformation throughout the structure.

At this point, the breakwater is unlikely to provide any meaningful resistance to the tsunami, as settlement values are far beyond acceptable limits for stability. The widespread nature of the settlement contours also suggests that the foundation of the breakwater is experiencing significant stress, which could lead to foundational failure in addition to structural collapse.

The settlement behaviour of the NMPA breakwater under varying tsunami heights highlights the importance of considering dynamic loading conditions in breakwater design. As tsunami height increases, settlement and overall deformation of the breakwater increase correspondingly, with the most significant impact observed when the tsunami height exceeds the breakwater height. This parametric study demonstrates that while the breakwater may perform adequately under small to moderate tsunami conditions, it becomes highly vulnerable to failure when subjected to large tsunamis.

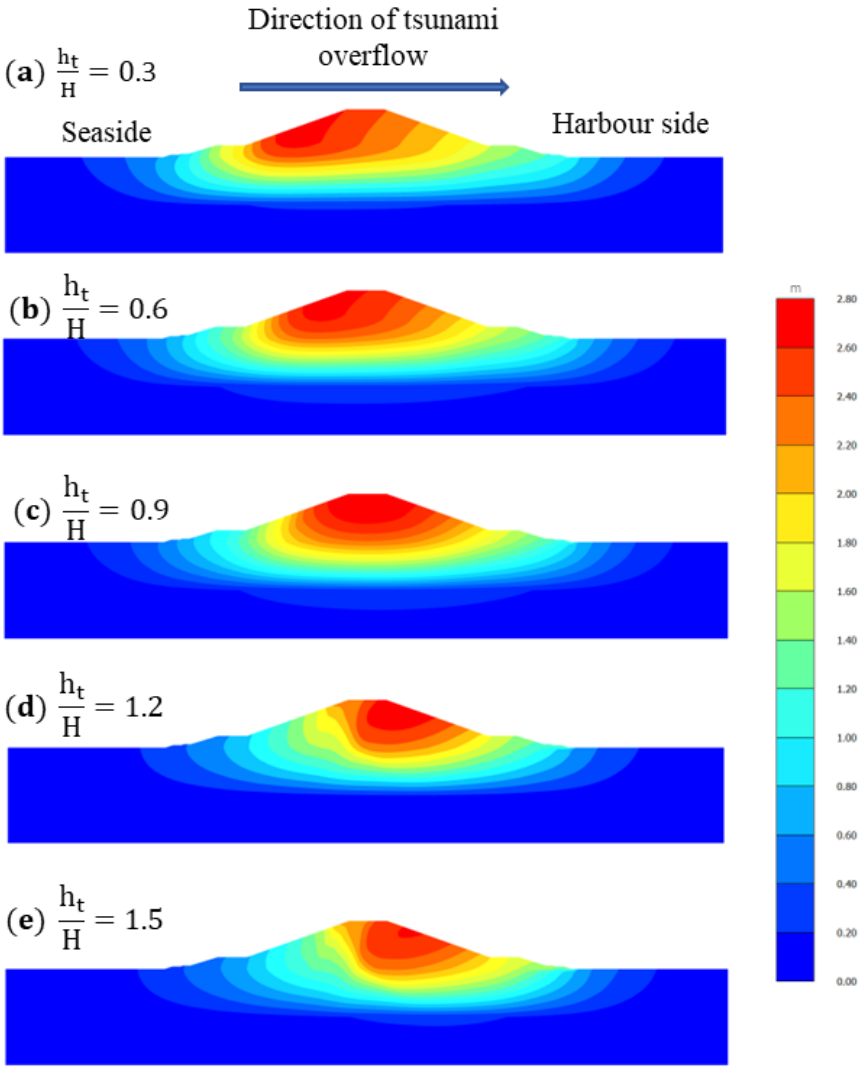

Fig. 9.14 Settlement of the breakwater under various tsunami heights

Lateral Displacement of the Breakwater

For the smallest tsunami height, represented by h_t/H =0.3, the breakwater crest undergoes limited displacement, reaching approximately 2 meters by the end of the simulation, as shown in Figure 9.15. In this case, tsunami height is much smaller than the breakwater height, and the structure maintains relative stability. The low displacement indicates that the breakwater can withstand the wave impact, with only minor deformation occurring over the 30-minute period. As the value of h_t/H increases to 0.6, the lateral displacement becomes more pronounced, reaching about 4 meters at 30 minutes. The increase in tsunami height results in higher hydrodynamic forces acting on the breakwater, leading to greater deformation. However, the breakwater still exhibits a relatively controlled response, indicating that it remains functional, though subjected to increased stress.

The trend continues as h_t/H rises to 0.9, where the lateral displacement reaches around 6 meters by the end of the simulation. In this case, the tsunami height approaches height of the breakwater, and the impact forces become significant. The larger displacement suggests that the structure is experiencing considerable deformation, as the tsunami wave is capable of overtopping or exerting strong lateral forces on the breakwater. At this stage, the breakwater may begin to lose its effectiveness in resisting the wave action.

For h_t/H =1.2, lateral displacement increases sharply, reaching approximately 10 meters. Here, tsunami height exceeds the breakwater height, leading to a scenario where breakwater is overwhelmed by the wave. Hydrodynamic pressure exerted on the structure increases dramatically, resulting in large-scale deformation. The breakwater likely experiences both elastic and plastic deformation, and possibility of structural failure becomes more pronounced as lateral displacement continues to grow rapidly.

The largest tsunami height considered in this analysis corresponds h_t/H =1.5, where the displacement reaches approximately 12 meters by end of the overflow. In this scenario, tsunami is 1.5 times height of the breakwater, and the forces acting on the structure are extreme. The breakwater undergoes significant displacement, and its structural integrity is likely compromised. The graph shows that lateral displacement grows at an accelerated rate as the wave height increases, highlighting the severe impact of tsunamis that exceed the height of coastal defenses.

The relationship between tsunami height and lateral displacement can be understood in terms of the hydrodynamic forces generated by the tsunami wave. When a tsunami impacts a breakwater, it exerts lateral and vertical forces, which cause the structure to deform. The

magnitude of these forces is directly related to the height of the tsunami, with higher waves generating stronger forces. As the tsunami height increases, the pressure and velocity of the water impacting the breakwater also increase, leading to larger lateral displacements. This effect is particularly evident when the tsunami height exceeds the breakwater height, as the wave is able to pass over the structure, leading to severe deformation and potential failure. In the case of smaller values of h_t/H, such as 0.3 and 0.6, the breakwater remains relatively stable because the height of the wave is much smaller than the height of the breakwater. This allows the breakwater to effectively resist the wave action, with only moderate lateral displacements observed. However, as h_t/H approaches H, the breakwater begins to experience more significant deformation, as seen in the case of h_t/H =0.9. At this point, the tsunami height is comparable to the height of the breakwater, and the structure is subjected to greater hydrodynamic forces, leading to increased displacement.

When h_t/H exceeds 1.0, the breakwater is no longer able to provide effective protection against the tsunami. For h_t/H =1.2, and h_t/H =1.5 h, the lateral displacements grow rapidly, indicating that the breakwater is undergoing large-scale deformation. In these cases, the tsunami height exceeds the breakwater height, resulting in forces that the structure is not designed to withstand. The breakwater is likely to experience plastic deformation or even collapse under these extreme conditions, as indicated by the steep increase in displacement.

The results of this analysis have important implications for the design of breakwaters in tsunami-prone regions. Breakwaters are typically constructed to resist the forces generated by regular wave action, but additional considerations must be made in areas where tsunamis are a significant threat. The data suggests that breakwaters must be designed to withstand waves that exceed their height in order to prevent catastrophic failure during a tsunami. This may involve increasing height of the breakwater, reinforcing the structure, or incorporating other design elements to dissipate energy of the tsunami wave.

The tsunami height has a profound effect on the lateral displacement of the breakwater crest. As h_t/H increases, the lateral displacement grows significantly, with the most severe displacements occurring when tsunami height exceeds breakwater height. This analysis underscores the importance of designing breakwaters capable of withstanding the forces generated by tsunamis, particularly in regions where such events are likely to occur. The data presented in this report highlights the need for robust coastal defense structures that can maintain their integrity even under extreme conditions.

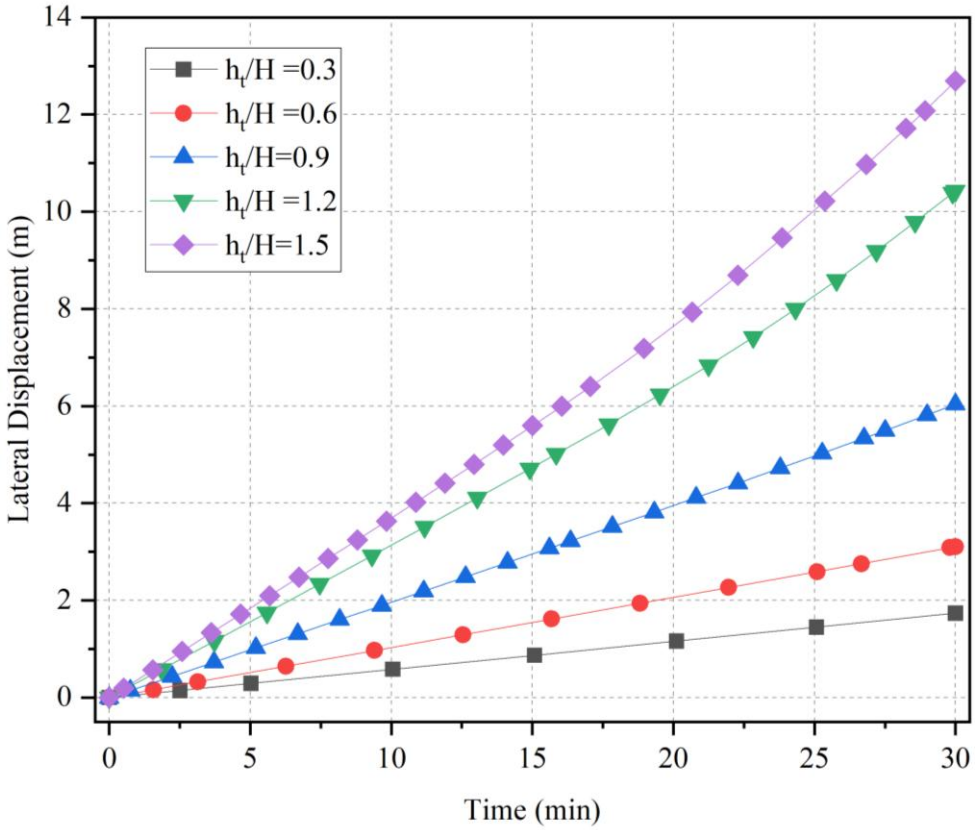

Fig. 9.15 Lateral displacement of the breakwater under various tsunami height

Stability of the Breakwater

The relationship between tsunami height and the factor of safety of a breakwater crest under various tsunami height-to-breakwater height ratios was analyzed. The factor of safety Msf has been computed using the strength reduction method, a widely used numerical tool for geotechnical analysis. The x-axis, representing the displacement of the breakwater crest, holds little significance in this case as it corresponds to displacement during the strength reduction process rather than actual structural response. Therefore, the focus of this sub-section is on the factor of safety values presented along the y-axis and how they vary with different tsunami heights, as shown in Figure 9.16.

The safety factor is critical in geotechnical engineering, reflecting structure stability under various loading conditions. A value greater than 1 indicates that the structure can withstand applied loads with some margin, while a value less than 1 implies impending failure. In this analysis, the safety of the factor is computed as a function of the tsunami height-to-breakwater height ratio, considering values of h_t/H = 0.3, 0.6, 0.9, 1.2, and 1.5. The goal is to determine how the stability of the breakwater is affected as the height of the tsunami increases.

For the smallest tsunami height, corresponding to h_t/H = 0.3, safety factor starts at a relatively high value, around 2.0. This indicates that the breakwater is highly stable under these

conditions, with a substantial margin of safety. The plot shows that safety factor remains consistently above 1.8 as displacement progresses during strength reduction process. This suggests that, even with minor displacements, the breakwater maintains a robust resistance to failure, highlighting the structure's ability to withstand tsunamis that are significantly smaller than its own height.

As the value of ht/H increases to 0.6, the safety factor decreases slightly, starting at around 1.8. Although the breakwater remains stable, the margin of safety is reduced compared to the previous case. The curve shows a gradual decline in the safety factor as the tsunami height approaches a value closer to the breakwater height. However, the safety factor still remains well above 1.6, suggesting that the breakwater can effectively resist forces generated by a tsunami of this magnitude, though it is subjected to greater stress than in the previous scenario.

For $h_t/H = 0.9$, the safety factor further decreases, starting at approximately 1.6. This value still indicates stability, but the reduced safety factor reflects the increasing challenge of resisting higher tsunami waves. As the strength reduction process progresses, the curve flattens, indicating that the breakwater is nearing its resistance limit. The lower safety factor, in this case, suggests that the breakwater is more vulnerable to deformation or potential failure when the tsunami height approaches the structure's height.

When the tsunami height exceeds the breakwater height, as in the case of $h_t/H = 1.2$, the safety factor starts at around 1.4 and decreases as displacement increases. The significantly reduced initial safety factor indicates that the breakwater is approaching a critical state where it may no longer be able to resist the forces imposed by the tsunami. The curve shows that the safety factor decreases more rapidly than in the previous cases, highlighting the increased risk of failure as the tsunami height surpasses the breakwater. This suggests that the breakwater is at a greater risk of large-scale deformation or collapse under such conditions.

The most extreme case considered in this analysis is $h_t/H = 1.5$, where the tsunami height is 1.5 times the height of the breakwater. In this scenario, the safety factor starts at approximately 1.0, indicating that the breakwater is at the failure threshold. A safety factor of 1.0 means that the forces acting on the structure are equal to its capacity to resist, with no margin for additional loads or uncertainties. As the curve progresses, the safety factor remains close to 1.0, underscoring the instability of the breakwater when faced with such a high tsunami. This suggests that the breakwater is at a high risk of structural failure when subjected to tsunamis that exceed its height by a significant margin. The results of this analysis provide valuable insights into the performance of breakwaters under varying tsunami conditions. The safety factor is directly influenced by the height of the tsunami, with larger waves resulting in a lower

factor of safety and, consequently, a higher risk of failure. In the case of smaller tsunamis, such as $h_t/H = 0.3$, the breakwater maintains a robust margin of safety, ensuring its stability even under challenging conditions. However, as the tsunami height increases, the margin of safety decreases, reflecting the increasing difficulty in resisting the forces generated by the wave.

When the tsunami height approaches or exceeds the height of the breakwater, the safety factor drops significantly, indicating that the structure is at risk of failure. In particular, the cases of $h_t/H = 1.2$ and $h_t/H = 1.5$) show that the breakwater is highly vulnerable to tsunamis that exceed its height. In these scenarios, the safety factor approaches 1.0, highlighting the potential for structural collapse if the wave forces surpass the breakwater's capacity to resist.

The strength reduction method employed in this analysis provides a clear understanding of breakwater's performance under different loading conditions. By systematically reducing the strength of the soil and structure, the method identifies the point at which the breakwater is no longer able to maintain stability. The resulting factor of safety values offers a quantitative measure of the breakwater's capacity to resist tsunami forces, providing critical information for the design and assessment of coastal defence structures.

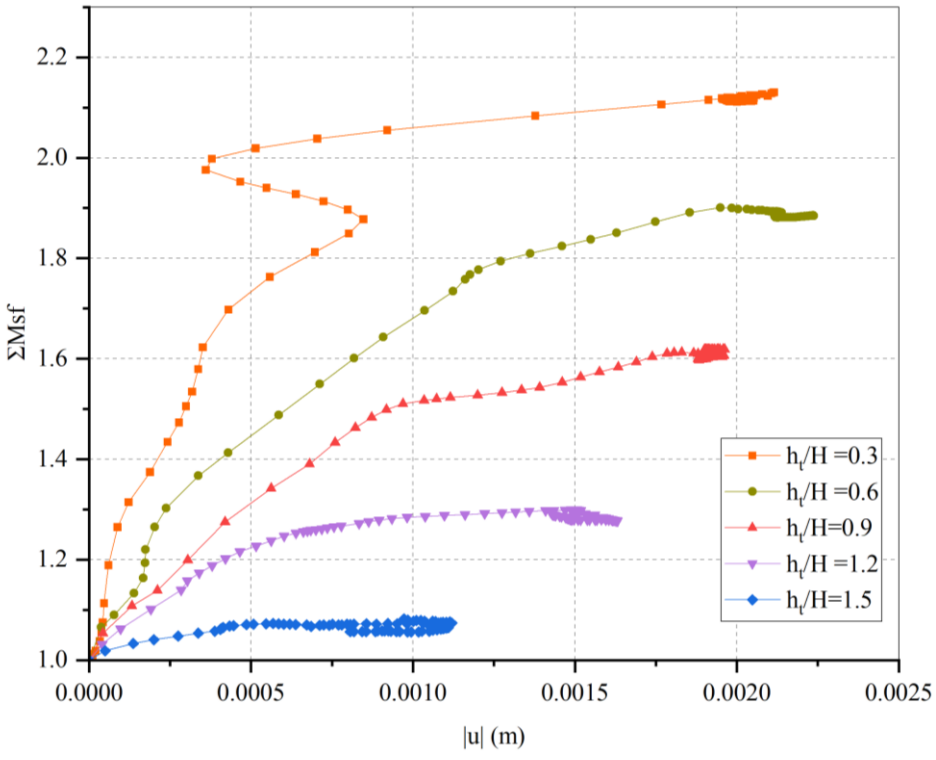

Fig. 9.16 Factor safety of breakwater subjected to different tsunami heights

The factor of safety of a breakwater is highly sensitive to height of tsunami. As tsunami height increases relative to breakwater height, safety factor decreases, with the most severe reductions occurring when the tsunami height exceeds the height of the structure. This analysis

underscores importance of designing breakwaters with sufficient capacity to withstand extreme tsunami events, particularly in regions where such events are likely to occur. The findings highlight the need for robust coastal defence systems that can maintain stability even under the most challenging conditions, ensuring the protection of coastal areas from the devastating impacts of tsunamis.

Development of Failure Envelope

The failure envelopes presented in this series of image in Figure 9.17 illustrate the progressive failure mechanisms of breakwater structure subjected to varying tsunami heights. These failure envelopes have been derived from stability analyses using numerical methods, and indicate regions within the breakwater that experience significant deformation or potential failure under different tsunami conditions. The colour contours in the figures represent the extent of failure, with the warmer colours (e.g., red) signifying regions of higher deformation.

In first case, where h_t/H =0.3, the tsunami height is relatively small compared to the breakwater height. The figure shows that there is no significant failure within the structure. The breakwater remains intact, with no noticeable deformation zones along its body. The absence of any colour changes indicates that the breakwater is well within its structural capacity and is able to resist the forces generated by the small tsunami. This result aligns with the higher factor of safety observed in previous analyses, confirming that the breakwater is highly stable under such low tsunami conditions.

As the tsunami height increases to h_t/H =0.6, the failure envelope begins to develop, primarily on the harbour side of the breakwater. A small, localized region of deformation appears near the crest, as indicated by the light blue colour. This suggests that the breakwater is starting to experience some internal stress, particularly on the side facing the harbour, where the tsunami impact forces are concentrated. The extent of the failure is still relatively minor, and the structure retains its overall stability. However, the emergence of a failure envelope at this stage indicates that the breakwater is beginning to reach its limit in certain regions, which may evolve further with increased tsunami height.

With a tsunami height of h_t/H =0.9, the failure envelope grows more prominent, extending deeper into the body of the breakwater and covering a larger area. The colour gradient now transitions from light blue to green and yellow, indicating a higher level of deformation compared to the previous case. The failure zone is still concentrated on the harbour side, but it now affects a more substantial portion of the structure. This suggests that the breakwater is experiencing significant stress, especially near its crest and upper slopes. The increasing size

of the failure envelope indicates that the breakwater is approaching a critical state where the potential for structural damage is much greater.

When the tsunami height reaches $h_t/H=1.2$, the failure envelope becomes much more extensive and severe. The warmer colours, including red and orange, dominate the harbour side of the breakwater, indicating that this region is undergoing substantial deformation. The failure zone now stretches from the crest of the breakwater down to the midsection, encompassing a significant portion of the structure. The extent of the failure suggests that the breakwater is no longer able to maintain its structural integrity in these regions, and significant damage or even collapse could occur if the loading continues. This result underscores the vulnerability of the breakwater when subjected to tsunami heights that exceed its own height, as the forces involved are far beyond the structure's capacity to resist.

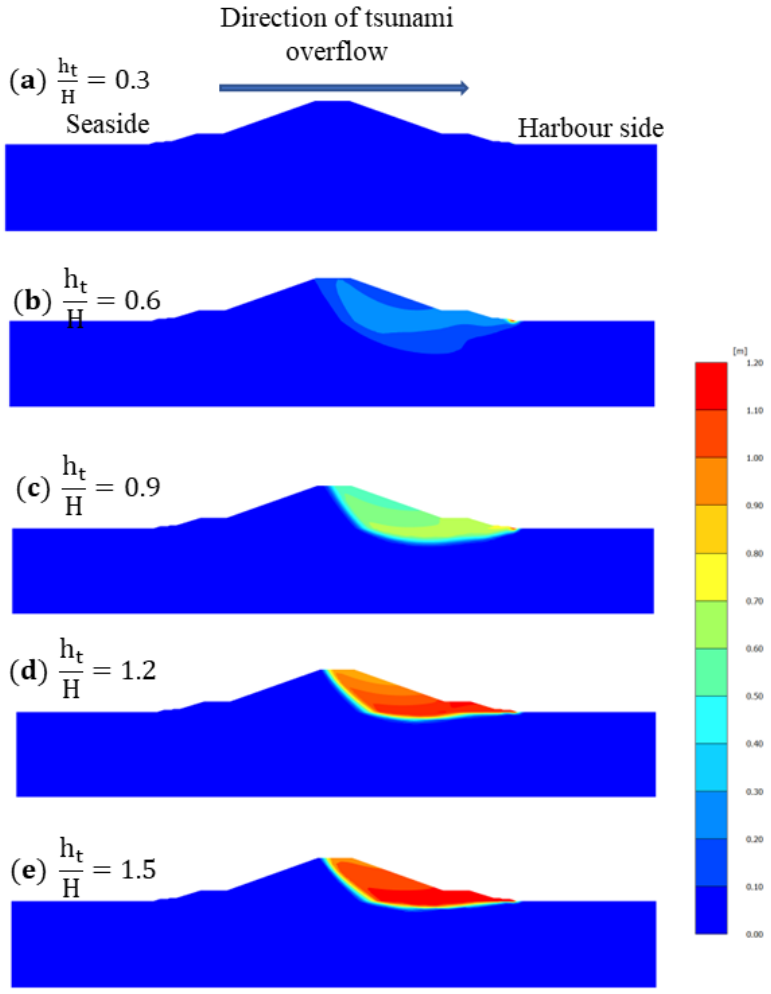

Fig. 9.17 Development of failure plane in the breakwater during tsunami overflow

In the most extreme case, where $h_t/H=1.5$, the failure envelope shows complete deformation of the harbour side of the breakwater. The red zone, indicating the highest level of deformation, spans a large area of the breakwater, with failure extending deep into the body of the structure.

The structure appears to have reached its limit, as it can no longer withstand the forces imposed by the tsunami. The substantial deformation on the harbour side suggests that the breakwater would likely collapse under these conditions. This result is consistent with the previous factor of safety analysis, which showed that the breakwater is at a high risk of failure when the tsunami height significantly exceeds its design height.

The progressive development of failure envelopes, as illustrated in these figures, reveals the increasing vulnerability of the breakwater as the tsunami height grows relative to its own height. At smaller tsunami heights, the breakwater remains stable, with no significant deformation zones. However, as the tsunami height increases, failure begins to develop on the harbour side, with the most severe deformations occurring when the tsunami height exceeds the breakwater height. The analysis shows that the harbour side of the breakwater is the most susceptible to failure, as the tsunami forces are concentrated in this region.

The failure envelopes provide valuable insights into the structural performance of the breakwater under extreme loading conditions. The results highlight the need for careful design and reinforcement of the harbour side of breakwaters, particularly in areas prone to tsunamis. By understanding the development of failure envelopes, engineers can better predict the points at which a structure will fail and implement design strategies to mitigate the risk of collapse during extreme events.

Drawdown Effects of Tsunami

(i) Displacements

Figure 9.18 illustrates displacement contours of the breakwater and its foundation soil when subjected to the drawdown effects of a tsunami from varying mean sea levels. The observed results provide valuable insights into the influence of the mean sea level on the stability and deformation patterns of the breakwater structure. When the tsunami drawdown occurred at a mean sea level equal to the height of the breakwater, the seaside experienced the most substantial displacements. This scenario represents a critical condition, where the hydraulic forces induced by the sudden drawdown exert maximum destabilizing effects on the breakwater and its foundation soil. Such significant displacements can compromise the structural integrity of the breakwater, highlighting the vulnerability of these structures under such conditions.

As the mean sea level decreased, a noticeable reduction in peak displacement was observed. For instance, when the mean sea level was set at 80% of the breakwater height, the peak displacement decreased by approximately 33%, demonstrating the mitigating influence of

reduced water levels on the structure's response. This trend continued as the mean sea level was further reduced. At 60% of the breakwater height, the displacement dropped significantly, with a reduction of around 58%. These reductions indicate that lower mean sea levels substantially alleviate the destabilizing forces caused by tsunami drawdown. At even shallower depths, the stabilizing effects became more pronounced. When the mean sea level was only 20% of the breakwater height, the observed displacements were negligible. This outcome emphasizes that under such low initial water levels, the drawdown forces are insufficient to induce meaningful displacements in the breakwater and its foundation soil.

The analysis clearly establishes that the mean sea level preceding a tsunami drawdown is a crucial parameter governing the stability of the breakwater. Higher mean sea levels amplify the hydrodynamic forces acting on the structure, leading to greater displacements and increased susceptibility to failure. Conversely, lower mean sea levels significantly reduce these forces, enhancing the structure's resilience against the drawdown effects.

These findings underline the importance of considering initial sea levels in the design and assessment of breakwater structures subjected to tsunami scenarios. Engineers and designers must account for these factors to optimize the stability and performance of such structures, especially in regions prone to high-magnitude tsunamis. Further investigations incorporating varying soil conditions, breakwater geometries, and dynamic loading scenarios could provide a more comprehensive understanding of the interplay between mean sea levels and breakwater stability during tsunami events.

The displacement contours presented in Figure 9.18 highlight the progressive reduction in the magnitude of displacements as the mean sea level (hs/H) decreases. At $h_s/H=1$, the displacement is most prominent on the seaside of the breakwater, as evidenced by the intense red and orange contours, indicating peak displacement zones. With the mean sea level lowered to $h_s/H=0.8$, the affected region and intensity of displacement notably diminish, transitioning to lighter shades of red and yellow. This trend continues as the mean sea level is further reduced to $h_s/H=0.6$, and $h_s/H=0.4$, with the contours shifting predominantly to cooler tones of blue and green, denoting lower displacement values. At $h_s/H=0.2$, the contours are uniformly blue, indicating negligible displacements. These visual representations emphasize the stabilizing effect of lower mean sea levels on the breakwater, as the hydrodynamic forces acting on the structure during tsunami drawdown are significantly attenuated.

The role of the breakwater's geometry and material properties in mitigating the impact of tsunami drawdown also warrants attention. Breakwaters with reinforced cores or hybrid designs incorporating geosynthetic materials, such as geogrids or gabions, may perform better under these conditions. These materials enhance structural integrity, reduce lateral displacements, and improve energy dissipation, providing a robust solution for coastal protection in high-risk areas.

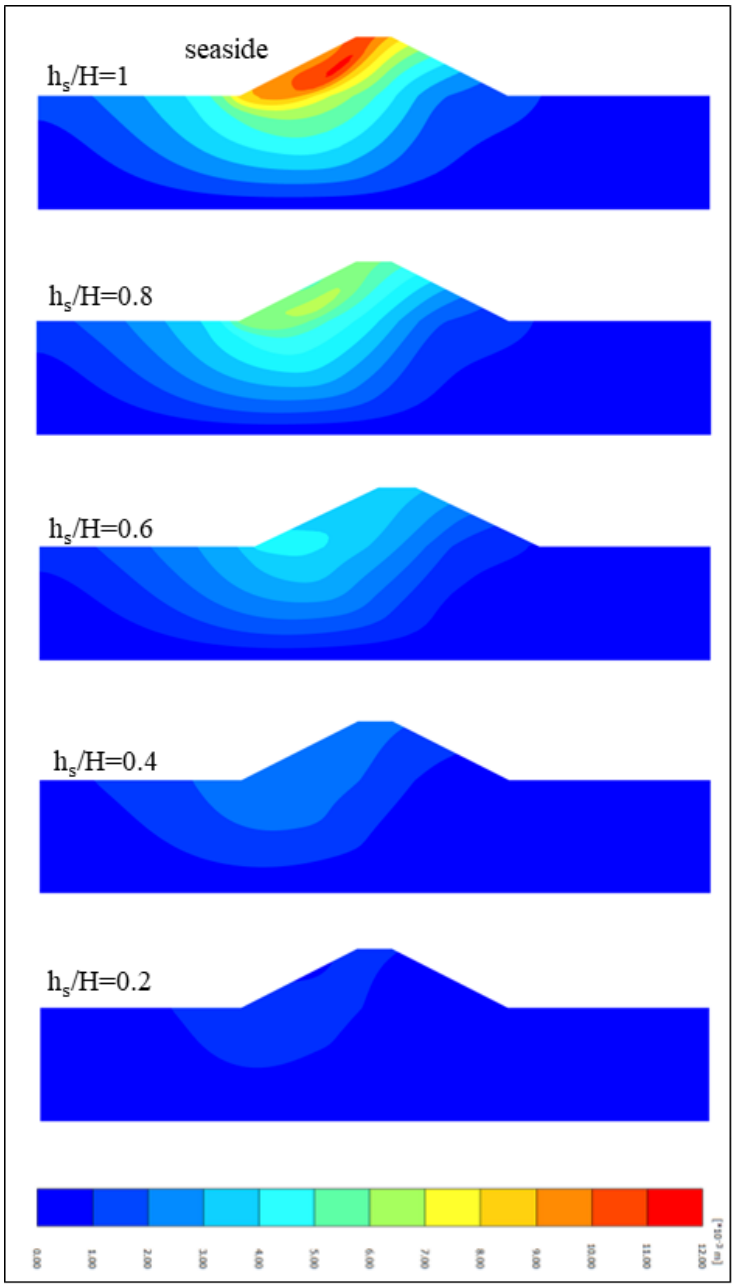

Fig. 9.18 Displacement contours of breakwater during the tsunami overflow

Additionally, the interaction between the foundation soil and the breakwater plays a pivotal role in determining the overall stability. Softer soils are more susceptible to settlement and lateral deformation, which can amplify the displacements observed during drawdown scenarios. Therefore, incorporating site-specific soil properties into numerical models and physical experiments is essential for accurate predictions and effective design interventions.

The broader implications of these findings on coastal management strategies should not be overlooked. The vulnerability of breakwater structures under high mean sea levels during tsunami events underscores the need for proactive measures, such as enhancing early warning systems and adopting adaptive construction practices. These approaches can help minimize damage and ensure the longevity and functionality of breakwater systems in safeguarding coastal infrastructure and communities.

(ii) Failure Mechanism

The sudden drawdown of sea levels during a tsunami event imposes significant hydrodynamic forces on coastal structures such as breakwaters, altering their internal stress distribution and potentially initiating failure. Figure 9.19 depicts the incremental displacement contours and provides critical insights into the evolving failure mechanisms of breakwaters subjected to drawdown. The displacement contours highlight the locations and paths along which failure is most likely to occur, offering valuable information for predicting and mitigating structural vulnerabilities.

When the mean sea level is at its highest, equivalent to the height of the breakwater, the failure plane extends into the foundation soil. This observation signifies that the high hydrostatic pressure caused by deep water levels compromises not only the breakwater structure but also its foundation. The displacement contours reveal that under these conditions, the structural instability propagates downward into the soil, indicating a base failure mode. Such a mechanism is particularly critical as it suggests that the breakwater's foundation is subjected to substantial stresses that can lead to settlement, rotation, or even collapse.

As the depth of the sea level decreases, the failure plane undergoes a noticeable shift. For sea levels reduced to $h_s/H=0.8$, the failure mechanism transitions from deep-seated foundation instability toward the crest and the face of the breakwater. This shift signifies a redistribution of stresses, where the hydrodynamic forces become more localized near the upper sections of the breakwater, rather than diffusing throughout the structure and

foundation.

When the mean sea level is further reduced to 60% or less of the breakwater height (hs/H=0.6), the failure mechanism transforms significantly. The contours indicate that the failure plane shifts from the base of the structure to its toe, marking a transition to toe failure. This behavior can be attributed to the reduced hydrostatic pressure acting on the foundation, which lessens the overall destabilizing forces at the base. Instead, the structural stresses concentrate near the toe, where the water flow exerts maximum drawdown-induced erosion and pressure.

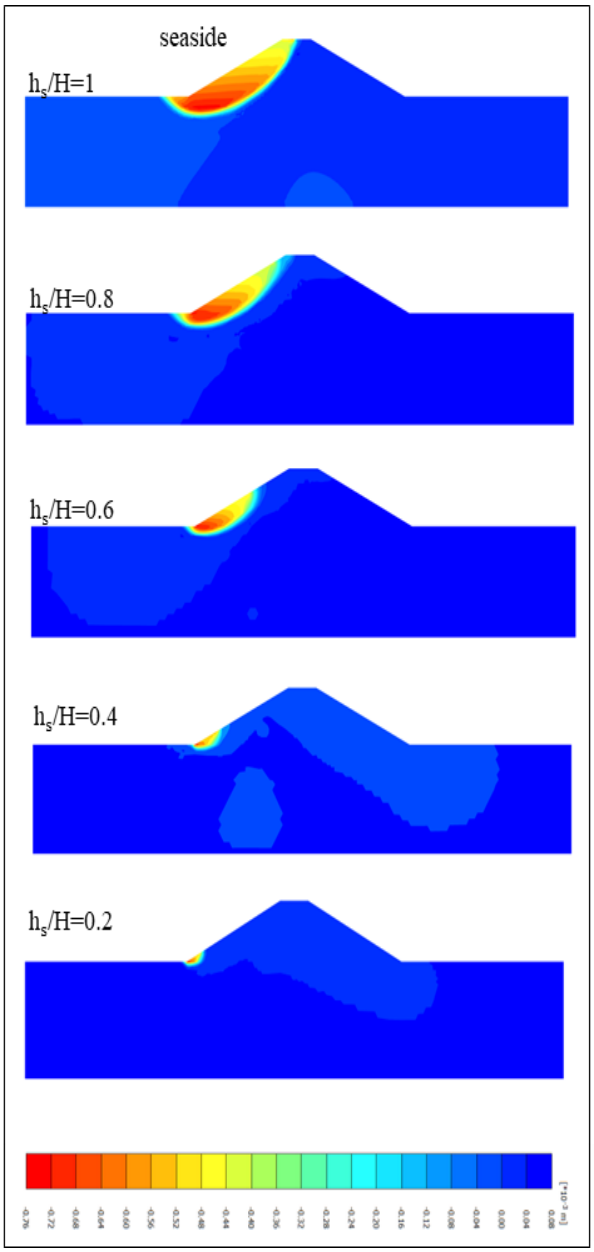

Fig. 9.19 Incremental displacement contours highlighting the possible failure mechanism

The shift from base failure to toe failure has significant implications for the structural design and resilience of breakwaters. Toe failure, while less catastrophic than base failure, can lead to progressive damage if left unaddressed. Erosion at the toe may undermine the stability of the breakwater over time, necessitating reinforcement strategies such as toe protection using geosynthetics, gabions, or rubble layers to resist scouring and displacement.

The drawdown of sea levels induces rapid changes in hydrostatic and hydrodynamic forces acting on the breakwater. During the drawdown process, the difference in water levels between the seaside and the lee side creates a pressure gradient, which intensifies as the sea level decreases. This pressure gradient generates significant shear forces along the failure plane, contributing to the observed displacement patterns. The contours in Figure 9.19 vividly illustrate how these forces influence the location and progression of failure planes.

The foundation soil plays a critical role in determining the extent and nature of failure mechanisms. Weaker/Softer soils are more prone to displacement under high hydrostatic pressures, leading to base failures as observed in deeper sea level scenarios (hs/H=1). Conversely, stiffer soils can resist deeper failures but may still exhibit localized instabilities near the toe. This highlights the importance of considering site-specific geotechnical properties during the design and analysis of breakwaters. The geometry of the breakwater also has a profound impact on the observed failure patterns. Structures with higher slopes or less robust foundations are more susceptible to shifting failure planes as the sea level changes. The incremental displacement contours suggest that flatter slopes and reinforced bases can help mitigate the transition from base to toe failure, enhancing overall stability during tsunami drawdown events. The failure modes observed at various sea levels underscore the dynamic response of breakwaters to changing hydrodynamic conditions. At high sea levels (hs/H=1), the failure is dominated by deep-seated foundation instability, while at intermediate levels (hs/H=0.6), the failure becomes more localized to the breakwater body. At low sea levels (hs/H=0.4and hs/H=0.2), the failure mechanism shifts entirely to the toe, suggesting a progressive stabilization of the foundation with decreasing water depth. The findings from Figure 9.19 highlight the need for adaptive design strategies to mitigate failure risks during tsunami events. Breakwaters must be designed to withstand a range of failure mechanisms, from base failure at high sea levels to toe failure at low levels. Reinforcement techniques, such as the use of geosynthetic materials, can enhance the structural integrity of both the breakwater and its foundation,

reducing the likelihood of displacement and failure. Numerical models play a vital role in understanding and predicting the failure mechanisms of breakwaters. By simulating the incremental displacement contours under various sea-level scenarios, engineers can identify critical failure planes and optimize structural designs accordingly. The observations from Figure 9.19 provide a basis for validating such models, ensuring their accuracy in predicting real-world behavior.

The failure mechanism of breakwaters during tsunami drawdown is a complex interplay of hydrodynamic forces, soil characteristics, and structural geometry. The incremental displacement contours in Figure 9.19 offer valuable insights into the shifting failure planes and their implications for breakwater stability. Future research should focus on integrating advanced materials, such as high-strength geogrids, into breakwater designs to enhance resilience. Additionally, experimental studies and field observations can complement numerical analyses, providing a comprehensive understanding of failure mechanisms and informing best practices for coastal protection in tsunami-prone regions.

(iii) Pore water Pressure

The pore water pressure within the breakwater structure plays a critical role in determining its overall stability during tsunami-induced rapid drawdown scenarios. As shown in Figure 9.20, the distribution of pore water pressure changes significantly with varying sea levels relative to the height of the breakwater, offering valuable insights into the hydraulic behavior of the structure under these conditions.

Initially, when the mean sea level is equal to the height of the breakwater, pore water pressure contours indicate higher pressures concentrated near the base of the breakwater. These pressures gradually decrease towards the crest, resulting in a pronounced pressure gradient. The high-pressure concentration at the base suggests a substantial hydraulic head acting on the structure, which could potentially lead to seepage forces if not adequately managed. This initial condition highlights the vulnerability of the base to higher hydraulic stresses.

As the sea level recedes to 80% of the breakwater height, the contours show a notable adjustment in the pressure distribution. The high-pressure zones remain concentrated near the lower regions, but the overall intensity of the pressures decreases. This redistribution reflects a reduction in the external hydraulic forces acting on the structure, which likely facilitates pore water pressure dissipation over time. However, the differential pressures

between the base and crest remain significant, indicating potential risks of destabilizing forces during the drawdown process.

When the sea level reaches 60% of the breakwater height, the pressure distribution further stabilizes, with the high-pressure regions becoming more confined to the lower portion of the structure. The gradient from the base to the crest becomes clearer and more uniform. This behavior suggests that the reduced hydraulic head allows the breakwater to dissipate pore pressures more effectively, which contributes to mitigating instability risks. However, the persistence of moderate pressures near the base emphasizes the need for structural resilience in this region.

At 40% of the breakwater height, the pressure contours exhibit a substantial reduction in overall intensity. While higher pressure zones remain near the base, their extent and magnitude are significantly diminished. Most of the structure is now subjected to lower pressure conditions, with only minor regions near the base experiencing moderate hydraulic forces. This transition indicates an increasingly favorable scenario for the breakwater's stability, as the external hydraulic forces become less pronounced.

For the case where the sea level is only 20% of the breakwater height, the pore water pressures throughout the structure are minimal. The contours show uniformity, with very low-pressure values observed across the breakwater. This scenario represents a highly stable condition, where the hydraulic forces acting on the breakwater are nearly negligible. The uniformity of the pressure distribution also suggests that the structure is no longer subjected to significant hydraulic gradients, reducing the likelihood of seepage-induced failure mechanisms.

The progression of pressure distributions across varying sea levels demonstrates the critical role of hydraulic head in influencing the pore water pressure dynamics within the breakwater. Higher sea levels correspond to more pronounced pressure gradients and higher stresses near the base, which could pose stability challenges. Conversely, the hydraulic forces diminish as the sea level recedes, leading to more uniform pressure distributions and enhanced stability.

Another key observation from the figure is the evolution of the pressure dissipation mechanism as the sea level changes. At higher sea levels, the dissipation of pore pressures is hindered by the significant hydraulic head, resulting in higher stresses near the base. As the sea level drops, the reduction in hydraulic head facilitates more effective dissipation, which is evident in the shifting and decreasing intensity of the pressure contours.

The differential pressures observed between the base and the crest at higher sea levels also underscore the importance of designing the breakwater with adequate drainage and filtration mechanisms. These features can help mitigate the risks associated with seepage forces and reduce the likelihood of instability during rapid drawdown scenarios.

Furthermore, the stability of the structure during the drawdown process is closely linked to the rate at which the pore pressures can dissipate. A rapid drawdown, as simulated in the figure, places the structure under significant stress, especially at the base, where hydraulic forces are concentrated. The findings suggest that slower drawdown rates could further enhance stability by allowing sufficient time for pressure dissipation.

The results also emphasize the need for rigorous geotechnical analysis during the design phase of such structures. Accounting for the dynamic nature of pore water pressures under fluctuating sea levels is essential to ensure that the breakwater can withstand extreme scenarios like tsunamis without experiencing structural failure.

The insights gained from the figure highlight the importance of regular monitoring and maintenance of breakwater structures in tsunami-prone regions. Implementing advanced monitoring systems to track pore water pressure dynamics in real time can provide early warnings of potential stability issues and enable timely interventions.

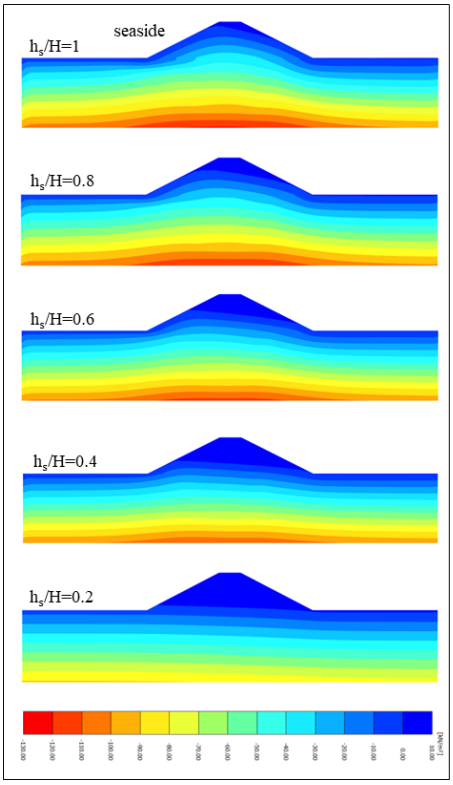

Fig. 9.20 Distribution of pore water pressure with varying sea levels relative to the height of the breakwater

CONCLUSIONS

Rubble mound (RM) breakwaters serve as critical coastal defence structures, but their vulnerability to seismic and tsunami-induced forces has been observed in past natural disasters, such as the 2004 Indian Ocean tsunami and the 2011 Great East Japan Earthquake. Existing literature on the failure mechanisms of RM breakwaters under such complex loading conditions remains limited, especially with respect to the role of seabed behaviour. Addressing this gap, the present study undertook a combined experimental and numerical approach to understand the dynamic response of conventional and reinforced RM breakwaters, aiming to develop effective countermeasures for improved resilience. The breakwater at New Mangalore Port was selected as a prototype for this investigation. A series of shake table and tsunami overflow tests were conducted on two configurations: a conventional model (without a crown wall) and a reinforced model featuring key enhancements such as *sheet piles embedded in the seabed, gabions along the outer slopes, and a crown wall at the crest.* The performance of the reinforced model was systematically evaluated against the conventional model to assess its effectiveness. Failure mechanisms were thoroughly examined in both cases. Additionally, numerical analysis was carried out to clarify the mechanisms involved in the response of breakwater when subjected to earthquake and tsunami loading.

Earthquake-Induced Effects: Experimental and Numerical Findings

Experimental Results: A series of shake table tests were conducted on conventional and reinforced RM breakwater models to investigate their seismic performance. The key observations include:

(i) The seismic response of the breakwater is influenced by various factors such as the acceleration amplitude of earthquake ground motion.

(ii) Settlement primarily arises due to these two factors: (a) the settling of the structure itself and (b) the lateral displacement and settlement of the foundation soil.

(iii) Settlement of the breakwater increases with higher acceleration amplitudes of earthquake ground motion. This higher acceleration amplitude give rise to the pore water pressure, which causes deformation in the foundation soils and an increase in shear strain. These factors ultimately reduce shear strength and diminish the bearing capacity of the foundation.

(iv) Lateral flow of foundation soils during the earthquake motion, primarily concentrated in the upper loose soil layer of the seabed, is a significant factor contributing to breakwater settlement. The presence of sheet piles effectively resists this lateral soil flow and

considerably reduces breakwater settlement. Also, the use of gabions on the slopes have added extra stability to the breakwater against the earthquake induced forces. During the main shock, the settlement and horizontal displacement was reduced by 49.3% and 37.3% respectively for reinforced model when compared to the conventional model without crown wall.

(v) In the reinforced model, the excess pore water pressure developed beneath the breakwater was reduced by 35.6% when compared to conventional breakwater (without crown wall). The reduction was attributed to the presence of sheet piles in the foundation soils.

(vi) From deformation pattern studies, the breakwater collapsed completely and sank into the sea due to loss in bearing capacity of foundation soils during the main shock for the conventional model. The increase in the acceleration amplitude caused pore water pressure to increase, and there was the intrusion of the breakwater main body. The development of shear strains led to shear deformation and slumping of core materials. Also, the outer armour layers and underlayer slumped and due to which the overall height was reduced. However, in the reinforced model, due to the presence of a crown wall at the crest, the overtopping of seawater was reduced after the breakwater model was subjected to earthquake loadings.

(vii) **Numerical Results:** Numerical modelling was performed using parameters such as depth and density of the loose sand layer, depth of the mean sea level, and dimensions of the reinforcements (sheet pile thickness and embedment depth).

- Deeper loose sand layers caused more settlement due to lower stiffness and increased compressibility.
- Higher densities of loose sand led to better load distribution and smaller displacements.
- Increasing sheet pile thickness and embedment depth notably improved lateral confinement and reduced foundation deformation.

Numerical results closely matched experimental observations, confirming that failure in conventional models was initiated due to the lateral spreading of loose soils, followed by progressive slumping and bearing failure beneath the core. Reinforced models showed increased structural stability, confinement and resistance to shear deformation.

<u>Effects of Tsunami overflow tests: Experimental and Numerical Findings</u>

Experimental Results: Tsunami overflow tests were performed to evaluate the performance of conventional and reinforced breakwaters. Key parameters such as settlement of the crest,

horizontal displacements, Incremental Pore Water Pressure (IPWP), deformation patterns, and damage analysis were scrutinized to assess the breakwater resilience and stability under extreme wave conditions. The major findings are:

(i) The settlement of the crest, a critical aspect of breakwater performance, revealed significant erosion of the protective armour layer during the tsunami overflow. However, the reinforced model exhibited remarkable resilience, with a substantial reduction of 94% in settlement attributed to incorporating gabions. The heavier weight of gabions and the larger contact area have prevented the scouring of rubbles from the armour layer of the breakwater.

(ii) Horizontal displacement along the crest poses a considerable threat during tsunami events, potentially compromising the breakwater's integrity. Integration of a crown wall with shear keys emerged as a pivotal solution, significantly reducing crest rubble displacement by an impressive 98%. The embedment of the shear key into the breakwater body offered extra resistance against horizontal tsunami force.

(iii) The assessment of Incremental Pore Water Pressure (IPWP) provided valuable insights into the stability of rubble mound breakwaters during tsunami overflow. Reinforced models demonstrated a lower 35 % IPWP, indicating reduced seepage and enhanced stability compared to conventional breakwaters.

(iv) Deformation pattern studies revealed the remarkable stability of reinforced breakwaters, with minimal scouring and deformation observed during tsunami overflow. The strategic placement of gabions, crown walls with shear keys, and sheet piles contributed to this resilience, highlighting the effectiveness of integrated countermeasure elements in mitigating adverse tsunami impacts.

(v) **Damage Analysis:** Damage quantification using relative displacement of armour units and eroded area showed clear superiority of the reinforced breakwater. Minimal dislodgement and scouring occurred, especially in the harbour, where wave attacks were most aggressive. The reinforced model maintained functional integrity post-tsunami impact.

Numerical Results:

- **Tsunami Height and Failure Envelopes:** The performance of a breakwater under varying tsunami heights, focusing on developing failure envelopes, settlement behaviour, and lateral displacement, is studied. Simulations showed that as ht/H increased:

- The failure envelopes demonstrate that significant deformation begins to emerge as the tsunami height increases relative to the breakwater, particularly on the harbour side in the conventional model, which is most exposed to hydrodynamic forces. When tsunami height reached 1.5 × breakwater height, the structure experienced widespread deformation and near-total collapse in the conventional model.
- For tsunamis exceeding the breakwater height, settlement reaches critical levels, indicating that the structural integrity is significantly compromised. This underscores the necessity for designing breakwaters that can endure regular wave action and extreme events like tsunamis.
- Numerical models of the reinforced breakwater showed a substantial reduction in maximum displacement and deformation zones, aligning closely with experimental results. The integration of sheet piles and crown walls effectively controlled seepage, delayed the onset of failure, and maintained structural coherence.

- **Tsunami Drawdown Analysis:** The analysis of breakwater performance under tsunami-induced drawdown scenarios provides critical insights into structural behaviour, stability mechanisms, and pore water pressure dynamics. Displacement patterns showed maximum movement on the seaside of the breakwater when the tsunami drawdown occurred at or above the breakwater height ($hs/H \geq 1$), indicating increased vulnerability. Lowering the mean sea level significantly reduced displacements—up to 58% at $hs/H = 0.6$—with negligible movement observed at $hs/H = 0.2$. Correspondingly, failure mechanisms shifted with sea level: base failure was predominant at high sea levels due to elevated hydrostatic pressure, while toe failure dominated at lower levels. The factor of safety decreased notably with rising sea levels, nearing failure at $hs/H \geq 0.4$, but remained high and stable at $hs/H = 0.2$. Pore water pressure followed a similar trend—intensifying near the base at higher water levels and dissipating under lower sea levels—further emphasizing the structural benefits of reduced hydraulic head. These findings highlight the need for targeted reinforcement, especially under high sea-level conditions.

Appendix I

Site Visit: NMPA Breakwater

A site visit for the northern breakwater of New Mangalore port was done on 2nd June 2023 in order to understand the ground condition of the breakwater. It was coordinated by the Executive Engineer (MW), NMPA, Er. Praveen Shenoy H.K. There were several locations where the settlement of the breakwater could be seen clearly. It might be due to the scouring of the rubble during high sea waves and storms in the past. In addition, seabed soils (below the breakwater) could attribute for the settlement. Therefore, it was requested to NMPA to provide the soil profile or bore logs data of the seabed soils which was done in the past. But unfortunately, those data was not available, therefore further investigation was not possible. In addition, some rubbles were scattered or scoured and were found in the sea (near to the breakwater). It might be due to the past high sea waves and storms. Figure A1 shows the settlement and scouring of the NMPA breakwater observed during the visit to the Northern Breakwater of New Mangalore Port.

Northern breakwater of New Mangalore Port

Settlement at the top of the breakwater

Settlement at the top of the breakwater

Settlement at the top of the breakwater.

Scattering/scouring of the rubbles of the breakwater.

Scattering scouring of the rubbles of the breakwater (at the end).

Fig. A1 Settlement and scouring observed during the visit to the Northern Breakwater of New Mangalore Port

As directed by NMPA officers, the PI of the project contacted Dr. Pruthviraj U., Associate Professor, NITK Surathkal for getting bathymetry survey details. Actually, bathymetry survey of NMPA breakwaters were done by Dr. Pruthviraj. Based on the report shared by Dr. Pruthviraj, the total displaced volume is given below:

Breakwater	**Total Displaced Volume**
Southern Breakwater	1916 m^3
Northern Breakwater	3227m^3

Appendix II

❖ **PhD (**partially benefitted from the project**)- 02**

(1) Dr Manu K Sajan

(2) Mr. Akarsh P.K.

❖ **M.Tech (**partially benefitted from the project**)- 03**

(1) Kaveri

(2) Sudhanshu Kumar

(3) Sudhansu Behera

❖ International Journals-03

(1) Akarsh, P.K., Chaudhary, B., Sajan, M.K., Sah, B., and Kumar, S (2024). "*Novel technique to mitigate the earthquake-induced damage of rubble mound breakwater*". **Geotextiles and Geomembranes** (Q1, Impact Factor 4.7), Elsevier, Volume 52, Issue 3, page 260-285. DOI: 10.1016/j.geotexmem.2023.11.001

(2) Akarsh, P.K., Chaudhary, B., Sajan, M.K., Kumar, S., and Sah, B. (2024). "*Seismic Stability Evaluation of Rubble Mound Breakwater: Shake Table Tests and Numerical Analyses*". **Soil Dynamics and Earthquake Engineering** (Q1, Impact Factor 4.2), Elsevier, Vol. 178, 108466. DOI: 10.1016/j.soildyn.2024.108466

(3) Akarsh, P.K., Sah, B., Chaudhary, B., Sajan, M.K., and Kumar, S. "*A Novel Geogrid-Wrapped Face Reinforcing Technique to Develop the Earthquake Resilient RM Breakwater*". **Acta Geotechnica**, Elsevier (Under review).

❖ Book Chapters-01

(1) Akarsh P.K., Kaveri, Chaudhary, B., Sajan, M.K., Kumar, S., and Sah, B, (2023) Numerical Simulations for Stability Evaluation of Breakwater Laying over Liquefiable Seabed Subjected to Irregular Seismic Motion, Indian Geotech Conference, IIT Roorkee, 2023.

❖ International Conferences-03

(1) Akarsh, P.K., **Chaudhary, B.,** Sajan, M.K., Kumar, S. (2024) Seismic Responses of Rubble Mound Breakwater: Numerical Analyses. Geo-Sustainnovation for Resilient Society (*Eds: Hazarika, H., Haigh, S.K., Chaudhary, B., Murai, M., Manandhar, S.*) CREST 2023, **Japan** proceedings. LNCE, vol 446, pg 237-246. Springer, Singapore. https://doi.org/10.1007/978-981-99-9219-5_22.

(2) Sajan, M.K., **Chaudhary, B.,** Akarsh, P.K., Kumar, S. (2024). Stability Analysis of Rubble Mound Breakwaters Under Tsunami Overflow. Geo-Sustainnovation for Resilient Society. (*Eds: Hazarika, H., Haigh, S.K., Chaudhary, B., Murai, M., Manandhar, S.*) CREST 2023, **Japan** proceedings. LNCE, vol 446, Pg 247-254. https://doi.org/10.1007/978-981-99-9219-5_23

(3) Kumar, S., **Chaudhary, B.,** Sajan, M.K., Akarsh, P.K. (2024). Response of Offshore Wind Turbine Foundation Subjected to Earthquakes, Sea Waves and Wind Waves: Numerical Simulations. Geo-Sustainnovation for Resilient Society. (*Eds: Hazarika, H., Haigh, S.K., Chaudhary, B., Murai, M., Manandhar, S.*) CREST 2023, **Japan** proceedings. LNCE, vol 446, pg 217-224. Springer Singapore. https://doi.org/10.1007/978-981-99-9219-5_20.

REFERENCES

Akarsh, P. K., Chaudhary, B., Sajan, M. K., and Kumar, S. (2024a). "Seismic responses of rubble mound breakwater: Numerical analyses." In: Hazarika, H., Haigh, S. K., Chaudhary, B., Murai, M., and Manandhar, S. (eds) *Geo-sustainnovation for resilient society. CREST 2023.* Lecture Notes in Civil Engineering, vol. 446, Springer, Singapore. https://doi.org/10.1007/978-981-99-9219-5_22

Akarsh, P. K., Chaudhary, B., Sajan, M. K., Kumar, S., and Sah, B. (2024c). "Seismic stability evaluation of rubble mound breakwater: shake table tests and numerical analyses." *Soil Dynamics and Earthquake Engineering* 178, 108466. https://doi.org/10.1016/j.soildyn.2023.12.005

Akarsh, P. K., Chaudhary, B., Sajan, M. K., Sah, B., and Kumar, S. (2024b). "Novel technique to mitigate the earthquake-induced damage of rubble mound breakwater." *Geotextiles and Geomembranes* 52(3), 260–285. https://doi.org/10.1016/j.geotexmem.2023.11.001

Aniel-Quiroga, Í., Vidal, C., Lara, J. L., González, M., and Sainz, Á. (2018). "Stability of rubble-mound breakwaters under tsunami first impact and overflow based on laboratory experiments." *Coastal Engineering* 135, 39–54. https://doi.org/10.1016/j.coastaleng.2018.01.004

Arikawa, T., Sato, M., Shimosako, K., and Gen, H. (2013). "Stability of breakwater under tsunami overflow." *Journal of Japan Society of Civil Engineers* 69(2), I_916–920 (in Japanese).

Arikawa, T., Sato, M., Shimosako, K., Hasegawa, I., Yoem, G. S., and Tomita, T. (2012). "Failure mechanism of Kamaishi breakwater due to the Great East Japan Earthquake tsunami." *Proceedings of the 33rd Conference on Coastal Engineering*, Santander, Spain, 1–13.

Banijamali, B., Alviri, A., Rastgoftar, E., and Soltanpour, M. (2017). "A case-study of rubble-mound breakwaters stability against Makran subduction zone tsunamis." *Coastal Engineering Proceedings* 1, structures.44. https://doi.org/10.9753/icce.v35.structures.44

Bolt, B. A. (2023). "Earthquake." *Encyclopedia Britannica*. https://www.britannica.com/science/earthquake-geology

Bricker, J. D., Francis, M., and Nakayama, A. (2012). "Scour depths near coastal structures due to the 2011 Tohoku Tsunami." *Journal of Hydraulic Research* 50, 637–641. https://doi.org/10.1080/00221686.2012.721015

Bricker, J. D., Nakayama, A., Takagi, H., Mitsui, J., and Miki, T. (2015). "Mechanisms of damage to coastal structures due to the 2011 Great East Japan Tsunami." In: *Handbook of Coastal Disaster Mitigation for Engineers and Planners*, 385–415. Elsevier Inc. https://doi.org/10.1016/B978-0-12-801060-0.00019-8

Broderick, L. (1984). "Riprap stability versus monochromatic and irregular waves." *Behavioral Ecology and Sociobiology*, Oregon State University.

Campos, Á., Molina-Sanchez, R., and Castillo, C. (2020). "Damage in rubble mound breakwaters. Part II: Review of the definition, parameterisation, and measurement of damage." *Journal of Marine Science and Engineering* 8(306). https://doi.org/10.3390/jmse8050306

Chaudhary, B., Hazarika, H., and Ishibashi, I., Abdullah, A. (2017a). "Sliding and overturning stability of breakwater under combined effect of earthquake and tsunami." *Ocean Engineering* 136, 106–116. https://doi.org/10.1016/j.oceaneng.2017.03.021

Chaudhary, B., Hazarika, H., and Manafi Khajeh Pasha, S. (2018a). "Countermeasures for breakwater foundation subjected to foreshocks and main shock of earthquake loading." *Marine Georesources and Geotechnology* 36, 308–322. https://doi.org/10.1080/1064119X.2017.1313342

Chaudhary, B., Hazarika, H., and Murakami, A., Fujisawa, K. (2019). "Development of resilient breakwater against earthquake and tsunami." *International Journal of Geomechanics* 19(1). https://doi.org/10.1061/(ASCE)GM.1943-5622.0001314

Chaudhary, B., Hazarika, H., and Nishimura, K. (2017b). "Effects of reinforcement on the performance of breakwater foundation subjected to earthquake loadings." *International Journal of Geotechnical Engineering* 11, 186–197. https://doi.org/10.1080/19386362.2016.1205167

Chaudhary, B., Hazarika, H., Murakami, A., and Fujisawa, K. (2018b). "Geosynthetic-sheet pile reinforced foundation for mitigation of earthquake and tsunami induced damage of breakwater." *Geotextiles and Geomembranes* 46, 597–610. https://doi.org/10.1016/j.geotexmem.2018.04.011

Chaudhary, B., Hazarika, H., Murakami, A., and Fujisawa, K. (2018c). "Countermeasures for enhancing the stability of composite breakwater under earthquake and subsequent tsunami." *Acta Geotechnica* 13, 997–1017. https://doi.org/10.1007/s11440-017-0615-4

Cihan, K., and Yuksel, Y. (2011). "Deformation of rubble-mound breakwaters under cyclic loads." *Ocean Engineering* 58, 528–539. https://doi.org/10.1016/j.oceaneng.2011.02.002

Cihan, K., and Yuksel, Y. (2013). "Deformation of breakwater armoured artificial units under cyclic loading." *Applied Ocean Research* 42, 79–86.

Cihan, K., Yuksel, Y., Berilgen, M., and Cevik, E. O. (2012). "Behavior of homogeneous rubble mound breakwater materials under cyclic loads." *Soil Dynamics and Earthquake Engineering* 34, 1–10. https://doi.org/10.1016/j.soildyn.2011.10.009

CIRIA C683 (2007). *The Rock Manual: The Use of Rock in Hydraulic Engineering*, 2nd edn.

Dave, T., and Murty, D. (2012). "Assessment of portable traveling pluviator to prepare reconstituted sand specimens." *Geomechanics and Engineering* 4, 79–89. https://doi.org/10.12989/gae.2012.4.2.079

Dentale, F., Reale, F., Di Leo, A., and Carratelli, E. P. (2018). "A CFD approach to rubble mound breakwater design." *International Journal of Naval Architecture and Ocean Engineering* 10, 644–650. https://doi.org/10.1016/j.ijnaoe.2017.10.011

Dou, H., and Byrne, P. M. (1997). "Model studies of boundary effect on dynamic soil response." *Canadian Geotechnical Journal* 34(3), 460–465. https://doi.org/10.1139/t97-006

Edge, B., Eskijian, M., Boudreau, R., Carbuccia, M., Jaradat, O., Percher, M., Serrano, J., and Arulmoli, A. (2011). "Investigation of the damage to areas of coastal Chile due to the Maule MW 8.8 earthquake of February 27, 2010." *Solutions to Coastal Disasters Conference 2011*, American Society of Civil Engineers, Reston, VA.

Esteban, M., Takagi, H., Thao, N. D., and Yamamoto, L. (2015). "Stability of shallow rubble mound breakwaters under climate change induced sea level rise." In: Esteban, M., Takagi, H., and Shibayama, T. (eds.), *Handbook of Coastal Disaster Mitigation for Engineers and Planners*, Butterworth-Heinemann (Elsevier), Oxford, UK.

Franco, L., Geeraerts, J., Briganti, R., Willems, M., Bellotti, G., and De Rouck, J. (2009). "Prototype measurements and small-scale model tests of wave overtopping at shallow rubble-mound breakwaters: the Ostia-Rome yacht harbour case." *Coastal Engineering* 56(2), 154–165. https://doi.org/10.1016/j.coastaleng.2008.03.009

Ghalandarzadeh, A., Ghalandarzadeh, S., and Abdi, F. (2021). "Experimental study on the seismic deformations of rockfill breakwaters." *Soil Dynamics and Earthquake Engineering* 147, 106782. https://doi.org/10.1016/j.soildyn.2021.106760

Goseberg, N., Wurpts, A., and Schlurmann, T. (2013). "Laboratory-scale generation of tsunami and long waves." *Coastal Engineering* 79, 57–74.

Guler, H. G., Arikawa, T., Oei, T., and Yalciner, A. C. (2015). "Performance of rubble mound breakwaters under tsunami attack: a case study—Haydarpasa Port, Istanbul, Turkey." *Coastal Engineering* 104, 43–53. https://doi.org/10.1016/j.coastaleng.2015.07.007

Gunbak, A. R., Muyesser, O., and Yuksel, Y. (2000). "Damages recorded at the coastal and port structures around Izmit Bay under the August 17, 1999 earthquake." In: *Proceedings of PIANC Buenos Aires Conference*, pp. 1–19.

Hara, T., Okawara, M., Osumi, T., Yamanaka, M., Ishihara, Y., and Tsunekawa, Y. (2012). "Damages in south-central coastal area of Iwate prefecture in 2011 off the Pacific Coast of Tohoku Earthquake." *Japanese Geotechnical Journal* 7(1), 25–36. https://doi.org/10.3208/jgs.7.25

Hazarika, H., Chaudhary, B., Nozu, A., Kohama, E., Suzuki, K., Murakami, A., and Fujisawa, K. (2019). "Modeling of soil-structure interaction for reinforced breakwater foundation subjected to earthquake and tsunami loading." In: Silvestri, F., and Moraci, N. (eds.), *Earthquake Geotechnical Engineering for Protection and Development of Environment and Constructions*, Taylor & Francis, London, p. 18.

Hazarika, H., Hara, T., Chaudhary, B., Monji, N., Nishimura, K., Yamasaki, N., and Kasama, K. (2017). "Seismic resistant of breakwater foundation reinforced by steel sheet pile and gabion—evaluation through element test." *16th World Conference on Earthquake Engineering*.

Hazarika, H., Kasama, K., Suetsugu, D., Kataoka, S., and Yasufuku, N. (2013). "Damage to geotechnical structures in waterfront areas of northern Tohoku due to the March 11, 2011 tsunami disaster." *Indian Geotechnical Journal* 43(2), 137–152.

Hazarika, H., Kataoka, S., Kasama, K., Kaneko, K., and Suetsugu, D. (2012). "Composite ground disasters caused by the earthquake and tsunami in Aomori, Iwate Prefecture, northern Japan." *Geotechnical Engineering Journal*, Special Issue on 2011 Great East Japan Earthquake 7(1), 13–23 (in Japanese).

Hazarika, H., Nishimura, K., and Chaudhary, B. (2015). "Model testing on resilient solution for breakwater protection against tsunami." *Japanese Geotechnical Society Special Publication* 3, 40–44. https://doi.org/10.3208/jgssp.v03.j05

Hudson, R. Y. (1959). Laboratory investigation of rubble-mound breakwaters. *Transactions of the American Society of Civil Engineers* 126(4), 610–659.

Iai, S. (1989). "Similitude for shaking table tests on soil-structure-fluid model in 1g gravitational field." *Soils and Foundations* 29(1), 105–118. https://doi.org/10.3208/sandf1972.29.105

Iai, S., and Sugano, T. (1999). "Soil-structure interaction studies through shaking table tests." In: *Earthquake Geotechnical Engineering*, Vol. 3, Balkema, 927–940.

IS 1893-Part 1 (2016). *Criteria for earthquake-resistant design of structures. Part 1: General provisions and buildings* (Fifth revision). Bureau of Indian Standards, New Delhi.

IS 2720-Part 4 (1985). *Methods of test for soils: Part 4—Grain size analysis*. Bureau of Indian Standards, New Delhi.

Jianhong, Y., Dongsheng, J., Wang, R., and Changqi, Z. (2013). "Numerical study of the stability of breakwater built on a sloped porous seabed under tsunami loading." *Applied Mathematical Modelling* 37, 9575–9590.

Kazama, M., and Noda, T. (2012). "Damage statistics (summary of the 2011 off the Pacific Coast of Tohoku Earthquake damage)." *Soils and Foundations* 52(5), 780–792.

Kikuchi, Y., Kawabe, S., Takaenaka, S., and Moriyasu, S. (2015). "Horizontal loading experiments on reinforced gravity type breakwater with steel walls." *Japanese Geotechnical Society Special Publication* 2(35), 1267–1272.

Knodel, P., Lo Presti, D., Pedroni, S., and Crippa, V. (1992). "Maximum dry density of cohesionless soils by pluviation and by ASTM D 4253-83: a comparative study." *Geotechnical Testing Journal* 15, 180. https://doi.org/10.1520/GTJ10239J

Koshimura, S., Hayashi, S., and Gokon, H. (2014). "The impact of the 2011 Tohoku earthquake tsunami disaster and implications to the reconstruction." *Soils and Foundations* 54(4), 560–572.

Lykke Andersen, T., Burcharth, H. F., and Gironella, X. (2011). "Comparison of new large and small scale overtopping tests for rubble mound breakwaters." *Coastal Engineering* 58(4), 351–373.

Maheshwari, B., Singh, H., and Saran, S. (2012). "Effects of reinforcement on liquefaction resistance of Solani sand." *Journal of Geotechnical and Geoenvironmental Engineering* 138(7), 831–840. https://doi.org/10.1061/(ASCE)GT.1943-5606.0000645

Memos, C. D. (2000). "Experimental investigation of the seismic response of rubble-mound breakwaters." In: Brebbia, C. A., and Olivella, J. (eds.), *Maritime Engineering and Ports II*, WIT Press. ISBN 1-85312-829-5.

Memos, C. D., and Protonotarios, J. N. (1992). "Patras breakwater failure due to seismic loading." In: *Proceedings of the 23rd International Conference on Coastal Engineering*, American Society of Civil Engineers, 3343–3356.

Memos, C. D., Bouckovalas, G. D., and Tsiachris, A. (2001). "Stability of rubble-mound breakwaters under seismic action." *Coastal Engineering*, 1585–1598.

MLIT (2011). *Earthquake and tsunami resistant measures against ports in Tohoku area*. Technical Committee Report No. 3, Ministry of Land, Infrastructure, Transport and Tourism, Government of Japan (in Japanese).

MLIT (2013). *Guidelines for tsunami resistant design of the breakwater*. Bureau of Port and Harbor, Ministry of Land, Infrastructure, Transport and Tourism, Japan (in Japanese).

Mondal, G., and Rai, D. C. (2008). "Performance of harbour structures in Andaman Islands during 2004 Sumatra earthquake." *Engineering Structures* 30, 174–182.

Murthy, C. V. R. (2002). "Learning Earthquake Design and Construction." *IITK-BMTPC Earthquake Tips*.

Muttray, M. O., and Oumeraci, H. (2005). “Theoretical and experimental study on wave damping inside a rubble mound breakwater.” *Coastal Engineering* 52, 709–725. https://doi.org/10.1016/j.coastaleng.2005.05.001

Najma, A., and Ghalandarzadeh, A. (2019). “Experimental study on the seismic behavior of composite breakwaters located on liquefiable seabed.” *Ocean Engineering* 186.

Nakano, Y. (2008). “Design load evaluation for tsunami shelters based on damage observations after Indian Ocean Tsunami disaster due to 2004 Sumatra earthquake.” *Journal of Architecture and Building Science*, Architectural Institute of Japan 13(25), 337–340.

Narayan, J. P., Sharma, M. L., and Maheshwari, B. K. (2005). “Run-up and inundation pattern developed during the Indian Ocean tsunami of December 26, 2004 along the coast of Tamil Nadu (India).” *Gondwana Research (Gondwana Newsletter Section)* 8(4), 611–616.

NILIM (2013). *Research report of the National Institute for Land and Infrastructure Management*. No. 52, Ministry of Land, Infrastructure, Transport and Tourism, Japan (in Japanese).

Oka, F., Tsai, P., Kimoto, S., and Kato, R. (2012). “Damage patterns of river embankments due to the 2011 off the Pacific Coast of Tohoku Earthquake and a numerical modeling of the deformation of river embankments with a clayey subsoil layer.” *Soils and Foundations* 52(5), 890–909.

Patnaik, K. V. K. R., Kumar, A. S. V. V., Ramu, C. V., and Prasad, K. V. S. R. (2012). “Observational analysis on the run-up height and inundation along the Andhra coast during December 26, 2004 Indian Ocean tsunami.” *Journal of Asian Earth Sciences* 45, 239–246.

PIANC. (2001). *Seismic design guidelines for port structures*. Netherlands: Permanent International Association of Navigation Congresses, A. A. Balkema Publishers.

PLAXIS 3D (2023). *PLAXIS 3D 2023.01 – Finite element code for soil and rock analyses*. Bentley Systems, Inc., Delft, Netherlands.

RAPSODI. (2016). “Risk assessment and design of prevention structures for enhanced tsunami disaster resilience/Euro-Japan collaboration.” *Coastal Engineering Journal* 58(4), 1–37.

Recio, J., and Oumeraci, H. (2008). “Hydraulic permeability of structures made of geotextile sand containers: Laboratory tests and conceptual model.” *Geotextiles and Geomembranes* 26, 473–487. https://doi.org/10.1016/j.geotexmem.2008.05.006

Sajan, M. K., Chaudhary, B., Akarsh, P. K., and Kumar, S. (2024b). “Geosynthetic reinforced rubble mound breakwater for mitigation of tsunami-induced damage.” *Geotextiles and Geomembranes* 52(1), 72–94. https://doi.org/10.1016/j.geotexmem.2023.09.003

Sajan, M. K., Chaudhary, B., Akarsh, P. K., and Sah, B. (2025). “Developing tsunami resilient rubble mound breakwater: novel gabion-based technique.” *Natural Hazards Review* 26(1). https://doi.org/10.1061/NHREFO/NHENG-2183

Sajan, M. K., Chaudhary, B., Akarsh, P. K., Kumar, S., and Sah, B. (2024a). “Novel techniques for reinforcing rubble-mound breakwater against tsunamis.” *Journal of Geotechnical and Geoenvironmental Engineering* 150(3). https://doi.org/10.1061/JGGEFK.GTENG-11773

Sassa, S., Takahashi, H., Morikawa, Y., and Takano, D. (2016). “Effect of overflow and seepage coupling on tsunami-induced instability of caisson breakwaters.” *Coastal Engineering* 117, 157–165.

Sugano, T., Nozu, A., Kohama, E., Shimosako, K. I., and Kikuchi, Y. (2014). “Damage to coastal structures.” *Soils and Foundations* 54(4), 883–901.

Sumer, B. M., Ansal, A., Cetin, K. O., Damgaard, J., Gunbak, A. R., Hansen, N. O., Sawicki, A., Synolakis, C. E., Yalciner, C. A., Yuksel, Y., and Zen, K. (2007). “Earthquake-induced liquefaction around marine structures.” *Journal of Waterway, Port, Coastal, and Ocean Engineering* 133(1), 55–82. https://doi.org/10.1061/(ASCE)0733-950X(2007)133:1(55)

Suppasri, A., Muhari, A., Ranasinghe, P., Mas, E., Shuto, N., Imamura, F., and Koshimura, S. (2012). “Damage and reconstruction after the 2004 Indian Ocean tsunami and the 2011 Great East Japan tsunami.” *Journal of Natural Disaster Science* 34(1), 19–39.

Suppasri, A., Shuto, N., Imamura, F., Koshimura, S., Mas, E., and Yalciner, A. C. (2013). “Lessons learned from the 2011 Great East Japan tsunami: performance of tsunami countermeasures, coastal buildings, and tsunami evacuation in Japan.” *Pure and Applied Geophysics* 170, 993–1018.

Takagi, H., and Bricker, J. D. (2015). "Breakwater damage and the effect of breakwaters on mitigation of inundation extent during tsunamis: Case study of the 2011 Great East Japan Earthquake and Tsunami." In: *Handbook of Coastal Disaster Mitigation for Engineers and Planners*, Elsevier Inc., 363–383.

Takahashi, H., Sassa, S., Morikawa, Y., Takano, D., and Maruyama, K. (2014). "Stability implications to the reconstruction." *Soils and Foundations* 54(4), 560–572.

Takahashi, S., Kuriyama, Y., Tomita, T., Kawai, Y., Arikawa, T., Tatsumi, D., and Negi, T. (2011). "Urgent survey for 2011 Great East Japan Earthquake and Tsunami disaster in ports and coasts – Part I (Tsunami)." *Technical Note of the Port and Airport Research Institute* 1231 (English Abstract).

Ulker, M. B. (2014). "Dynamic response of seabed–rubble mound breakwater system under seismic waves." *Second European Conference on Earthquake Engineering and Seismology*, Istanbul, 1–12.

United States Army Corps of Engineers (2002). *Coastal engineering manual, EM 110-2-1100 (Part VI), Change 3 (28 September 2011).* Washington, DC, USA: United States Army Corps of Engineers.

Van Gent, M. R. A., and Van Der Werf, I. M. (2019). "Influence of oblique wave attack on wave overtopping and forces on rubble mound breakwater crest walls." *Coastal Engineering* 151, 78–96. https://doi.org/10.1016/j.coastaleng.2019.04.001

Vidal, C., Martin, F. L., Negro, V., Gironella, X., Madrigal, B., and García-Palacios, J. (2004). "Measurement of armor damage on rubble mound structures: Comparison between different methodologies." In: *Coastal Structures 2003*, American Society of Civil Engineers, Reston, VA, 189–200.

Wang, H., Yang, C. Y., Lamison, C. W., and Chen, S. S. (1978). "Loadings on rubble mound breakwaters due to earthquakes." *Coastal Engineering*.

Wilson, B. W., and Torum, A. (1972). "Effects of the tsunamis: An engineering study." In: *The Great Alaska Earthquake of 1964: Oceanography and Coastal Engineering*, National Academy of Sciences, 361–523.

Ye, J. H., and Jeng, D. S. (2013). "Three-dimensional dynamic transient response of a poro-elastic unsaturated seabed and a rubble mound breakwater due to seismic loading." *Soil Dynamics and Earthquake Engineering* 44, 14–26.

Yuksel, Y., Cetin, K. O., Ozguven, O., Isik, N. S., Cevik, E., and Sumer, B. M. (2004). "Seismic response of a rubble mound breakwater in Turkey." *Proceedings of the Institution of Civil Engineers – Maritime Engineering* 157, 151–161. https://doi.org/10.1680/maen.2004.157.4.151

Zhang, Y., and Ye, J. (2023). "Seismic dynamics of revetment breakwater built on reclaimed coral sand foundation in the SCS: Insight from 1 g shaking table tests." *Bulletin of Engineering Geology and the Environment* 82, 134. https://doi.org/10.1016/j.apor.2025.104512

Zhao, H. Y., Liang, Z. D., Jeng, D., Zhu, J. F., Guo, Z., and Chen, W. Y. (2018). "Numerical investigation of dynamic soil response around a submerged rubble mound breakwater." *Ocean Engineering* 156, 406–423. https://doi.org/10.1016/j.oceaneng.2018.03.005

Zhao, M., Zhang, G., Wang, P., Du, X., and Zhang, X. (2020). "An accurate frequency-domain model for seismic responses of breakwater–seawater–seabed–bedrock system." *Ocean Engineering* 197, 1–23.

****